

Afferents Integration and Neural Adaptive Control of Breathing

by

Chung Tin

B.Eng., Mechanical Engineering, The University of Hong Kong, 2002

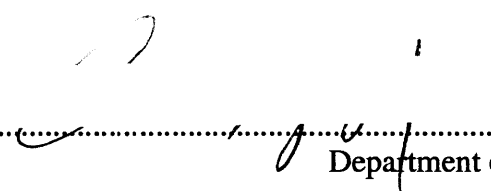
S.M., Mechanical Engineering, Massachusetts Institute of Technology, 2004

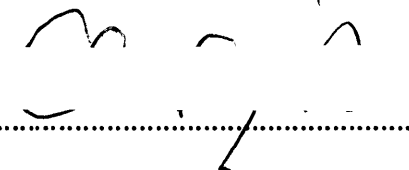
SUBMITTED TO THE DEPARTMENT OF MECHANICAL ENGINEERING
IN PARTIAL FULFILLMENT OF THE REQUIREMENTS FOR THE DEGREE OF

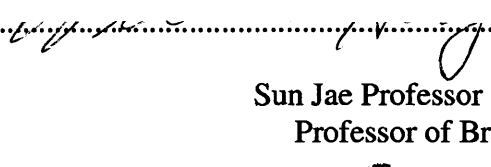
DOCTOR OF PHILOSOPHY IN MECHANICAL ENGINEERING
AT THE
MASSACHUSETTS INSTITUTE OF TECHNOLOGY


JUNE 2011

© 2011 Massachusetts Institute of Technology. All rights reserved.

Signature of Author.....
Department of Mechanical Engineering
May 19, 2011

Certified by
Chi-Sang Poon
Principal Research Scientist of Health Sciences & Technology
Thesis Supervisor

Certified by
Neville Hogan
Sun Jae Professor of Mechanical Engineering
Professor of Brain and Cognitive Sciences
Thesis Committee Chair

Accepted by
David E. Hardt
Ralph E. and Eloise F. Cross Professor of Mechanical Engineering
Chairman, Committee on Graduate Students

Afferents Integration and Neural Adaptive Control of Breathing

by

Chung Tin

Submitted to the Department of Mechanical Engineering
On May 19, 2011, in Partial Fulfillment of the
Requirements for the Degree of
Doctor of Philosophy in Mechanical Engineering

Abstract

The respiratory regulatory system is one of the most extensively studied homeostatic systems in the body. Despite its deceptively mundane physiological function, the mechanism underlying the robust control of the motor act of breathing in the face of constantly changing internal and external challenges throughout one's life is still poorly understood.

Traditionally, control of breathing has been studied with a highly reductionist approach, with specific stimulus-response relationships being taken to reflect distinct feedback/feedforward control laws. It is assumed that the overall respiratory response could be described as the linear sum of all unitary stimulus-response relationships under a Sherringtonian framework. Such a divide-and-conquer approach has proven useful in predicting the independent effects of specific chemical and mechanical inputs. However, it has limited predictive power for the respiratory response in realistic disease states when multiple factors come into play. Instead, vast amounts of evidence have revealed the existence of complex interactions of various afferent-efferent signals in defining the overall respiratory response.

This thesis aims to explore the nonlinear interaction of afferents in respiratory control. In a series of computational simulations, it was shown that the respiratory response in humans during muscular exercise under a variety of pulmonary gas exchange defects is consistent with an optimal interaction of mechanical and chemical afferents. This provides a new understanding on the impacts of pulmonary gas exchange on the adaptive control of the exercise respiratory response. Furthermore, from a series of in-vivo neurophysiology experiments in rats, it was discovered that certain respiratory neurons in the dorsolateral pons in the rat brainstem integrate central and peripheral chemoreceptor afferent signals in a hypoadditive manner. Such nonlinear interaction evidences classical (Pavlovian) conditioning of chemoreceptor inputs that modulate the respiratory rhythm and motor output. These findings demonstrate a powerful gain modulation function for control of breathing by the lower brain.

The computational and experimental studies in this thesis reveal a form of associative learning important for adaptive control of respiratory regulation, at both behavioral and neuronal levels. Our results shed new light for future experimental and theoretical elucidation of the mechanism of respiratory control from an integrative modeling perspective.

Thesis Supervisor:

Chi-Sang Poon

Principle Research Scientist of Health Sciences & Technology

Thesis Committee:

Neville Hogan (Thesis Committee Chair)

Sun Jae Professor of Mechanical Engineering

Professor of Brain and Cognitive Sciences

Kamal Youcef-Toumi

Professor of Mechanical Engineering

Acknowledgements

Earning a PhD. Degree is hard, especially from MIT. It would have been impossible for me without the help and support of many people throughout the process.

I would like to first thank my advisor, Dr. Chi-Sang Poon, who offered me the opportunity to pursue a research project totally distinct from my previous background. Furthermore, his advice and guidance throughout these years have paved the road for me towards becoming an independent scientist. I would also like to thank Prof. Neville Hogan and Prof. Kamal Youcef-Toumi for their invaluable feedback and guidance in shaping the thesis in its best possible form.

Members of Poon Lab have been wonderful. Dr. Gang Song has taught me all the neuroscience, physiological and experimental techniques that open my road towards biological research. Thank to Dr. Yunguo Yu for teaching me the skills for performing multielectrode recording, as well as for being a good friend. I am indebted to Dr. Ping Yu and Martha Adams for their generous help on carrying out the experiments. Dr. Paula Feinberg-Zadek has been very kind to help me proofread my thesis writing. I would also like to thank all the past and present members of Poon Lab for their friendship and support all these years. It has been a great time working with all of you.

I must thank our beloved Leslie Regan at the Graduate Office of Mechanical Engineering for her help and care in many occasions through my life as a graduate student in MIT.

I would like to thank the Croucher Foundation and American Heart Associative for their generous financial support for my graduate study.

I have been very lucky to meet so many fantastic friends here who have kept me moving toward the finish line. My special thank to Sally Kwok and Edmond Lee and their baby Natalie. Sally and Edmond have been like brother and sister to me and they treat me like one of their family. Natalie has been one of the best cheerleaders for me since she was born. I owe countless emotional, as well as nutritional, support from them. My special thanks also go to Samuel Au, who has been both a mentor and a friend to me. Thank to Sam for helping me to settle down in MIT when I first came. We have had enormous sharing both in science and in life over the years. I will always remember the fun times when we went playing soccer, snowboarding and hiking together.

My life here would have been a very different story without the friendship from all of you: Patrick Sit, Louis Wong, Ivy Lee, Raymond Lam, Ming Yan Poon, Preston Li, Albert Kong, Albert Lok, David Choa, Ricky Tong, Victor Yeung and many more. Thanks for your company and support and fun.

Thanks to my friends in Hong Kong and anywhere in the world. Thanks for being my friends and for caring about me since the day we met.

I owe my deepest gratitude to my parents. They have always offered me the best they could since the very first day and they support unconditionally every move I have made in life. I can never thank you enough.

Chung Tin
Cambridge, Massachusetts
May 2011

Table of Contents

Chapter 1	Introduction.....	15
1.1	THESIS OUTLINE	18
1.2	REFERENCES.....	19
Chapter 2	Background	21
2.1	RESPIRATORY FEEDBACK	21
2.1.1	Mechanical Feedback.....	22
2.1.2	Chemical Feedback.....	23
2.2	BRAINSTEM RESPIRATORY CONTROL CENTER.....	23
2.2.1	Dorsal respiratory group (DRG)	24
2.2.2	Ventral respiratory group (VRG).....	24
2.2.3	Pontine respiratory region.....	25
2.3	Traditional view of respiratory control and limitations	26
2.4	Evidence of intelligent respiratory control.....	27
2.4.1	Nonassociative learning in the chemical and mechanical feedback pathways 28	
2.4.2	Clinical implications from models of nonassociative learning.....	29
2.4.3	Associative interaction of vagal and carotid chemoafferent inputs	30
2.5	Summary	30
2.6	REFERENCES.....	31

Chapter 3 Integrative and Reductionist Approaches to Modeling of Control of Breathing..... 37

3.1 INTRODUCTION..... 37

3.2 REDUCTIONIST VIEW OF BIOLOGICAL MODELING 38

 3.2.1 The Physiome Project and Multiscale Model 39

3.3 ENGINEERING AND PHYSICS VIEW OF INTEGRATIVE MODELING .. 41

3.4 TOP-DOWN (INTEGRATIVE) VS BOTTOM-UP (REDUCTIONIST) APPROACH TO BIOLOGICAL MODELING 42

3.5 CRITERIA OF A GOOD MECHANISTIC MODEL 44

3.6 CONTROL OF BREATHING: REDUCTONISM VS INTEGRATION..... 45

 3.6.1 Limitations of classical reflex models: a case for sensorimotor integration45

 3.6.2 Optimal sensorimotor integration in respiratory control 47

 3.6.3 Hebbian feedback covariance learning model of respiratory motor control49

 3.6.4 Cheyne-Stokes breathing from different engineering control perspectives 54

3.7 REFERENCES..... 56

Chapter 4 Mechanical-Chemical Interaction underlies Optimal Respiratory Control in Gas Exchange Defects 61

4.1 INTRODUCTION..... 61

4.2 BACKGROUND..... 63

 4.2.1 Traditional notion of dead space..... 63

4.3 GENERALIZED GAS EXCHANGE EQUATION AND OPTIMAL RESPIRATORY CONTROL FOR PULMONARY GAS EXCHANGE DEFECTS .. 64

 4.3.1 Notion of dead space in gas exchange equation 64

 4.3.2 Role of dead space in optimal respiratory control 67

4.4 THE OPTIMIZATION MODEL (MODIFIED FROM POON’S MODEL)..... 68

4.5 GAS EXCHANGE EQUATION UNDER DIFFERENT PULMONARY GAS EXCHANGE DEFECTS..... 72

 4.5.1 Congestive heart failure 72

 4.5.2 Right-to-left shunts 73

 4.5.3 External Dead Space 74

4.6	THE EFFECT OF EXTERNAL DEAD SPACE, PARALLEL DEAD SPACE AND SHUNT ON OPTIMIZATION OF RESPIRATORY CONTROL	81
4.6.1	Congestive heart failure	81
4.6.2	Right-to-left shunts	83
4.6.3	External Dead Space	84
4.7	DISCUSSION	86
4.7.1	Optimization as a framework for afferent interaction in homeostatic control 87	
4.7.2	Different mechanisms underlying isocapnic augmented exercise hyperpnea in CHF and shunt	88
4.7.3	Mechanisms of potentiation of exercise ventilatory response by added dead space: Optimization vs. short term modulation	89
4.7.4	Influence of chemical afferent signal on breathing pattern revealed by comparing airway CO ₂ and dead space loading	89
4.8	CONCLUSIONS.....	90
	Appendix A: Numerical simulation for external dead space	91
4.9	REFERENCES.....	95
Chapter 5 Central-peripheral Chemoreceptors Interaction Revealed a Form of Pavlovian Conditioning		101
5.1	INTRODUCTION.....	101
5.2	METHODS.....	103
5.2.1	Animal preparation	103
5.2.2	Microelectrode arrays	104
5.2.3	Recording.....	104
5.2.4	Protocols	106
5.2.5	Data analysis	106
5.2.6	Histology.....	108
5.3	RESULTS.....	109
5.3.1	Interaction of hypercapnia and hypoxia in phrenic motor output.....	109
5.3.2	Neuronal recording loci	110
5.3.3	Neuronal response to hypoxia and hypercapnia	111

5.4	DISCUSSION	126
5.4.1	Controversy about chemoreceptors interaction in phrenic motor output..	126
5.4.2	Recording loci of respiratory neurons.....	127
5.4.3	Role of dl-pons in chemoafferent signaling.....	127
5.4.4	Associative learning (Pavlovian conditioning) in respiratory chemoreflex control	128
5.4.5	Implications for respiratory rhythmogenesis, respiratory instability/apnea and acclimatization	130
5.5	CONCLUSIONS	131
5.6	REFERENCES.....	132
Chapter 6 Conclusions and Future Work		139
6.1	FUTURE WORKS.....	140
6.1.1	Modeling.....	140
6.1.2	Experimental.....	142
6.2	REFERENCES.....	143

List of Figures

Figure 3.1 Two views for respiratory control (a) Classical reflex model assumes additive, reducible and superposable characteristics of chemical, mechanical and exercise stimuli; (b) The optimization model integrates various afferent-efferent signals in a single model to characterize the complex interactions among these signals. (Poon *et al.*, 2007)..... 46

Figure 3.2 Simplified block diagram of the optimization model of respiratory control. Sensorimotor feedback signals are integrated by an intelligent controller which produces optimal ventilatory drive and breathing pattern that are most cost-effect for meeting metabolic demands, subject to the constraints imposed by the mechanical plant and chemical plant. The functional block “G” represents the transmission gains for sensorimotor integration. 53

Figure 3.3 Hebbian Feedback Covariance Control Paradigm 53

Figure 3.4 Limit cycle a) Stable, b) unstable, c) semi-stable (Slotine & Li, 1991)..... 55

Figure 4.1 Expired CO₂ trace with illustration of “dead space”. Total “dead space” normally comprises alveolar and airway dead space 65

Figure 4.2 Block diagram of optimal respiratory CO₂ control 67

Figure 4.3 Simulated breathing pattern fitted to clinical data to determine parameter values for mechanical work index. 71

Figure 4.4 Illustration of parallel dead space, V_D, and the corresponding expired CO₂ trace..... 72

Figure 4.5 Illustration of right-to-left shunt and the corresponding expired CO ₂ trace....	74
Figure 4.6 Distribution of P _{CO2} along the airway over a breath cycle in the presence of an external dead space. Tube volume $V_{Dex} = 1L$	77
Figure 4.7 Expired CO ₂ trace at mouth (red) and at end of tube (blue). Two components of ΔP_{CO2} are illustrated.....	78
Figure 4.8 Change of ΔP_{CO2} as a function of external dead space volume. (A) 200ml; (B) 600ml; (C) 1000ml.....	79
Figure 4.9 Dependence of ΔP_{CO2} on breathing pattern (1) rapid shallow (dashed lines); (2) normal (solid line) and (3) slow deep (dash-dot lines) with constant total ventilation. (Red lines represent expired CO ₂ trace at mouth and blue lines represent expired CO ₂ trace at end of tube.)	79
Figure 4.10 (A) ΔP_{CO2} as a function of total ventilation and breathing frequency; (B) ΔP_{CO2} as a function of VE at three levels of V_{CO2} (V_T and breathing frequency are obtained from minimization of Eq.4.12). ($V_{Dex} = 1L$).	80
Figure 4.11 Simulated exercise respiratory response of CHF patient compared with normal subject. CHF patients demonstrated augmented ventilation, with a rapid shallow pattern. The dashed lines are clinical data adopted from (Wasserman, K., Y.-Y. Zhang, et al., Circulation, 1997.). Prediction of breathing pattern is characterized by adj-R ² values.	82
Figure 4.12 (A) Simulated exercise respiratory response of two levels of right-to-left shunt compared with normal. Increased shunt fraction is associated with augmented ventilation. (B) Change of ΔP_{CO2} as a function of shunt fraction and metabolic CO ₂	84
Figure 4.13 Simulated exercise respiratory response of external dead space loading compared with normal and inhaled CO ₂ . External dead space resulted in a stronger augmented exercise ventilatory response than inhaled CO ₂ . Both cases results in hypercapnia with normal breathing pattern.	86
Figure 4.14 Compartment model indicating pulmonary gas exchange defect problem under present study.	87
Figure 4.15 Schematic diagram of external dead space simulation.....	94
Figure 5.1 A. Local field potential recording in one channel of multielectrode array. B. PCA decomposition of signals in (A) indicating that the neuron cluster is readily distinguishable from the noise cluster.....	105

Figure 5.2 Response of phrenic discharge amplitude and timing components to hypoxia under varying CO₂ backgrounds in one rat. 110

Figure 5.3 Recording loci. (A) Electrolytic lesion was made at the end of the experiment to mark the recording site. (B) Loci of 4 types of respiratory-related neurons in KFN and LPBN exhibiting hypoadditive CO₂- O₂ interaction..... 111

Figure 5.4 A sample pure-I neuron (A) Firing pattern of neuron presented as perievent raster referenced to respiratory cycle; (B) Hypoxic response (separated into inspiratory and expiratory components) under different CO₂ background showing hypoadditive interaction; (C) Time-stamped spike trains representaiton of hypoxic response under different CO₂ background. 115

Figure 5.5 A sample E-I neuron (A) Firing pattern of neuron presented as perievent raster referenced to respiratory cycle; (B) Hypoxic response (separated into inspiratory and expiratory components) under different CO₂ background showing hypoadditive interaction; (C) Time-stamped spike trains representaiton of hypoxic response under different CO₂ background. 116

Figure 5.6 A sample eE neuron (A) Firing pattern of neuron presented as perievent raster referenced to respiratory cycle; (B) Hypoxic response (separated into inspiratory and expiratory components) under different CO₂ background showing hypoadditive interaction; (C) Time-stamped spike trains representaiton of hypoxic response under different CO₂ background. 117

Figure 5.7 A sample wE/lateE neuron (A) Firing pattern of neuron presented as perievent raster referenced to respiratory cycle; (B) Hypoxic response (separated into inspiratory and expiratory components) under different CO₂ background showing hypoadditive interaction; (C) Time-stamped spike trains representaiton of hypoxic response under different CO₂ background. 118

Figure 5.8 Mutliexponential curve fitting to breath-by-breath phrenic data, using the same time constants over three different CO₂ background. Results suggested that hypercapnic input altered only the gains of the learning dynamics but had little influence on its time course. 120

Figure 5.9 Mutliexponential curve fitting to breath-to-breath neuronal firing (top: E-I inspiratory firing; bottom: wE/late-E expiratory firing) data, using the same time constants over three different CO₂ background. Results suggested that hypercapnic input altered only the gains of the learning dynamics but had little influence on its time course. 122

Figure 5.10 Left panels: Averaged gains of multiexponential curve fitting (normalized to normocapnic condition) for phrenic and neuronal activity over three different CO₂ background during hypoxia stimulation. Right panels: Correlation between gains of phrenic T_I/T_E and I/E-neurons mutliexponential curve fitting. (A) Phrenic T_I vs. I-neurons (n=12); (B) Phrenic T_E vs. E-neurons (n=7). * indicates statistically significant difference from normal CO₂ condition (p<0.05)..... 124

Figure 5.11 Left panels: Averaged gains of multiexponential curve fitting (normalized to normocapnic condition) for phrenic and neuronal activity over three different CO₂ background during post-hypoxia recovery. Right panels: Correlation between gains of phrenic T_I/T_E and I/E-neurons mutliexponential curve fitting. (A) Phrenic T_I vs. I-neurons (n=12); (B) Phrenic T_E vs. E-neurons (n=7). * indicates statistically significant difference from normal CO₂ condition (p<0.05)..... 125

Chapter 1 Introduction

The essence of living organism survival is the maintenance of a stable constant internal environment of the body. From glucose to temperature, water to oxygen, the body continually strives to regulate all its physiological states in the face of various disturbances. Claude Bernard, the founder of modern physiology, coined the concept of *milieu intérieur*, and he suggested that:

The constancy of the internal environment is the condition that life should be free and independent... So far from the higher animal being indifferent to the external world, it is on the contrary in a precise and informed relation with it, in such a way that its equilibrium results from a continuous and delicate compensation, established as by the most sensitive of balances. (Bernard, 1878, 1974)

It would take nearly fifty years before this concept of biological stability received renewed attention. To describe this concept, physiologist Walter B. Cannon coined the term *homeostasis* in 1926 in his seminal work, The Wisdom of the Body (Cannon, 1932), which presented the first notions of a biological automatic controller. However, the body's high-dimensional organization and sophisticated dynamical interactions largely preclude thorough understanding of such a robust regulation mechanism (Somjen, 1992; Dworkin, 1993; Poon & Siniaia, 2000).

The respiratory system is probably one of the most extensively studied physiological systems. Current understanding of respiratory control is built upon a variety of classic respiratory reflex responses such as CO₂ or hypoxic chemoreflex, lung inflation and deflation reflexes and exercise hyperpnea reflex, etc. Such Sherringtonian stimulus-response analyses are useful in predicting the independent effects of specific chemical and mechanical inputs, from a traditional reductionist view. All of these reflex responses have been extensively studied and, for the most part, independently of one another for the sake of simplicity. However, the predictive power of these reflex models is limited when multiple factors come into play together. A major limitation of the classical chemoreflex model is that it cannot explain the isocapnia hyperpnea response during exercise. This discrepancy has led to the general postulation of a distinct “exercise stimulus” that feeds forward to the chemoreflex feedback loop as an “exercise reflex” (Grodins, 1950). However, despite extensive explorations for over a century, the putative “exercise stimulus” has remained elusive to this date (Forster, 2000).

In contrast to the assumption of afferents independence of the classical Sherringtonian reflex model, considerable evidence indicates that distinct classes of respiratory afferent inputs might interact with one another when applied concomitantly. For example, it has long been recognized that lung stretch receptors activation may interact with chemical drive in control of inspiratory and/or expiratory muscle activity (Kelsen *et al.*, 1977; Mitchell *et al.*, 1982; Mitchell *et al.*, 1990; Ainsworth *et al.*, 1992). Such afferent interactions have potential significance in certain clinical applications such as positive end-expiratory pressure (PEEP) or continuous positive airway pressure (CPAP), or certain disease states such as chronic obstructive pulmonary disease or lung transplant, where the resultant exaggeration (due to lung inflation) or total absence (deafferentation) of vagal afferent inputs may alter the chemoreflex regulation of breathing. Such interactions also have important physiological implications in that they indicate a much more complex central processing of these respiratory afferent inputs than the conventional reflex models imply.

Presently, there is limited information about how afferent information arising from chemoreceptors and mechanoreceptors are processed and integrated centrally and

how they may interact with one another. Bajić et al. (1994) reported that peripheral chemoreceptor and pulmonary stretch receptor inputs interact linearly in modulating certain medullary neurons in the dorsal respiratory group and caudal ventral respiratory group in dogs, and a nonadditive interaction in other caudal VRG neurons. Tonkovic-Capin et al. (2000) showed that the interaction between arterial CO₂ tension and pulmonary stretch receptor-mediated modulations of caudal medullary, expiratory bulbospinal neuron activity is mainly additive, but synergism between P_{aCO₂} and excitatory inputs is also present. However, little is known about how these afferent inputs affect the activities of other pontomedullary neurons when presented together and how such interactions may influence respiratory activity.

The mammalian lower brain has traditionally received little attention in regard to its intelligence. However, as evidenced by the precision, robustness, versatility and reliability in physiological control, the traditional reductionist view is inadequate in explaining the common complex scenario of physiological control especially when multiple factors come into play. In fact, the respiratory system demonstrates sustained capability of adaption and memory as in the higher brain (reviewed in (Eldridge & Millhorn, 1986a); (Poon & Siniaia, 2000)). Examples of such processes are numerous and include responses to the following inputs: carotid sinus nerve and carotid chemoreceptors (Eldridge, 1974; Eldridge & Gill-Kumar, 1978; Millhorn *et al.*, 1980; Zhang & Mifflin, 1995; Mifflin, 1997), hypoglossal nerve (Jiang *et al.*, 1991), hypoxia (Fregosi, 1991b; Georgopoulus *et al.*, 1992; Bisgard & Neubauer, 1995; Bach & Mitchell, 1996), and vagal nerve fibers from pulmonary stretch receptors (Stanley *et al.*, 1975; Karczewski *et al.*, 1976).

In this thesis, we explore the interactions of respiratory afferents and their implications for intelligent respiratory control from both experimental and modeling aspects. We show that nonlinear interactions between respiratory afferents provide a consistent picture over a wide range of experimental and physiological scenarios, that contradicts the assumptions of additivity, reducibility and superposition characteristics in the classical reflex model. Such interactions have been emphasized in the rapidly growing fields of systems biology and systems medicine, which are important in

advancing our understanding of how our body works as an integrated system (Ahn *et al.*, 2006b, a).

1.1 THESIS OUTLINE

Chapter 2 provides a review of the organization of the respiratory system, anatomically and functionally. We provide evidence that respiratory control is not merely a simple reflex but possess more sophisticated computation.

Chapter 3 contrasts integrative and reductionist approaches in biological system modeling, with particular emphasis on the respiratory system. This chapter sets the stage for the integrative approach taken in this thesis.

Chapter 4 investigates the interaction of mechanical and chemical feedback signals from a computational approach. We hypothesize that an optimal respiratory control model provides consistent prediction for the exercise respiratory control under various pulmonary gas exchange defective conditions by integrating both chemical and mechanical respiratory signals. The optimization framework is shown to provide a convenient mathematical tool to predict a wide range of respiratory responses with a conceptually simple but generalized theory.

Chapter 5 investigates the interaction of peripheral and central chemoreceptors using an experimental approach. We test the influence of the CO₂ background on the subsequent hypoxic response in both phrenic motor output and dorsolateral pons respiratory neurons activity. Furthermore, we demonstrate the important role of dorsolateral pons in the CO₂-O₂ interaction. We also show that gain modulation of hypoxic response by central input represents a form of associative learning in respiratory control. Several clinical implications regarding this interaction are suggested.

Chapter 6 summarizes the findings and suggests directions for future investigation.

1.2 REFERENCES

- Ainsworth DM, Smith CA, Johnson BD, Eicker SW, Henderson KS & Dempsey JA. (1992). Vagal modulation of respiratory muscle activity in awake dogs during exercise and hypercapnia. *J Appl Physiol* **72**, 1362-1367.
- Bach KB & Mitchell GS. (1996). Hypoxia-induced long-term facilitation of respiratory activity is serotonin dependent. *Respir Physiol* **104**, 253-260.
- Bajic J, Zuperku EJ, Tonkovic-Capin M & Hopp FA. (1994). Interaction between chemoreceptor and stretch receptor inputs at medullary respiratory neurons. *The American journal of physiology* **266**, R1951-1961.
- Bernard C. (1878, 1974). *Lectures on the phenomena of life common to animals and plants. (Lecons sur les phénomènes de la vie communs aux animaux et aux végétaux.)*. Thomas, Springfield, Ill.
- Bisgard GE & Neubauer A. (1995). Peripheral and central effects of hypoxia. In *Regulation of Breathing*, ed. Dempsey JA & Pack AI, pp. 617-668. Marcel Dekker, Inc., N.Y. Basel, Hong Kong.
- Cannon WB. (1932). *The wisdom of the body*. W.W. Norton & Company, New York,.
- Dworkin BR. (1993). *Learning and Physiological Regulation*. University of Chicago Press, Chicago.
- Eldridge FL. (1974). Central neural respiratory stimulatory effect of active respiration. *J Appl Physiol* **37**, 723-735.
- Eldridge FL & Gill-Kumar P. (1978). Lack of effect of vagal afferent input on central neural respiratory afterdischarge. *J Appl Physiol* **45**, 339-344.
- Eldridge FL & Millhorn DE. (1986). Oscillation, gating, and memory in the respiratory control system. In *Handbook of Physiology: The Respiratory System*, ed. Fishman AP, Cherniack NS & Widdicombe JG, pp. 93-114. Amer. Phys. Soc., Bethesda.
- Forster HV. (2000). Exercise hyperpnea: where do we go from here? *Exerc Sport Sci Rev* **28**, 133-137.
- Fregosi RF. (1991). Short-term potentiation of breathing in humans. *J Appl Physiol* **71**, 892-899.
- Georgopoulos D, Giannouli E, Tsara V, Argiropoulou P, Patakas D & Anthonisen N. (1992). Respiratory short-term poststimulus potentiation (after-discharge) in patients with obstructive sleep apnea. *Am Rev Respir Dis* **146**, 1250-1255.

- Grodins FS. (1950). Analysis of factors concerned in regulation of breathing in exercise. *Physiol Rev* **30**, 220-239.
- Jiang C, Mitchell GS & Lipski J. (1991). Prolonged augmentation of respiratory discharge in hypoglossal motoneurons following superior laryngeal nerve stimulation. *Brain Res* **538**, 215-225.
- Karczewski WA, Budzinska K, Gromysz H, Herczynski R & Romaniuk JR. (1976). Some response of the respiratory complex to stimulation of its vagal and mesencephalic inputs. In *Respiratory Centers and Afferent System*, ed. Duran E, pp. 107-115. INSERM.
- Kelsen SG, Altose MD & Cherniack NS. (1977). Interaction of lung volume and chemical drive on respiratory muscle EMG and respiratory timing. *J Appl Physiol* **42**, 287-295.
- Mifflin S. (1997). Short-term potentiation of carotid sinus nerve inputs to neurons in the nucleus of the solitary tract. *Respir Physiol* **110**.
- Millhorn DE, Eldridge FL & Mitchell GS. (1980). Prolonged stimulation of respiration by a new central neuronal mechanism. *Respir Physiol* **41**, 87-103.
- Mitchell GS, Cross BA, Hiramoto T & Scheid P. (1982). Interactions between lung stretch and PaCO₂ in modulating ventilatory activity in dogs. *J Appl Physiol* **53**, 185-191.
- Mitchell GS, Douse MA & Foley KT. (1990). Receptor interactions in modulating ventilatory activity. *The American journal of physiology* **259**, R911-920.
- Poon CS & Siniaia MS. (2000). Plasticity of cardiorespiratory neural processing: classification and computational functions. *Respir Physiol* **122**, 83-109.
- Somjen GG. (1992). The missing error signal - regulation beyond negative feedback. *News Physiol Sci* **7**, 184-185.
- Stanley NN, Altose MD, Cherniack NS & Fishman AP. (1975). Changes in strength of lung inflation reflex during prolonged inflation. *J Appl Physiol* **38**, 474-480.
- Tonkovic-Capin M, Zuperku EJ, Stuth EA, Bajic J, Dogas Z & Hopp FA. (2000). Effect of central CO₂ drive on lung inflation responses of expiratory bulbospinal neurons in dogs. *American journal of physiology* **279**, R1606-1618.
- Zhang W & Mifflin SW. (1995). Expiratory amino-acid receptors contribute to carotid sinus and vagus nerve evoked excitation of neurons in the nucleus of the tractus solitarius. *J Auton Nerv Syst* **55**, 50-56.

Chapter 2 Background

The respiratory control system is a multi-input multi-output nonlinear system (Poon, 2000). The system comprises a mechanical plant (respiratory mechanics and muscles) and a chemical plant (pulmonary gas exchange) that are controlled by respiratory neurons in the medulla and pons regions of the brainstem. Extensive studies over the past century have accumulated an enormous collection of knowledge about the respiratory system. Translating these scientific findings into clinical practice becomes critical, as in many other biological research fields (Saijo, 2002; Mankoff *et al.*, 2004; Horig *et al.*, 2005).

2.1 RESPIRATORY FEEDBACK

The two major inputs to the respiratory control system for normal autonomic respiratory regulation are the mechanical and chemical feedbacks. These two sensory modalities play the most significant role in modulating the respiratory rhythm in terms of tidal volume and phase durations (i.e. inspiratory and expiratory durations). These feedback pathways are also critical for proper responses during various acute or chronic stressful conditions that occur during exercise or chronic lung disease, for example.

2.1.1 Mechanical Feedback

The motor act of breathing rhythmically inflates/deflates the lungs by altering the pleural pressure. The change in lung volume is sensed by slowly adapting pulmonary stretch receptors (SARs) in the airways. These receptors transmit information to the dorsal respiratory neurons and pontine nuclei via myelinated afferent fibers of the vagus nerve (Ezure *et al.*, 1998). The SARs are phasically stimulated by lung expansion and exhibit small tonic activities throughout the respiratory cycle. The classic Hering-Breuer inflation reflex (HBIR) describes the inhibitory effect of lung inflation and subsequent SAR activation on inspiration (Breuer, 1868b; Breuer, 1868a). This 'reflex' is presumed to protect the lungs from overexpansion. Recent studies have revealed that the fictive HBIR in rats undergoes dynamical changes in the form of non-associative learning (habituation and desensitization) that provides necessary temporal and frequency filtering. The dynamics are modulated by NMDA (N-methyl-D-aspartate) receptors (Poon *et al.*, 2000a; Siniiaia *et al.*, 2000a; Poon & Siniiaia, 2000b; Poon & Young, 2006b; MacDonald *et al.*, 2009).

Other mechanical sensory receptors include the irritant and J-type receptors (Taylor *et al.*, 1989). The irritant receptors, or rapidly adapting receptors (RARs), are located in the lung epithelium, and respond to noxious chemical or mechanical agents. RARs activity is also transmitted via myelinated fibers of the vagus nerve, and is less sensitive to lung inflation compared to SARs. Stimulation of RARs causes bronchoconstriction, coughing, sneezing and general increases in ventilation.

The third receptor type called J-receptors are unmyelinated C-fiber vagal nerve endings that respond to vascular distension and fluid increases in the interstitium. Activation of these J-receptors can cause hyperpnea and dyspnea. Due to the high activation threshold of these unmyelinated C-fibers, small current stimulation of the vagus nerve is unlikely to activate them.

2.1.2 Chemical Feedback

The primary function of the respiratory system is to regulate blood gas concentration. There are two classes of chemoreceptors that continuously monitor the blood chemistry states, peripherally and centrally.

Two peripheral chemoreceptors exist: carotid and aortic bodies. The carotid bodies are located high in the neck at the bifurcation of the common carotid arteries. These receptors sense changes in arterial P_{O_2} , P_{CO_2} , and pH. Carotid body activity is transmitted to the brainstem via a small branch of the glossopharyngeal nerve called the carotid sinus nerve (CSN) (Black & Torrance, 1967) and also referred to as Hering's nerve. Carotid body is stimulated mainly by a decrease in P_{O_2} and increases in H^+/P_{CO_2} . In human, the aortic bodies play a smaller role in peripheral detection and do not respond to changes in P_{O_2} .

Unlike the peripheral chemoreceptors, the loci of central chemoreceptor are still being debated. A number of brainstem regions have been shown to be CO_2/H^+ sensitive, including ventrolateral medullary surface, nucleus of solitary tract, locus coeruleus, medullary raphe, retrotrapezoid nucleus (RTN), rostroventrolateral medullar, pre-Bötzinger's Complex (pre-BötC), cerebellar fastigial nucleus (reviewed in Dean & Nattie, 2010). In recent years, RTN at the ventrolateral medullar surface is suggested to be the principal site of intracranial CO_2/H^+ chemoreception (Guyenet *et al.*, 2008). Their tonic activity likely supplies a general background excitation to the respiratory central pattern generator (RCPG) (Duffin, 1991).

2.2 BRAINSTEM RESPIRATORY CONTROL CENTER

Respiratory neurons are densely populated in three main brainstem areas: the dorsal respiratory group (DRG), the ventral respiratory group (VRG) and the pontine respiratory group (PRG).

2.2.1 Dorsal respiratory group (DRG)

The DRG is comprised of mainly inspiratory neurons located in the ventrolateral subnucleus of the nucleus of the solitary tract (NTS) (Cohen & Feldman, 1984). Extensive monosynaptic excitatory projections to the phrenic nucleus in the spinal cord are identified from the neurons in the DRG (Fedorko *et al.*, 1983; de Castro *et al.*, 1994).

Furthermore, the NTS is the principal site of terminations of respiratory-related sensory afferents, including SARs, RARs, and peripheral chemoreceptors. Inhibitory projection to the Böttinger's Complex (BötC) and retrotrapezoid nucleus (RTN) have been identified. Commissural subdivision of NTS relays neurons for peripheral chemoreceptors and it provides important excitation to VRG (Takakura *et al.*, 2006; Takakura *et al.*, 2007).

2.2.2 Ventral respiratory group (VRG)

The VRG is a column of respiratory neurons in the ventrolateral medulla. It is commonly divided into the following subdivisions: para-facial respiratory group (pFRG), Böttinger's Complex (BötC), pre-Böttinger's Complex (pre-BötC), rostral VRG (primarily inspiratory neurons) and caudal VRG (primarily expiratory neurons). The inspiratory (I-Aug) neurons in rostral VRG project monosynaptically to motoneurons in the phrenic nucleus that innervate the diaphragm while expiratory (E-Aug) neurons in caudal VRG innervate the abdominal and expiratory intercostal motoneurons. The BötC consists of a large population of expiratory neurons that provides extensive inhibitory projections within VRG, to NTS and to the phrenic nucleus.

Pacemaker-like neurons have been identified in pre-BötC (Smith *et al.*, 1991) and pFRG (Onimaru *et al.*, 1987, 1988; Onimaru & Homma, 2003) which are thought to generate inspiratory and expiratory rhythms respectively. How the two rhythm generators coordinate with each other to set the respiratory rhythm remains unclear. Our recent

modeling work suggests that they interact in a two-way "handshake" process via a sequence of excitation-reverse inhibition-postinhibitory rebound excitation (Wittmeier *et al.*, 2008).

2.2.3 Pontine respiratory region

Respiratory neurons are mostly found in the dorsolateral (dl-pons) and the ventrolateral (vl-pons) pontine areas.

2.2.3.1 Dorsolateral pons

Two major structures constituting the dl-pons are the Kölliker-Fuse nucleus (KFN) and the parabrachial nucleus (lateral and medial), commonly termed the "pneumotaxic center" (Lumsden, 1923a). The dl-pons has extensive reciprocal projections with VRG, NTS and the phrenic motor nucleus. Using single-unit extracellular recording in combination with juxtacellular labeling, the functional taxonomy and topographic distribution of pneumotaxic respiratory neurons in the rat dl-pons have been systematically characterized (Song *et al.*, 2006). Six subtypes of respiratory neurons, phasic or phase-spanning have been identified.

The pneumotaxic center is traditionally thought to play an ancillary role in inspiratory-expiratory phase transition by providing a fail-safe mechanism for inspiratory off-switch (IOS) secondary to vagal proprioceptive feedback. Recently, the role of dl-pons in mediating chemoreflex responses has been increasingly recognized (Fournier & Kinkead, 2008; Nuding *et al.*, 2009; Song & Poon, 2009a, 2009b; Bonis *et al.*, 2010; Boon & Milsom, 2010).

2.2.3.2 Ventrolateral pons/A5 area

A5 is not a well-defined anatomical structure, it includes a noradrenergic cell group scattered in the vl-pons. The vl-pons has been shown to specifically control

expiration (Jodkowski *et al.*, 1997). Furthermore, the vl-pons has an important role in shaping the post-hypoxic depression of respiration (Dick & Coles, 2000).

2.3 TRADITIONAL VIEW OF RESPIRATORY CONTROL AND LIMITATIONS

Traditionally, control of breathing has been understood in terms of a set of stimulus-response relationships presumably reflecting various afferent feedback/feedforward control mechanism. Such Sherringtonian stimulus-response analyses are useful in predicting the independent effects of specific chemical and mechanical inputs under well-controlled experimental conditions. However, less attention has been put on the interaction of these inputs, that the response when different stimuli are presented simultaneously.

A long unresolved problem in respiratory control is the isocapnic exercise hyperpnea, defined as an automatic increase in respiratory ventilation geared to metabolic demands with near constancy of arterial CO₂ and pH levels. The chemoreflex/mechanoreflex feedback model implies the existence of a feedforward signal from an exercise-related input. However, despite extensive search over the past century, none of the hypothesized feedforward mechanisms have been demonstrated conclusively as the true “exercise stimulus” obligatory to exercise hyperpnea (Mateika & Duffin, 1995; Ward, 2000; Eldridge *et al.*, 2006; Secher *et al.*, 2006; Waldrop *et al.*, 2006; Yu & Poon, 2006).

Furthermore, the available evidence reveals a distinct multiplicative (synergistic) component in the ventilatory response to concomitant exercise and hypercapnia such that CO₂ responsiveness is potentiated during exercise (Poon & Greene, 1985; Poon, 1989; Mitchell & Babb, 2006). Ventilatory response to chemical or exercise input is also potentiated by increases in physiological dead space and shunt (e.g. in congestive heart failure patients). Such sensorimotor integration characteristics are ignored in the

oversimplified reflex model which mistakenly considers all respiratory inputs as additive to the “exercise stimulus”

Clearly, the deceptively mundane motor function of breathing is not a trivial task of “as-easy-as-breathing”. Breathing is regulated by the brain continually throughout life without fail in the face of constant physiologic and environmental challenges, which can easily surpass the most robust man-made controller. Accumulating evidences show that the respiratory control system undergoes more intelligent computation involving various memory, adaptation and gating mechanisms (Eldridge & Millhorn, 1986a; Poon & Siniaia, 2000).

2.4 EVIDENCE OF INTELLIGENT RESPIRATORY CONTROL

Two forms of intelligent behavior evidenced in respiratory control are nonassociative and associative learning.

Habituation and sensitization are two common forms of nonassociative learning that are exhibited in many neuronal structures of mammalian and invertebrate nervous systems (Thompson & Spencer, 1966; Groves & Thompson, 1970; Poon, 1996a; Cohen *et al.*, 1997). According to the classic Dual-Process Theory (Groves & Thompson, 1970), habituation is a progressive reduction in physiological response that occurs upon repetitive application of the same stimulus. On the other hand, sensitization is the progressive amplification of a response following a repetitive stimulus. In simple invertebrate nervous systems, habituation and sensitization have been shown to result from activity-dependent phasic depression and enhancement of synaptic efficacy respectively (Kandel, 1978; Cohen *et al.*, 1997).

Associative learning is the learning process that is dependent on the pairing of two inputs. Two forms of associative learning have been extensively studied: operant conditioning and classical (Pavlovian) conditioning.

In operant conditioning, an individual modifies an action-outcome association by reinforcement/punishment. On the other hand, classical (or Pavlovian) conditioning involves repeatedly pairing an unconditioned stimulus (which unfailingly evokes a reflexive response) with another previously neutral stimulus (which does not normally evoke the response). Upon learning, response occurs both to the unconditioned stimulus and to the other, originally neutral stimulus (now referred to as the "conditioned stimulus"). The response to the conditioned stimulus is termed a *conditioned response*.

2.4.1 Nonassociative learning in the chemical and mechanical feedback pathways

Recent studies have demonstrated various forms of nonassociative learning that process mechanical and peripheral chemical feedback afferent signals in respiratory control (Siniatia *et al.*, 2000a; Young *et al.*, 2003b; Poon & Young, 2006a). For instance, the inspiratory duration is modulated by peripheral chemical feedback through short-term potentiation (STP) of the inspiratory motor activity which can be modeled as leaky integrators that are only intact during inspiratory phrase but not expiratory phrase (or they are logically gated to inspiratory circuitry). On the other hand, the expiratory circuit is modulated by a hypoxia-induced short-term depression (STD), with post-stimulus rebound, of respiratory frequency mediated by neurons in the ventrolateral pons.

Such STD behavior is also revealed in the classic Hering-Breuer inflation reflex through vagal modulation of the expiratory circuitry. Blockade of N-methyl-D-aspartate receptors (NMDA-R) has been shown to slow the response of these learning processes (Poon *et al.*, 1999b; Siniatia *et al.*, 2000b).

STP can function to nullify the steady-state errors in homeostatic regulation and STD may help to filter out any large and undesired tonic bias and hence, recalibrate the controller's sensitivity to new operating states. NMDA-R may serve to adaptively adjust the optimal response speed of such nonassociative learning mechanisms.

2.4.2 Clinical implications from models of nonassociative learning

These nonassociative learning mechanisms have important implications for respiratory control in various respiratory disorders (Young, 2002). During hypoxia, the initial increase in respiratory frequency may be compensated by the adaptation in the primary and secondary chemical feedback pathways that act to restore the expiration time. In the absence of such adaptation, it can be predicated that prolonged hypoxia may provoke unremitting tachypnea along with impaired pulmonary gas exchange due to premature emptying of the lungs, resulting in an adverse departure from homeostasis with increased breathing effort.

In certain chronic obstructive pulmonary diseases such as emphysema, bronchitis and asthma characterized by over-inflation of the lungs, pontine desensitization could protect against possible apnea resulting from the Hering-Breuer reflex due to augmented vagal feedback. Alternatively, the pontine respiratory center may be viewed as a “fail-safe” mechanism for averting apneusis in the event of vagal feedback breakdown, which accompanies certain chronic or acute restrictive lung diseases.

Our recent report showed that overexpression of either sensitization or desensitization of the Hering-Breuer inflation reflex occurs in two contrasting mutant mouse models of Rett syndrome. Rett syndrome is an autism-spectrum disorder caused by mutations in the X-linked gene encoding methyl-CpG-binding protein 2 (MECP2) (Amir *et al.*, 1999). *Mecp2* mutant mice exhibit either spontaneous repetitive apnea (Viemari *et al.*, 2005; Poon & Song, 2007; Stettner *et al.*, 2007; Abdala *et al.*, 2010) or tachypnea (Song *et al.*, 2011) depending on whether the Hering-Breuer reflex is sensitized or desensitized. Another important translational application is our recent demonstration that abolition of desensitization by pontine lesion in vagi-intact rats may disrupt the entrainment of the respiratory rhythm to mechanical ventilation (MacDonald *et al.*, 2007).

2.4.3 Associative interaction of vagal and carotid chemoafferent inputs

Associative learning in respiratory control similar to classical studies in *Aplysia* (Glanzman, 1995) and cerebellum (Thompson, 1988) has not been widely investigated. However, preliminary data in our previous studies indicate that these vagal mechanical and carotid chemoafferent inputs may also interact associatively, evidencing strong chemical-mechanical interaction. Importantly, the adaptation to carotid sinus nerve (CSN) input was greatly attenuated by vagal input but *not* vice versa, suggesting that the vagal pathway may inhibit the CSN pathway but not the other way around.

A possible neural correlate for such associative interaction is suggested by our preliminary data. These data show that late-E neurons (expiratory neurons firing in the late expiratory phase with an augmenting pattern (Song *et al.*, 2006)) in dl-pons receive convergent inhibitory vagal input and excitatory CSN input, such that any CSN adaptation effect on T_E mediated by these neurons would be necessarily suppressed by vagal feedback.

Previous modeling study demonstrated that a Hebbian feedback covariance learning rule is a plausible mechanism to achieve optimal respiratory control by correlating mechanical and chemical feedback in order to adapt the controller gain (Poon, 1996c).

2.5 SUMMARY

Section 2.4 shows evidence that the respiratory control system undergoes various form of learning processes. It is apparent that the traditional simple reflex model does not provide the full picture of the system behavior. Instead, a wide variety of complex respiratory behaviors may arise as a learned behavior from sophisticated computation in the brainstem. In this thesis, we demonstrate how afferent interactions may contribute to various learned respiratory behaviors.

2.6 REFERENCES

- Abdala AP, Dutschmann M, Bissonnette JM & Paton JF. (2010). Correction of respiratory disorders in a mouse model of Rett syndrome. *Proc Natl Acad Sci U S A* **107**, 18208-18213.
- Amir RE, Van den Veyver IB, Wan M, Tran CQ, Francke U & Zoghbi HY. (1999). Rett syndrome is caused by mutations in X-linked MECP2, encoding methyl-CpG-binding protein 2. *Nat Genet* **23**, 185-188.
- Black AMS & Torrance RW. (1967). Chemoreceptor effects in the respiratory cycle. *J Physiol* **189**, 59-61P.
- Bonis JM, Neumueller SE, Krause KL, Kiner T, Smith A, Marshall BD, Qian B, Pan LG & Forster HV. (2010). The pontine respiratory group, particularly the Kolliker-Fuse nucleus, mediates phases of the hypoxic ventilatory response in unanesthetized goats. *J Appl Physiol* **108**, 1321-1335.
- Boon JA & Milsom WK. (2010). The role of the pontine respiratory complex in the response to intermittent hypoxia. *Respir Physiol Neurobiol* **171**, 90-100.
- Breuer J. (1868a). Self-steering of respiration through the nerves vagus. In *Breathing: Hering-Breuer Centenary Symposium*, ed. Porter R, pp. 365-394. Churchill, London.
- Breuer J. (1868b). Self-steering of respiration through the nerves vagus.
- Cohen MI & Feldman JL. (1984). Discharge properties of dorsal medullary inspiratory neurons: relation to pulmonary afferent and phrenic efferent discharge. *J Neurophysiol* **51**, 753-776.
- Cohen TE, Kaplan SW, Kandel ER & Hawkins RD. (1997). A simplified preparation for relating cellular events to behavior: mechanisms contributing to habituation, dishabituation, and sensitization of the *Aplysia* gill-withdrawal reflex. *Journal of Neuroscience* **17**, 2886-2899.
- de Castro D, Lipski J & Kanjhan R. (1994). Electrophysiological study of dorsal respiratory neurons in the medulla oblongata of the rat. *Brain Research* **639**, 49-56.
- Dean JB & Nattie EE. (2010). Central CO₂ chemoreception in cardiorespiratory control. *Journal of Applied Physiology* **108**, 976.
- Dick TE & Coles SK. (2000). Ventrolateral pons mediates short-term depression of respiratory frequency after brief hypoxia. *Respir Physiol* **121**, 87-100.

- Duffin J. (1991). A model of respiratory rhythm generation. *NeuroReport* **4**, 1215-1218.
- Eldridge FL & Millhorn DE. (1986). Oscillation, gating, and memory in the respiratory control system. In *Handbook of Physiology: The Respiratory System*, ed. Fishman AP, Cherniack NS & Widdicombe JG, pp. 93-114. Amer. Phys. Soc., Bethesda.
- Eldridge FL, Morin D, Romaniuk JR, Yamashiro S, Potts JT, Ichiyama RM, Bell H, Phillipson EA, Killian KJ, Jones NL & Nattie E. (2006). Supraspinal locomotor centers do/do not contribute significantly to the hyperpnea of dynamic exercise in humans. *J Appl Physiol* **100**, 1743-1747.
- Ezure K, Tanaka I & Miyazaki M. (1998). Pontine projections of pulmonary slowly adapting receptor relay neurons in the cat. *NeuroReport* **9**, 411-414.
- Fedorko L, Merrill EG & Lipski J. (1983). Two descending medullary inspiratory pathways to phrenic motoneurons. *Neuroscience Letters* **43**, 285-291.
- Fournier S & Kinkead R. (2008). Role of pontine neurons in central O₂ chemoreflex during development in bullfrogs (*Lithobates catesbeiana*). *Neuroscience* **155**, 983-996.
- Glanzman DL. (1995). The cellular basis of classical conditioning in *Aplysia californica*—it's less simple than you think. *Trends Neurosci* **18**, 30-36.
- Groves PM & Thompson RF. (1970). Habituation: a dual-process theory. *Physiological Reviews* **77**, 419-450.
- Guyenet PG, Stornetta RL & Bayliss DA. (2008). Retrotrapezoid nucleus and central chemoreception. *The Journal of Physiology* **586**, 2043-2048.
- Horig H, Marincola E & Marincola FM. (2005). Obstacles and opportunities in translational research. *Nature medicine* **11**, 705-708.
- Jodkowski JS, Coles SK & Dick TE. (1997). Prolongation in expiration evoked from ventrolateral pons of adult rats. *J Appl Physiol* **82**, 377-381.
- Kandel ER. (1978). *A Cell-Biological Approach to Learning*. Society for Neuroscience, Bethesda, MD.
- Lumsden T. (1923). Observations on the respiratory centres in cat. *J Physiol London* **57**, 153-160.
- MacDonald SM, Song G & Poon CS. (2007). Nonassociative learning promotes respiratory entrainment to mechanical ventilation. *PLoS ONE* **2**, e865.

- MacDonald SM, Tin C, Song G & Poon CS. (2009). Use-dependent learning and memory of the Hering-Breuer inflation reflex in rats. *Exp Physiol* **94**, 269-278.
- Mankoff SP, Brander C, Ferrone S & Marincola FM. (2004). Lost in Translation: Obstacles to Translational Medicine. *J Transl Med* **2**, 14.
- Mateika JH & Duffin J. (1995). A review of the control of breathing during exercise. *Eur J Appl Physiol Occup Physiol* **71**, 1-27.
- Mitchell GS & Babb TG. (2006). Layers of exercise hyperpnea: modulation and plasticity. *Respir Physiol Neurobiol* **151**, 251-266.
- Nuding S, Segers L, Shannon R, O'Connor R, Morris K & Lindsey B. (2009). Central and peripheral chemoreceptors evoke distinct responses in simultaneously recorded neurons of the raphé-pontomedullary respiratory network. *Philosophical Transactions of the Royal Society B: Biological Sciences* **364**, 2501.
- Onimaru H, Arata A & Homma I. (1987). LOCALIZATION OF RESPIRATORY RHYTHM-GENERATING NEURONS IN THE MEDULLA OF BRAIN-STEM SPINAL-CORD PREPARATIONS FROM NEWBORN RATS. *Neuroscience Letters* **78**, 151-155.
- Onimaru H, Arata A & Homma I. (1988). PRIMARY RESPIRATORY RHYTHM GENERATOR IN THE MEDULLA OF BRAIN-STEM SPINAL-CORD PREPARATION FROM NEWBORN RAT. *Brain Research* **445**, 314-324.
- Onimaru H & Homma I. (2003). A Novel Functional Neuron Group for Respiratory Rhythm Generation in the Ventral Medulla. *The Journal of Neuroscience* **23**, 1478-1486.
- Poon C-S. (1996a). Synaptic Plasticity and Respiratory Control. In *Bioengineering Approaches to Pulmonary Physiology and Medicine*, ed. Khoo MCK, pp. 93-113. Plenum, Los Angeles.
- Poon C-S & Greene JG. (1985). Control of exercise hyperpnea during hypercapnia in humans. *J Appl Physiol* **59**, 792-797.
- Poon C-S & Siniatia MS. (2000b). Plasticity of cardiorespiratory neural processing: classification and computational functions. *Respir Physiol* **122**, 83-109.
- Poon C-S, Siniatia MS & Young DL. (2000a). High-pass filtering of carotid-vagal influences on expiration in rat: role of NMDA receptors. *Neurosci Letters* **284**, 5-8.

- Poon C-S & Young D. (2006a). Nonassociative learning as gated neural integrator and differentiator in stimulus-response pathways. *Behavioral and Brain Functions* **2**, 29.
- Poon C-S & Young D. (2006b). Nonassociative learning as gated neural integrator and differentiator in stimulus-response pathways. *Behavioral and Brain Functions* **2**, 29.
- Poon CS. (1989). Effects of inspiratory resistive load on respiratory control in hypercapnia and exercise. *J Appl Physiol* **66**, 2391-2399.
- Poon CS. (1996b). Self-tuning Optimal Regulation of Respiratory Motor Output by Hebbian Covariance Learning. *Neural Netw* **9**, 1367-1383.
- Poon CS. (2000). Respiratory models and control. In *Biomedical Engineering Handbook*, 2nd edn, ed. Bronzion JD, pp. 161. CRC Press, Boca Raton, Fl.
- Poon CS & Siniatia MS. (2000). Plasticity of cardiorespiratory neural processing: classification and computational functions. *Respir Physiol* **122**, 83-109.
- Poon CS, Siniatia MS, Young DL & Eldridge FL. (1999). Short-term potentiation of carotid chemoreflex: an NMDAR-dependent neural integrator. *Neuroreport* **10**, 2261-2265.
- Poon CS & Song G. (2007). Habituation, desensitization and sensitization of the Hering-Breuer reflex in normal and Mecp2-/y knockout mice. *J Physiol* **584**, 359-360; author reply 361.
- Saijo N. (2002). Translational study in cancer research. *Internal medicine (Tokyo, Japan)* **41**, 770-773.
- Secher N, Poon C-S, Ward S, Whipp B & Duffin J. (2006). Supraspinal locomotor centers do/do not contribute significantly to the hyperpnea of dynamic exercise in humans. *J Appl Physiol* **100**, 1417-1418.
- Siniatia MS, Young DL & Poon C-S. (2000a). Habituation and desensitization of the Hering-Breuer reflex in rat. *J Physiol* **523.2**, 479-491.
- Siniatia MS, Young DL & Poon C-S. (2000b). NMDA receptor-dependent short-term depression of neurotransmission from vagal C-fibers in NTS. In *Soc Neurosci Annual Conf*.
- Smith J, Ellenberger H, Ballanyi K, Richter D & Feldman J. (1991). Pre-Botzinger complex: a brainstem region that may generate respiratory rhythm in mammals. *Science* **254**, 726-729.

- Song G & Poon C-S. (2009a). Lateral parabrachial nucleus mediates shortening of expiration during hypoxia. *Respiratory physiology & neurobiology* **165**, 1-8.
- Song G & Poon C-S. (2009b). Lateral parabrachial nucleus mediates shortening of expiration and increase of inspiratory drive during hypercapnia. *Respiratory physiology & neurobiology* **165**, 9-12.
- Song G, Tin C, Giacometti M & Poon C-S. (2011). Habituation without NMDA receptor-dependent desensitization of Hering-Breuer apnea reflex in a *Mecp2*^{+/-} mutant mouse model of Rett syndrome. *Frontiers in Integrative Neuroscience* (Accepted).
- Song G, Yu Y & Poon CS. (2006). Cytoarchitecture of pneumotaxic integration of respiratory and nonrespiratory information in the rat. *J Neurosci* **26**, 300-310.
- Stettner GM, Huppke P, Brendel C, Richter DW, Gartner J & Dutschmann M. (2007). Breathing dysfunctions associated with impaired control of postinspiratory activity in *Mecp2*^{-/-} knockout mice. *The Journal of physiology* **579**, 863-876.
- Takakura AC, Moreira TS, West GH, Gwilt JM, Colombari E, Stornetta RL & Guyenet PG. (2007). GABAergic Pump Cells of Solitary Tract Nucleus Innervate Retrotrapezoid Nucleus Chemoreceptors. *Journal of Neurophysiology* **98**, 374-381.
- Takakura ACT, Moreira TS, Colombari E, West GH, Stornetta RL & Guyenet PG. (2006). Peripheral chemoreceptor inputs to retrotrapezoid nucleus (RTN) CO₂-sensitive neurons in rats. *The Journal of Physiology* **572**, 503-523.
- Taylor AE, Rehder K, Hyatt RE & Parker JC. (1989). *Clinical Respiratory Physiology*. Saunders, Philadelphia.
- Thompson RF. (1988). The neural basis of basic associative learning of discrete behavioral responses. *Trends Neurosci* **11**, 152-155.
- Thompson RF & Spencer WA. (1966). Habituation: A model phenomenon for the study of neuronal substrates of behavior. *Psychological Review* **73**, 16-46.
- Viemari JC, Roux JC, Tryba AK, Saywell V, Burnet H, Pena F, Zanella S, Bevenegut M, Barthelemy-Requin M, Herzing LB, Moncla A, Mancini J, Ramirez JM, Villard L & Hilaire G. (2005). *Mecp2* deficiency disrupts norepinephrine and respiratory systems in mice. *J Neurosci* **25**, 11521-11530.
- Waldrop TG, Iwamoto GA & Haouzi P. (2006). Point:Counterpoint: Supraspinal locomotor centers do/do not contribute significantly to the hyperpnea of dynamic exercise. *J Appl Physiol* **100**, 1077-1083.

- Ward SA. (2000). Control of the exercise hyperpnoea in humans: a modeling perspective. *Respir Physiol* **122**, 149-166.
- Wittmeier S, Song G, Duffin J & Poon C-S. (2008). Pacemakers handshake synchronization mechanism of mammalian respiratory rhythmogenesis. *Proceedings of the National Academy of Sciences* **105**, 18000-18005.
- Young DL. (2002). Neural adaptive mechanisms in respiratory regulation: theory and experiments. In *Mechanical Engineering*. Massachusetts Institute of Technology, Cambridge.
- Young DL, Eldridge FL & Poon CS. (2003). Integration-differentiation and gating of carotid afferent traffic that shapes the respiratory pattern. *J Appl Physiol* **94**, 1213-1229.
- Yu Y & Poon C-S. (2006). Critique of 'Control of arterial PCO₂ by somatic afferents'. *J Physiol* **572**, 897-898.

Chapter 3 Integrative and Reductionist Approaches to Modeling of Control of Breathing¹

3.1 INTRODUCTION

Systems biology is a classic discipline which has its root when Norbert Wiener (Wiener, 1948) first coined the term “cybernetics”. Engineers have a long history of getting inspirations from biology. The wings of Icarus might be considered one of the first “flying machine” models of birds. Although it is just a Greek myth, it shows human’s innate appreciation for modeling biological designs. Today, mathematical or computer modeling of biological systems is used to improve our understanding of biological phenomena in their full complexity. The traditional approach adopted by biologists for analyzing biological systems is via a strategy of reductionism (Lazebnik 2002; Sorger 2005; Strange 2005; Ahn, Tewari et al. 2006; Ahn, Tewari et al. 2006; Pugh and Andersen 2008). A complementary approach is via the method of integrative modeling based on physical principles. This integrative framework will likely facilitate the collaboration of researchers from such diverse disciplines as biology, chemistry,

¹ To appear as the opening chapter of Lecture Notes in Mathematics (LNM BIOS) for Graz volume

physiology, engineering, computer science, and mathematics to bring out the best of systems biology. S

In this chapter, we examine the criteria of a good *mechanistic* model based on reductionist or integrative approaches. We then discuss the reductionist view and integrated view in the modeling of the respiratory control system.

3.2 REDUCTIONIST VIEW OF BIOLOGICAL MODELING

Reductionism is a divide-and-conquer approach to tackle complex phenomena by parsing the problem into smaller, simpler and more tractable components. It has served as an important guiding principle which has proved tremendously useful in understanding many biological problems. However, there are also drawbacks to this approach. Organisms are definitely more than just the sum of their individual parts. The reductionist approach makes several key assumptions in studying biological systems:

1. A singular factor determines each behavior.

The goal of reductionism is to isolate a single factor to account for each observed behavior. The pharmaceutical community believes that there is a single malfunction for each disease that needs to be cured. Hence, a miracle drug targeting the site of malfunction will solve the problem. Although this is a reasonable assumption for many cases, it does not always apply for more complex situations. For instance, how living habit and genetic factors together affect a person's health (Ahn *et al.*, 2006b)? A young immuno-compromised man with pneumococcal pneumonia will get the same antibiotics treatment as an elderly woman with the same infection. A 'personalized medicine' approach is more desirable but is infeasible with the reductionist view (Wellstead *et al.*, 2008).

2. Response is linearly additive of several factors

Reductionism partitions the problem into many pieces, each studied separately. The total response is then viewed as the superposition of these individual effects. This approach is easily executable but it neglects any nonlinear interactions among components.

3. Only static or steady-state response matters

Cannon(1932) in his book *The Wisdom of the Body* first coined the term “homeostasis”, describing how our body maintains stability and constancy robustly in the face of stress. However, the focus on constancy in the steady state ignores the ubiquity of dynamic behaviors like oscillations and chaos, which may also be important for our body to function. For instance, circadian rhythms and heart rate variability are examples of periodic and chaotic behaviors that may be integral to the maintenance of homeostasis.

3.2.1 The Physiome Project and Multiscale Model

The Physiome Project is one of the major efforts to integrate physiology and engineering (Hunter & Borg, 2003). It provides a coherent framework to integrate the vast amount of DNA sequences, protein structures and signal transduction pathways data into mathematical models which can facilitate the analysis of complex interaction among these systems of different sizes and time scales. It is an important international effort to apply systems engineering approach to physiological modeling and develop standard languages to facilitate sharing of models and information among different research teams.

The Physiome Project is premised on the notion of “multiscale modeling” in which components on different spatial and temporal scales are integrated into a single model.

This is accomplished by combining physiology from molecular level to cell, organ and systems levels. Although the term “multiscale modeling” has been often interpreted as multi-structural modeling across spatiotemporal scales (White *et al.*, 2009), it is increasingly recognized that this modeling approach has its limitations also as it may risk under- or overfitting of parameters and the resulting errors could propagate between models and across spatiotemporal scales (although the benefits of model integration are sometimes considered to outweigh such error costs) (Ortoleva *et al.*, 2009; Qutub *et al.*, 2009). Broadly speaking, multiscale modeling could involve any analytical approach that allows increased predictivity (without sacrificing robustness) by extension or generalization of *any* modeling “scale,” including structural or spatiotemporal scale, analytical scale (Ortoleva *et al.*, 2009) or computational scale (Taufer *et al.*, 2009).

Current models of chemoreflex or exercise hyperpnea are predictive of the ventilatory responses to chemical and metabolic challenges respectively but are generally non-predictive of breathing pattern variables. On the other hand, classical optimization models from the 1950’s that consider work of breathing as an objective function for respiratory control have been limited to the prediction of pattern variables such as respiratory frequency but not total ventilation (e.g. Mead (1960a)). Generalized optimization models that integrate both chemical challenges and work of breathing into an overall control objective (Poon *et al.*, 1992a) can be highly predictive and multiscale (*multi-functional* scale) in that they can simultaneously predict both total ventilation and breathing pattern responses (including instantaneous inspiratory motor output) to a combination of chemical, mechanical and metabolic challenges (see Eq. 4.5) as encountered in a variety of physiological and clinical states (on a *multi-disease* scale).

3.3 ENGINEERING AND PHYSICS VIEW OF INTEGRATIVE MODELING

The field of physics is traditionally highly reductionistic and multiscale in that it seeks to identify the elemental particles or forces of nature on the smallest spatiotemporal scale that underlie physical phenomena on a macroscale. On the other hand, it is also highly integrative in its quest to discover the physical laws (Newton's law, thermodynamics etc.) that unify diverse physical phenomena from quantum to cosmic scales in order to predict complex behaviors based on first principles. Integrative modeling aims to describe how different system components interacting based on physical principles may give rise to emergent behavior of the system. Elucidation of the integrative mechanisms is important for a conceptual understanding on the working principle of the system behavior, as opposed to an empirical or phenomenological (black box) model.

Engineering and physics approach to integrative modeling has a long history in studying mechanical, fluid, thermal, chemical, electronic and other physical systems. Engineering and physical system equations help to specify the behaviors of individual components and their interactions based on physical laws. The strength of such an integrative modeling approach is that it provides a quantitative description of the interaction of different variables in the system based on the physical mechanisms involved. This leads to an experimentally testable unified theory which can span multiple system scales. Hence, engineers have the right analytical tools for designing complex machines. There are several basic performance measures of any engineering control system: stability, robustness and sensitivity. Stability requires a system's states to remain within a finite space over time with a bounded input. Robustness states that a system can favorably maintain its performance under conditions that it is not designed for. Sensitivity states how small a change can a system detect and respond to.

Engineering systems theory has provided the necessary mathematical tools for us to design and evaluate the performance of control systems, and to understand the underlying mechanisms. During the 1940s, the introduction of frequency-domain methods (e.g. Nyquist, Bode) made it possible for engineers to design linear closed-loop control systems that satisfied some performance requirements. Root-locus method was then developed by Evans in the early 1950s. Nowadays, engineers commonly have to deal with multiple-input-multiple-output (MIMO) and nonlinear systems. Classical control theory, which deals with only linear single-input-single-output (SISO) systems, has become inadequate.

There are many reasons for studying nonlinear systems. First, linear control assumes a small range of operation. Its performance is inevitably compromised or the model may become unstable when the required operation range is large and hence nonlinearity becomes significant. Furthermore, some systems may not be linearizable even within a small working range. These “hard” nonlinearities include Coulomb friction, saturation, dead-zones, backlash and hysteresis. Nonlinear controllers are generally more robust to model uncertainties. Since most systems are inherently nonlinear, a good nonlinear controller model can be paradoxically simpler and more intuitive than a linear model (Slotine & Li, 1991; Ogata, 1997).

3.4 TOP-DOWN (INTEGRATIVE) VS BOTTOM-UP (REDUCTIONIST) APPROACH TO BIOLOGICAL MODELING

Integration and reductionism represent two complementary approaches to study complex biological systems (Young & Poon, 2001b). Reductionism lays the groundwork for biological modeling by providing experimental evidence of discrete system elements at the microscopic scale. This bottom-up approach is an efficient strategy to match observed microscopic evidence with observed macroscopic behavior. For instance, gene-targeting

studies attempt to correlate defects of a single gene with abnormalities at the behavioral level. Although this approach will undoubtedly generate useful information for inductive reasoning, the correlation between microscopic and macroscopic events may not be straightforward for complex biological systems (Gerlai, 2001). Thus, direct combination of prime data at the microscopic level may not always lead to understanding of biological mechanisms and prediction of behaviors at the macroscopic level. On the other hand, top-down approach translates integrated phenomena at the macroscopic scale into hypotheses about various microscopic system elements and their interactions. Such deductive reasoning helps to formulate a general integrative principle for the system under study.

Both top-down and bottom-up approaches are necessary for studying biological systems which are typically highly complex and multidimensional. Over the past decades, biological research has accumulated so much data that the underlying system is beyond comprehension without formal analytical tools. Lazebnik (2002) tells how a biologist might attempt to fix a radio in a different way than does an engineer. Thus, biologists may construct a system diagram of the radio in the form of “all-too-well recognizable diagrams, in which a protein is placed in the middle and connected to everything else with two-way arrows”. It is of very slim chance that a radio can be fixed this way. The key difference is that engineers have a formal set of language to describe an electronic device systematically and quantitatively (resistance, capacitance, Kirchhoff's circuit laws, etc). Hence, a trained electronics engineer can unambiguously comprehend a circuit diagram of the radio or any other electronic devices. This shows that reductionism becomes powerless when dealing with multi-dimensional problems.

Yet, top-down approach is necessarily speculative and controversial, especially when the system is complex. Advances in bottom-up approach facilitate top-down investigation. On the other hand, controversies in top-down approach raise scientific inquiries which can lead to potential revolutionary ideas. The process of proving or disproving these ideas will lead to new insights for reducing the search space in the bottom-up approach. Hence,

proper combination of top-down and bottom-up approaches is necessary to elucidate complex biological systems. A model is fully validated when bottom-up meets top-down.

3.5 CRITERIA OF A GOOD MECHANISTIC MODEL

Biologists and engineers see modeling in different ways. So then, what is a good model? Pugh and Andersen (Pugh & Andersen, 2008) suggested seven characteristics of a good model. We summarize below four key criteria that we think are most important for a model to be useful.

1. Embody first principles of the system based on physical and chemical laws

A good model should be physically realistic and reasonable. It also means the model should incorporate all applicable first principles *quantitatively* and *dynamically*.

2. A minimum model

A good model does not have to include every fine details of the system. A model is a tool to provide the intuition to understand the mechanisms underlying a system. An overly complex model may obscure understanding of the system. A *simple* yet sufficient model should be the best model.

3. Summarize existing results with mechanistic insight

The *sine qua non* of a good model is that it is consistent with existing observed phenomena, both qualitatively and quantitatively. A good model should be *general* enough to be consistent with a wide variety of system behaviors. A curve fit to the data is not sufficient; a good model should provide mechanistic insight.

4. Predict behaviors distinct from the data the model is based on

A useful model necessarily has to *predict* phenomena beyond those it is based on. If a model has no prediction power, it is simply a curve fitting machine. A good model can predict a wide range of different phenomena that may be surprising or even

counterintuitive, such as predicting the Earth is round instead of flat. The prediction will help to guide further experiments to uncover more mechanisms underlying the system.

3.6 CONTROL OF BREATHING: REDUCTONISM VS INTEGRATION

3.6.1 Limitations of classical reflex models: a case for sensorimotor integration

The respiratory control system is a multi-input multi-output nonlinear system (Poon, 2000). The system comprises a mechanical plant (respiratory mechanics and muscles) and a chemical plant (pulmonary gas exchange) that are controlled by respiratory neurons in the medulla and pons regions of the brainstem. Extensive studies over the past century have accumulated an enormous collection of knowledge about the respiratory system. Translating these scientific findings into clinical practice becomes critical, as in many other biological research fields (Saijo, 2002; Mankoff *et al.*, 2004; Horig *et al.*, 2005).

However, the effectiveness of such translational research has been limited by the traditional reductionist paradigm which assumes a simple reflex model of respiratory control (Wasserman *et al.*, 1986; Haouzi, 2006; Waldrop *et al.*, 2006). This classical reflex model assumes additive, reducible and superposable characteristics of afferent signals (Figure 3.1a) from chemical, mechanical and exercise stimuli (Mateika & Duffin, 1995; Ward, 2000; Eldridge *et al.*, 2006; Secher *et al.*, 2006; Waldrop *et al.*, 2006; Yu & Poon, 2006).

In fact, a complex physiological system is more than simply the sum of its parts (Strange, 2005). There is evidence that various afferent and efferent signals are integrated by the respiratory controller in a sophisticated way to define the overall ventilatory response (Figure 3.1b). For instance, the available evidence reveals a distinct multiplicative (synergistic) component in the ventilatory response to concomitant exercise and hypercapnia such that CO₂ responsiveness is potentiated during exercise, and vice versa (Poon & Greene, 1985; Poon, 1989; Mitchell & Babb, 2006). Ventilatory response to chemical or exercise input is also potentiated by increases in physiological dead space and shunt (e.g. in congestive heart failure patients). Such sensorimotor integration characteristics are ignored in the oversimplified reflex model which mistakenly considers all respiratory inputs as additive to the “exercise stimulus” (Figure 3.1a). Hence, translational research cannot be effectively conducted without a unified model of respiratory sensorimotor integration that can account for such complex behaviors. The optimization model of ventilatory control first proposed in (Poon, 1983a) has proved to hold promise for this purpose.

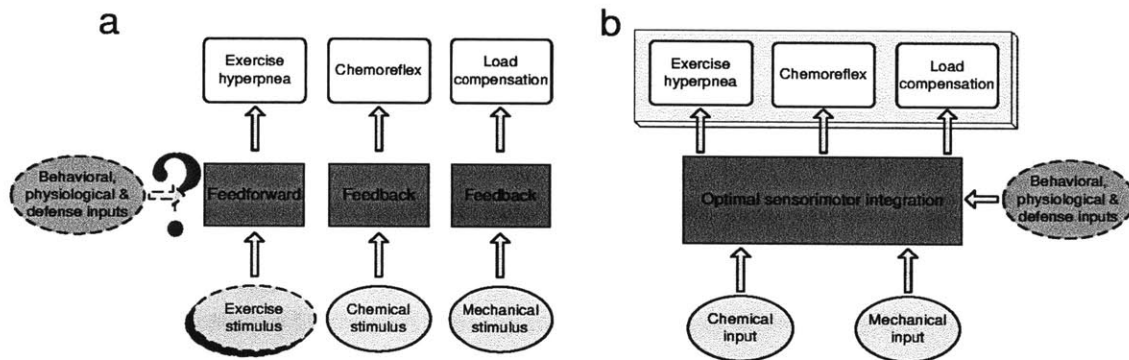


Figure 3.1 Two views for respiratory control (a) Classical reflex model assumes additive, reducible and superposable characteristics of chemical, mechanical and exercise stimuli; (b) The optimization model integrates various afferent-efferent signals in a single model to characterize the complex interactions among these signals. (Poon *et al.*, 2007)

3.6.2 Optimal sensorimotor integration in respiratory control

a. Formulation of the model

M.J. Purves once queried (Purves, 1979): “What do we breathe for?”.

The primary purpose of breathing is to meet metabolic demands, as evidenced by the apparent respiratory homeostasis during exercise. An implicit objective is to maintain chemical homeostasis as well as minimize the energy consumption in the act of breathing. Furthermore, the respiratory system also faces constant challenges of many other causes such as the need for varying behavioral (feeding, smelling, blowing, vocalization, breath-holding, posture, emotion, defecation), physiological (panting, thermal hyperpnea) or defense (coughing, sneezing, emesis, eructation, hiccup) measures. Apparently, the respiratory control system is intelligent enough to maintain a delicate balance between these conflicting objectives.

Poon (1983b, 1987b) first introduced the following cost function to integrate the chemical and mechanical costs of breathing (Figure 3.2) :

$$J = J_c + J_m = [\alpha(P_{aCO_2} - \beta)]^2 + \ln \dot{W}_o^2 \quad (3.1)$$

The terms J_c , J_m in Eq. 3.1 represent the competing chemical and mechanical costs of breathing (α , β are parameters) in conformance to Steven’s power law and Weber-Fechner law of psychophysics respectively (Stevens, 1961). The term \dot{W}_o is a measure of the work rate of breathing subject to the mechanical limitation of the respiratory system.

The optimal total ventilation \dot{V}_E is one that minimizes J (Eq. 3.1) subject to the gas exchange process and mechanical constraint thus weighing the chemoafferent feedback against the respiratory motor output. The resultant optimal solution simulates

the linear $\dot{V}_E - P_{aCO_2}$ relationship during CO_2 inhalation and proportional $\dot{V}_E - \dot{V}CO_2$ relationship during exercise as follows (Poon, 1983b, 1987b):

$$\dot{V}_{E0} = 863\alpha^2(P_{aCO_2} - \beta) \frac{\dot{V}_{CO_2}}{(1 - V_D/V_T)} \quad (3.2)$$

$$\dot{V}_E = \frac{\dot{V}_{E0}}{1 + \dot{V}_{E0}/\dot{V}_{max}} \quad (3.3)$$

Hence, the controller gain is not constant but may be adjusted to track the metabolic $\dot{V}CO_2$.

Equation 3.1 has been extended (Poon *et al.*, 1992a) to model the integrative control of \dot{V}_E and respiratory pattern, by expressing \dot{W}_o explicitly in terms of the isometric respiratory driving pressure $P(t)$. The mechanical plant in this case is defined by the following equation of motion:

$$P(t) = \dot{V}(t)R_{rs} + V(t)E_{rs} \quad (3.4)$$

whereby all ventilatory variables can be derived successively from the $P(t)$ waveform as follows:

$$P(t) \rightarrow \dot{V}(t), V(t) \rightarrow V_T, T_I, T_E \rightarrow \dot{V}_E \quad (3.5)$$

where R_{rs} , E_{rs} are respectively the total (extrinsic and intrinsic) respiratory resistance and elastance; $\dot{V}(t)$, $V(t)$ are instantaneous respiratory airflow and volume; T_I and T_E are inspiratory and expiratory durations. V_T, T_I and T_E together determine the total ventilation. This integrated model captures both the optimal ventilatory response characteristics of Eq. 3.2, and the corresponding optimal respiratory pattern.

Glossary

J	Total cost of breathing
J_c	Chemical cost of breathing
J_m	Mechanical cost of breathing
P_{aCO_2}	Arterial CO ₂ partial pressure
α	Chemoreceptor sensitivity
β	Chemoreceptor response threshold
\dot{W}_o	Work rate of breathing
\dot{V}_E	Total ventilation
\dot{V}_{max}	Maximal ventilatory output
$\dot{V}CO_2$	Metabolic CO ₂ production rate
R_{rs}	Total respiratory resistance
E_{rs}	Total respiratory elastance
$\dot{V}(t)$	Instantaneous respiratory airflow rate
$V(t)$	Instantaneous respiratory volume
T_I	Inspiratory duration
T_E	Expiratory duration
$P(t)$	Isometric inspiratory driving pressure measured at functional residual capacity (FRC)

3.6.3 Hebbian feedback covariance learning model of respiratory motor control

The optimization model represents an intelligent control system in our breathing. The next question is: what is the brain mechanism that optimizes our breathing? A Hebbian feedback covariance adaptive control paradigm which conforms to the neurophysiological system was proposed based on the Hebbian covariance learning rule (Figure 3.3). Figure 3.3 is hence an engineering realization of the respiratory optimal controller (Figure 3.2). The synaptic weight that determines the optimal input-output

relationship is computed by correlating the corresponding intrinsic fluctuations that are ubiquitous in physiological signals (Young & Poon, 1998).

Hebbian synaptic plasticity was first postulated by Hebb over 50 years ago as a mechanism of learning and memory (Hebb, 1949). The classical Hebbian model (Hebb, 1949) states that the strength (or gain) C of a synaptic connection is modified according to an adaptation law of the form:

$$\frac{dC}{dt} = k(y \cdot u) \quad (3.6)$$

where y , u are mean firing rates of input and output neurons, respectively, and k is an adaptation constant. This synaptic adaptation law has been widely taken as the basis of NMDA receptor-dependent long-term potentiation (LTP) in some hippocampal and neocortical neurons.

However, there are some limitations to the classical Hebbian model, not the least the inevitable occurrence of runaway instability and irreversible saturation resulting from sustained or random coactivity of interacting neurons, leading to difficulties in its implementation (Poon, 1996d; Young, 1997; Young & Poon, 2001c). Moreover, the dependence of the classical Hebbian model on pre- and post-synaptic activities local to the adapting neuron does not lend itself to feedback control applications. To circumvent these difficulties, a stochastic synaptic adaptation law called *Hebbian feedback covariance adaptation* has been proposed (Young & Poon, 2001c). Instead of pairing the mean input and output activities of the controller neuron, the new adaptation law modifies the synaptic strength by correlating the temporal variations of the pre- and post-synaptic neural activities about their respective mean values. Here, the pre- and post-synaptic activities of the controller neuron correspond to the feedback signal and control signal, respectively. This adaptive control paradigm can be viewed as a reinforcement

learning system driven by spontaneous, random perturbations in the control and feedback variables (Figure 3.3). The new adaptation law becomes,

$$\frac{dC}{dt} = k_1(\delta y \cdot \delta u) - k_2 C \cdot g(\delta y, \delta u; y, u) \quad (3.7)$$

where δu and δy are the temporal variations of the pre- and post-synaptic neural activities about their respective mean values and $g(\cdot)$ is some positive definite function, which acts as a decay term to avoid saturation. Depending on the sign of the constant k_1 , the algorithm can describe synaptic LTP (for $k_1 > 0$) or LTD (long-term depression) (for $k_1 < 0$).

The Hebbian feedback covariance controller is stochastic in nature and employs a direct adaptive control approach. The controller gain, C , is updated according to the input/output relationship of the system, without explicit estimation of the plant parameters. In addition, the adaptive controller can be designed in such a way to optimize a certain objective function (which is essentially the Lyapunov function (Slotine & Li, 1991)). By applying the Barbalat's lemma (Slotine & Li, 1991), the objective can be guaranteed to converge to a minimum value at steady state.

The discussions of the algorithm so far have focused on static input-output relationship only. In reality, systems are usually governed by dynamical relationships as a result of, for instance, slow time constants and time delays. Young and Poon (2001c) modified the original algorithm for dynamical systems by introducing a near-term objective function, Q . The Hebbian covariance feedback law is applied to the near-term objective function which, with some suitable transformations of the state variables, will lead to minimization in the long term.

To illustrate, consider a first-order nonlinear system,

$$\dot{y} = q(y, u) \quad (3.8)$$

The steady state solution is obtained as,

$$y_0 = f(u_0) \quad (3.9)$$

An intermediate variable z is defined as a filtered version of the original state variable y ,

$$z(y, \dot{y}, u) = f(u) \quad (3.10)$$

such that $z \rightarrow y_0$ as $f(u) \rightarrow f(u_0)$. Hence, the system becomes static in z , and the same algorithm can be applied on this intermediate (or filtered) state variable with a near-term objective function defined in z and u . In steady state, the near-term objective function converges to the long-term objective function. The same approach is generally applicable to systems of higher order.

The Hebbian feedback covariance control is computationally simple compared to conventional self-tuning or model-reference adaptive control, which generally require a prescribed reference model or desired trajectory. On the other hand, it is also a form of reinforcement learning with an implicit reinforcement signal, namely the covariance of the filtered state and the control signals.

Hebbian feedback covariance control has been successfully applied to the modeling of the respiratory system to predict the optimal adaptation behaviors during exercise and CO₂ inhalation (Young, 1997; Young & Poon, 1998). Moreover, robustness to noise disturbances is also verified with simulations. Further experimental evidence is required to identify the neural correlates of such an algorithm in respiratory control. This Hebbian feedback covariance control has a substantial mathematical background. It shows an example in which reverse engineering is applied to a physiological system toward developing a biologically-inspired engineering control paradigm. Such a

paradigm may transcend its biological counterpart to suggest a general engineering control theory that is applicable to any practical system.

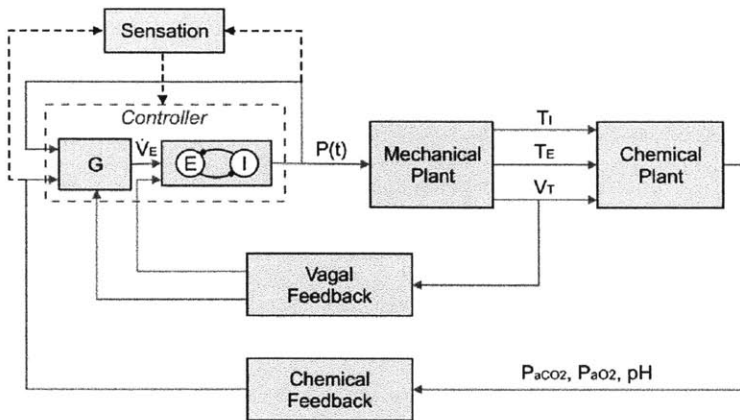


Figure 3.2 Simplified block diagram of the optimization model of respiratory control. Sensorimotor feedback signals are integrated by an intelligent controller which produces optimal ventilatory drive and breathing pattern that are most cost-effect for meeting metabolic demands, subject to the constraints imposed by the mechanical plant and chemical plant. The functional block “G” represents the transmission gains for sensorimotor integration.

Dyspnea (respiratory discomfort) may involve the processing of similar signals by the higher brain (the somatosensory cortex and limbic system).

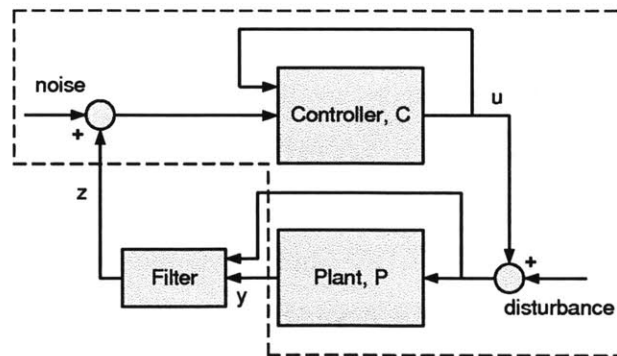


Figure 3.3 Hebbian Feedback Covariance Control Paradigm

The controller gain, C , is adapted based on the covariance between the input (y) and output (u) signals. Dotted line indicates the original control scheme for static system. To account for system dynamics, a filter is added to transform the plant output, y into an intermediate variable.

3.6.4 Cheyne-Stokes breathing from different engineering control perspectives

Cheyne-Stokes breathing is of significant clinical concern. It is a respiratory abnormality when a person's breathing wax and wane periodically. It is occurring more frequently in patients with chronic heart failure and left ventricular systolic dysfunction, normals at high altitude, or during sleep. There have been extensive analytical studies about the mechanism of Cheyne-Stokes. Three possible views are discussed below.

Cheyne-Stokes breathing as system instability

Cheyne-Stokes breathing has been studied on the basis of engineering stability. It has been suggested that Cheyne-Stokes breathing is a result of instability of the respiratory control system based on chemoreflex, as the above mentioned conditions increase the gain and/or phase lag of the system. A vast variety of engineering theory is concerned about the stability of a control system, especially linear time-invariant system. Khoo (1982) has performed an extensive analytical study, based on Nyquist's stability criterion, on the dependence of stability of respiratory control system on different parameters and physiological conditions. The analysis determines the local stability of the system about the equilibrium state using a linearized system. An unstable combination of system parameters will diverge the states from the equilibrium, and will be bounded by saturations in chemoreceptors, gas exchange process and mechanical limitation of actuators, and hence oscillate. This study represents one of the very successful systematic applications of engineering theories in the study of cardiorespiratory phenomena. It has led to many subsequent studies of Cheyne-Stoke breathing and the mechanisms of possible treatment.

Cheyne-Stokes breathing as limit cycle

It should be noted that Cheyne-Stoke breathing can also be interpreted as a stable limit cycle. Limit cycle is an important phenomenon in nonlinear systems, and is distinct

from the oscillation in linear systems (Figure 3.4). A marginally stable linear system may also oscillate. However, the amplitude of a limit cycle is independent of the initial condition, while the oscillation of a marginally stable linear system has its amplitude determined by its initial condition. Furthermore, the oscillation of a marginally stable linear system is not robust and is very sensitive to changes in system parameters. On the other hand, limit cycle may be viewed as a “stable” state. A unique mathematical tool for determining existence and stability of limit cycle is available (Slotine & Li, 1991) and may be useful in further study of Cheyne-Stokes breathing .

Cheyne-Stokes breathing as an optimal pattern

Ghazanshahi and Khoo (1993) has suggested that Cheyne-Stokes breathing is actually an optimal breathing pattern at high altitude when the respiratory system is highly stressed. They suggested that Cheyne-Stokes, or more generally periodic breathing, is a cost effective way to breathe when respiratory demand is high. They showed that despite the large fluctuation in blood gas concentration, on average gas transport is more efficient in periodic breathing, and it also saves muscular efforts. The chemical cost is lowered by the large breath to reduce dead space ventilation hence maintaining blood gas homeostasis; while mechanical cost is lowered by the apnea period which partially offset the increased work during the breathing phase.

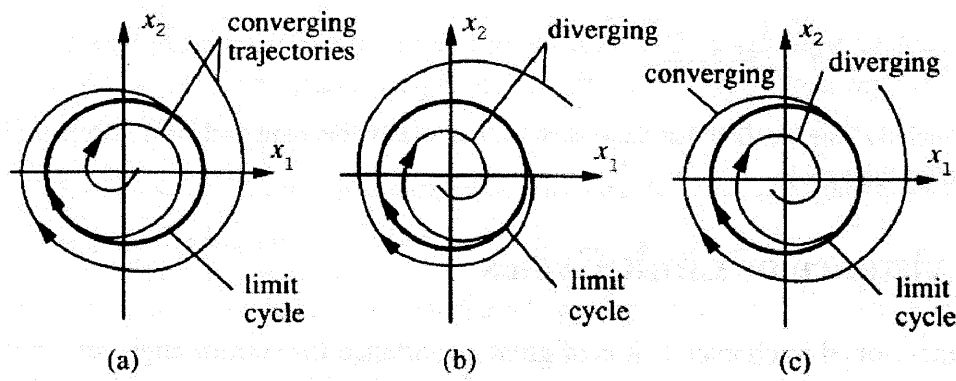


Figure 3.4 Limit cycle a) Stable, b) unstable, c) semi-stable (Slotine & Li, 1991)

3.7 REFERENCES

- Ahn AC, Tewari M, Poon CS & Phillips RS. (2006). The limits of reductionism in medicine: could systems biology offer an alternative? *PLoS Med* **3**, e208.
- Cannon WB. (1932). *The wisdom of the body*. W.W. Norton & Company, New York,.
- Eldridge FL, Morin D, Romaniuk JR, Yamashiro S, Potts JT, Ichiyama RM, Bell H, Phillipson EA, Killian KJ, Jones NL & Nattie E. (2006). Supraspinal locomotor centers do/do not contribute significantly to the hyperpnea of dynamic exercise in humans. *J Appl Physiol* **100**, 1743-1747.
- Gerlai R. (2001). Gene targeting: technical confounds and potential solutions in behavioral brain research. *Behav Brain Res* **125**, 13-21.
- Ghazanshahi SD & Khoo MC. (1993). Optimal ventilatory patterns in periodic breathing. *Ann Biomed Eng* **21**, 517-530.
- Haouzi P. (2006). Theories on the nature of the coupling between ventilation and gas exchange during exercise. *Respir Physiol Neurobiol*.
- Hebb DO. (1949). *The Organization of Behavior*. Wiley, New York.
- Horig H, Marincola E & Marincola FM. (2005). Obstacles and opportunities in translational research. *Nature medicine* **11**, 705-708.
- Hunter PJ & Borg TK. (2003). Integration from proteins to organs: the Physiome Project. *Nat Rev Mol Cell Biol* **4**, 237-243.
- Khoo MC, Kronauer RE, Strohl KP & Slutsky AS. (1982). Factors inducing periodic breathing in humans: a general model. *J Appl Physiol* **53**, 644-659.
- Lazebnik Y. (2002). Can a biologist fix a radio?--Or, what I learned while studying apoptosis. *Cancer Cell* **2**, 179-182.
- Mankoff SP, Brander C, Ferrone S & Marincola FM. (2004). Lost in Translation: Obstacles to Translational Medicine. *J Transl Med* **2**, 14.
- Mateika JH & Duffin J. (1995). A review of the control of breathing during exercise. *Eur J Appl Physiol Occup Physiol* **71**, 1-27.
- Mead J. (1960). Control of respiratory frequency. *J Appl Physiol* **15**, 325-336.
- Mitchell GS & Babb TG. (2006). Layers of exercise hyperpnea: modulation and plasticity. *Respir Physiol Neurobiol* **151**, 251-266.

- Ogata K. (1997). *Modern Control Engineering*. Prentice Hall, Englewood Cliffs, New Jersey.
- Ortoleva P, Adhangale P, Cheluvvaraja S, Fontus M & Shreif Z. (2009). Deriving principles of microbiology by multiscaling laws of molecular physics. *IEEE Eng Med Biol Mag* **28**, 70-79.
- Poon C-S. (1983a). Optimal control of ventilation in hypoxia, hypercapnia and exercise. In *Modeling and Control of Breathing*, ed. Whipp & Wiberg. Elsevier, New York.
- Poon C-S & Greene JG. (1985). Control of exercise hyperpnea during hypercapnia in humans. *J Appl Physiol* **59**, 792-797.
- Poon C-S, Lin SL & Knudson OB. (1992). Optimization character of inspiratory neural drive. *J Appl Physiol* **72**, 2005-2017.
- Poon CS. (1983b). Optimal control of ventilation in hypoxia, hypercapnia and exercise. In *Modelling and Control of Breathing*, ed. Whipp BJ & Wiberg DW, pp. 189-196. Elsevier, New York.
- Poon CS. (1987). Ventilatory control in hypercapnia and exercise: optimization hypothesis. *J Appl Physiol* **62**, 2447-2459.
- Poon CS. (1989). Effects of inspiratory resistive load on respiratory control in hypercapnia and exercise. *J Appl Physiol* **66**, 2391-2399.
- Poon CS. (1996). Self-tuning optimal regulation of respiratory motor output by Hebbian covariance learning. *Neural Network* **8**, 1-17.
- Poon CS. (2000). Respiratory models and control. In *Biomedical Engineering Handbook*, 2nd edn, ed. Bronzion JD, pp. 161. CRC Press, Boca Raton, FL.
- Poon CS, Tin C & Yu Y. (2007). Homeostasis of exercise hyperpnea and optimal sensorimotor integration: the internal model paradigm. *Respiratory physiology & neurobiology* **159**, 1-13; discussion 14-20.
- Pugh EN, Jr. & Andersen OS. (2008). Models and mechanistic insight. *J Gen Physiol* **131**, 515-519.
- Purves MJ. (1979). What do we breathe for? In *Central Nervous Control Mechanisms in Breathing (Wenner-Gren Center Int Symp Ser)*, ed. von Euler C & Lagercrantz H, pp. 7-12. Pergamon, Oxford, UK.
- Qutub A, Gabhann F, Karagiannis E, Vempati P & Popel A. (2009). Multiscale models of angiogenesis. *IEEE Eng Med Biol Mag* **28**, 14-31.

- Saijo N. (2002). Translational study in cancer research. *Internal medicine (Tokyo, Japan)* **41**, 770-773.
- Secher N, Poon C-S, Ward S, Whipp B & Duffin J. (2006). Supraspinal locomotor centers do/do not contribute significantly to the hyperpnea of dynamic exercise in humans. *J Appl Physiol* **100**, 1417-1418.
- Slotine J-JE & Li W. (1991). *Applied Nonlinear Control*. Prentice-Hall, Englewood Cliffs, NJ 07632.
- Stevens SS. (1961). To honor Fechner and repeal his law. *Science* **133**, 80-86.
- Strange K. (2005). The end of "naive reductionism": rise of systems biology or renaissance of physiology? *Am J Physiol Cell Physiol* **288**, C968-974.
- Taufer M, Armen R, Chen J, Teller P & Brooks C. (2009). Computational multiscale modeling in protein--ligand docking. *IEEE Eng Med Biol Mag* **28**, 58-69.
- Waldrop TG, Iwamoto GA & Haouzi P. (2006). Point:Counterpoint: Supraspinal locomotor centers do/do not contribute significantly to the hyperpnea of dynamic exercise. *J Appl Physiol* **100**, 1077-1083.
- Ward SA. (2000). Control of the exercise hyperpnoea in humans: a modeling perspective. *Respir Physiol* **122**, 149-166.
- Wasserman K, Whipp BJ & Casaburi R. (1986). Respiratory control during exercise. In *Handbook of physiology*, ed. Cherniack NS & Widdicombe JG, pp. 595-620. American Physiological Society, Bethesda, MD.
- Wellstead P, Bullinger E, Kalarnatianos D, Mason O & Verwoerd M. (2008). The role of control and system theory in systems biology. *Annu Rev Control* **32**, 33-47.
- White R, Peng G & Demir S. (2009). Multiscale modeling of biomedical, biological, and behavioral systems (Part 1). *IEEE Eng Med Biol Mag* **28**, 12-13.
- Wiener N. (1948). *Cybernetics; or, Control and communication in the animal and the machine*. Technology Press, [Cambridge, Mass.].
- Young DL. (1997). Hebbian Covariance Learning and Self-Tuning Optimal Control. In *Mechanical Engineering*. M.I.T, Cambridge, MA.
- Young DL & Poon C-S. (2001a). Soul searching and heart throbbing for biological modeling. *Behavioral and Brain Sciences* **24**, 1080-1081.

Young DL & Poon CS. (1998). Hebbian covariance learning. A nexus for respiratory variability, memory, and optimization? *Adv Exp Med Biol* **450**, 73-83.

Young DL & Poon CS. (2001b). A Hebbian Feedback Covariance Learning Paradigm for Self-tuning Optimal Control. *IEEE Transactions on Systems, Man, and Cybernetics - Part B: Cybernetics* **31**, 173-186.

Yu Y & Poon C-S. (2006). Critique of 'Control of arterial PCO₂ by somatic afferents'. *J Physiol* **572**, 897-898.

Chapter 4 Mechanical-Chemical Interaction underlies Optimal Respiratory Control in Gas Exchange Defects²

4.1 INTRODUCTION

Breathing is an innate motor act that is basic to survival. This deceptively mundane (“as-easy-as-breathing”) motor function is regulated by the brain continually throughout life without fail in the face of constant physiologic and environmental challenges. In cardiopulmonary diseases, control of breathing is compromised but remains surprisingly sturdy as compensatory mechanisms set in to restore homeostasis until the disease progresses to the point of breakdown with acute/chronic respiratory failure. Precisely how such robust automatic control is accomplished and what makes it finally fail in disease states remains poorly understood.

² Research supported by American Heart Association Pre-doctoral Fellowship

Classical models of respiratory control assume a simple, fixed reflexogenic controller with additive, reducible and superposable characteristics of chemoreceptor and mechanoreceptor afferent signals. This chemoreflex/mechanoreflex feedback model implies the existence of a feedforward signal from an exercise-related input in order to explain the control of exercise hyperpnea – an automatic increase in respiratory ventilation geared to metabolic demands with near constancy of arterial CO₂ and pH levels. However, despite extensive search over the past century, none of the hypothesized feedforward mechanisms has been demonstrated conclusively as the true “exercise stimulus” that is obligatory to exercise hyperpnea (Mateika & Duffin, 1995; Ward, 2000; Eldridge *et al.*, 2006; Secher *et al.*, 2006; Waldrop *et al.*, 2006; Yu & Poon, 2006). These controversies raise serious questions regarding the validity of such oversimplified models.

A novel model of respiratory control based on a general optimality principle proposed previously (Poon, 1983a) has proved to be capable of synthesizing a vast array of respiratory phenomena. The model addresses the important question of how the respiratory controller balances multiple competing objectives in order to optimize the work of breathing while striving to maintain homeostasis of arterial CO₂ and pH levels in a unified framework. The resultant optimal controller encapsulates many salient characteristics of respiratory control including distinct ventilatory responses to exercise, CO₂ inhalation and increased respiratory dead space (V_D) to tidal volume (V_T) ratio as well as CO₂-exercise and V_D/V_T -exercise interactions and ventilatory load compensation, all without the need for an explicit putative “exercise stimulus”. The success of coherent predictions by the optimization model over a wide variety of physiological conditions makes it a more useful tool than the conventional reflex model for translation between clinical observations and physiological mechanisms. The present study will explore the capability of such optimization model on predicting the exercise ventilatory response imposed by various clinical and physiological conditions that compromise gas exchange efficiency. Specifically, our study will explain the difference that increased dead space in congestive heart failure leads to normocapnic exercise response while in external dead space breathing, it leads to hypercapnia.

4.2 BACKGROUND

4.2.1 Traditional notion of dead space

Oxygenation of blood and elimination of carbon dioxide from the blood requires efficient pulmonary ventilation and gas exchange. Nevertheless, ventilation is never perfect and a portion of the ventilation of every breath is inevitably wasted, physically and/or functionally (dead space). Such waste is further exaggerated under various cardiorespiratory diseases and physiological conditions. Increased dead space fraction has been shown to be a useful diagnostic measure for predicting mortality in acute respiratory distress syndrome (Nuckton *et al.*, 2002). Furthermore, mechanical ventilation tubing imposes additional apparatus dead space to the respiratory circuit. Understanding its impact on patients' respiration will suggest necessary precautions to minimize its adverse effects (Mapleson, 1954; De Robertis *et al.*, 1999; De Robertis *et al.*, 2010).

The notion of “dead space” has a century-old history and is important in characterizing the defects of gas exchange efficiency under various conditions. Riley's three compartment model provides a simple idealized picture of imperfect gas exchange in respiration (Riley & Cournand, 1949, 1951). In his model, the three compartments are an ideal lung unit, a dead space volume and shunt in blood stream. Dead space is the volume that is being ventilated but not perfused; while shunt is the part that is perfused but not ventilated. Neither of them contributes to gas exchange.

Bohr (Bohr, 1891) first calculated the dead space (V_D) using the following equation based on mass balance:

$$\frac{V_D}{V_T} = 1 - \frac{F_{\bar{E}CO_2}}{F_{ACO_2}} \quad (4.1)$$

where

V_T = tidal volume

$F_{\bar{E}CO_2}$ = Average volumetric fraction of carbon dioxide in mixed expired gas

F_{ACO_2} = Average volumetric fraction of carbon dioxide in alveolar gas

(equivalently, P_{CO_2} can be used instead of F_{CO_2})

With the difficulty of defining F_{ACO_2} unequivocally, especially in the presence of inhomogeneity, Enghoff (Enghoff, 1938) modified Bohr's equation by replacing alveolar partial pressure with arterial (P_{aCO_2}) and the dead space is now named physiological dead space.

The physiological dead space is commonly divided into two compartments. The first compartment, anatomical dead space, is the volume of the conducting airways and tubing in the ventilator circuitry. The second, alveolar dead space, is commonly referred to as the volume of nonperfused alveoli and can include effects due to ventilation/perfusion mismatch.

4.3 GENERALIZED GAS EXCHANGE EQUATION AND OPTIMAL RESPIRATORY CONTROL FOR PULMONARY GAS EXCHANGE DEFECTS

4.3.1 Notion of dead space in gas exchange equation

Traditionally, the problem of pulmonary gas exchange is captured as the quantity V_D/V_T in the steady state gas exchange equation as follow:

$$P_{aCO_2} = P_{ICO_2} + \frac{K\dot{V}_{CO_2}}{\dot{V}_E(1 - V_D/V_T)} \quad (4.2)$$

where P_{ICO_2} is the partial pressure of inhaled CO_2 ; \dot{V}_{CO_2} is the metabolic CO_2 production rate; \dot{V}_E is the total ventilation; V_D/V_T is the dead space to tidal volume ratio; $K = 863$ is a constant to reconcile STPD (standard temperature (0 °C), barometric pressure at sea level

(101.3 kPa) and dry) and BTPS (body temperature, pressure and saturated) conditions and for unit conversion.

Clinical measure of V_D/V_T using Enghoff-Bohr's equation is useful for quantifying severity of disease in a patient. However, various causes of gas exchange defects may confuse or complicate the measurement of dead space (Fletcher *et al.*, 1981; Tang *et al.*, 2005; Drummond & Fletcher, 2006; Hedenstierna & Sandhagen, 2006). Furthermore, the quantity V_D/V_T itself does not provide a full picture for the impact of the gas exchange defects on respiratory control without understanding the specific nature of the gas exchange problem.

To provide a better understanding of the problem of gas exchange, especially for its impact on control of breathing, we will look into the problem from the first principle.

Dead space is commonly investigated using a single breath test for carbon dioxide (SBT-CO₂), whereby expired carbon dioxide fraction is plotted against expired volume (Figure 4.1). The area under the expired CO₂ curve represents the volume of CO₂ being eliminated in the tidal volume. On the other hand, the area between the P_{aCO_2} line and the curve represents the volume of CO₂ that is not eliminated by the tidal volume due to any non-ideal gas exchange condition, which commonly includes contribution from alveolar dead space and airway dead space (Fowler, 1948; Bartels *et al.*, 1954; Langley *et al.*, 1976; Fletcher *et al.*, 1981; Lucangelo & Blanch, 2004; Drummond & Fletcher, 2006).

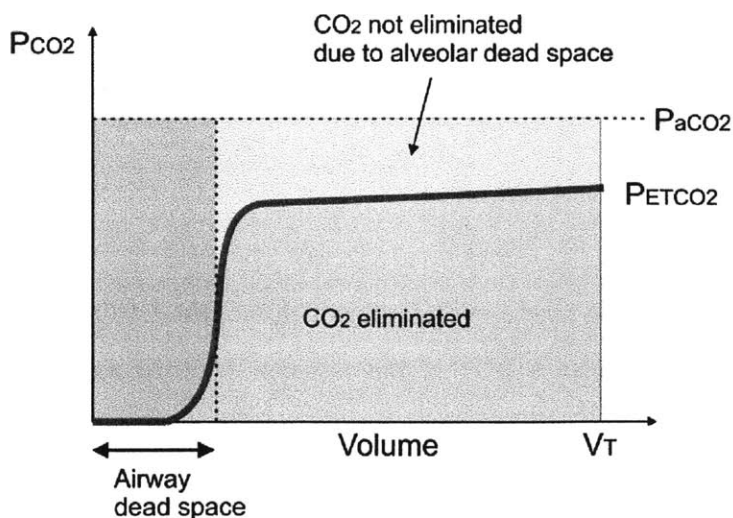


Figure 4.1 Expired CO₂ trace with illustration of “dead space”. Total “dead space” normally comprises alveolar and airway dead space

The amount of CO₂ removed by ventilation of volume V_T with gas at CO₂ tension of P_{aCO₂} at steady state is equal to the metabolic production of CO₂, V_{CO₂}.

$$\begin{aligned}
 KV_{CO_2} &= \int_{V_T} P_{CO_2} \cdot dV \\
 &= V_T \times \frac{\int_{V_T} P_{CO_2} \cdot dV}{V_T} \\
 &= V_T \times P_{\bar{E}CO_2}
 \end{aligned} \tag{4.3}$$

where P _{$\bar{E}CO_2$} is the mixed expired CO₂.

Under ideal condition, assuming homogenous and steady state condition, arterial, alveolar, end-tidal and mixed expired CO₂ are indistinguishable from one another.

$$P_{\bar{E}CO_2} = P_{aCO_2} \tag{4.4}$$

However, in reality or under any gas exchange defects, mixed expired CO₂ partial pressure P _{$\bar{E}CO_2$} deviates from P_{aCO₂}. Without loss of generality, the gas exchange equation can be written as

$$KV_{CO_2} = V_T \times (P_{aCO_2} - \Delta P_{CO_2}) \tag{4.5}$$

or in the equivalent form using total ventilation ($\dot{V}_E = V_T \times freq$) instead of tidal volume (V_T), the gas exchange equation becomes:

$$P_{aCO_2} = \frac{K\dot{V}_{CO_2}}{\dot{V}_E} + \Delta P_{CO_2} \tag{4.6}$$

where ΔP_{CO_2} is a measure to indicate the average deviation of the expired CO₂ trace from the P_{aCO₂} level and hence V_T × ΔP_{CO₂} represents the area between the horizontal line indicating P_{aCO₂} level and the expired CO₂ curve. This area is commonly used as a measure of the “dead space”. but it actually has a broader meaning incorporating different situations of gas exchange defects (e.g. shunts, non-uniform gas mixing, etc.). It also

represents the inhaled CO₂ (P_{ICO₂}) as in the traditional gas exchange equation. It will be helpful for our understanding of the respiratory response to various clinical and physiological conditions.

4.3.2 Role of dead space in optimal respiratory control

The impact of gas exchange defects on respiratory control is considered in the framework of optimal respiratory control. Consider the optimization problem similar to (Poon, 1987a):

$$\begin{aligned} \min_{\dot{V}_E} J &= \min_{\dot{V}_E} (J_c + J_m) = \min_{\dot{V}_E} \left\{ \alpha (P_{aCO_2} - \beta) \right\}^2 + \ln \dot{V}_E^2 \\ \text{s.t.} \quad P_{aCO_2} &= \Delta P_{CO_2} + \frac{K \dot{V}_{CO_2}}{\dot{V}_E} \end{aligned} \quad (4.7)$$

The total cost of breathing is the sum of chemical (J_c) and mechanical (J_m) cost (α , β are parameters). The optimization is constrained by the gas exchange equation (Eq. 4.6).

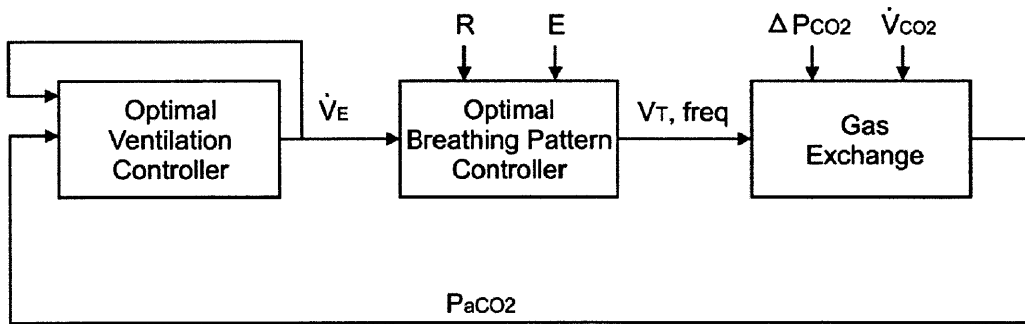


Figure 4.2 Block diagram of optimal respiratory CO₂ control

To obtain the optimal \dot{V}_E ,

$$\begin{aligned} \frac{\partial J}{\partial \dot{V}_E} &= 0 \\ \Rightarrow 2\alpha^2 (P_{aCO_2} - \beta) \frac{\partial P_{aCO_2}}{\partial \dot{V}_E} + \frac{2}{\dot{V}_E} &= 0 \end{aligned} \quad (4.8)$$

where

$$\begin{aligned} \frac{\partial P_{aCO_2}}{\partial \dot{V}_E} &= -\frac{K\dot{V}_{CO_2}}{\dot{V}_E^2} + \frac{\partial \Delta P_{CO_2}}{\partial \dot{V}_E} \\ \Rightarrow \dot{V}_E^* &= \alpha^2 (P_{aCO_2} - \beta) \left(K\dot{V}_{CO_2} - \dot{V}_E^2 \frac{\partial \Delta P_{CO_2}}{\partial \dot{V}_E} \right) \end{aligned} \quad (4.9)$$

The term $-\dot{V}_E^2 \frac{\partial \Delta P_{CO_2}}{\partial \dot{V}_E}$ in Eq. 4.9 accounts for the impact of various pulmonary gas exchange defects on the optimal respiratory response. This will be elaborated in several different conditions in the following sections.

4.4 THE OPTIMIZATION MODEL (MODIFIED FROM POON'S MODEL)

In the present study, the optimization is performed as follow:

$$\min_{\dot{V}_E} J = \min_{\dot{V}_E} \left\{ \alpha (P_{aCO_2} - \beta) \right\}^2 + \ln \frac{\dot{V}_E^2}{\left(1 - \frac{\dot{V}_E}{\dot{V}_{E \max}} \right)^4} \quad (4.10)$$

$$s.t. \quad P_{aCO_2} = \Delta P_{CO_2} + \frac{K\dot{V}_{CO_2}}{\dot{V}_E}$$

$$\Rightarrow \min_{V_T, freq} \dot{W} \quad (4.11)$$

$$s.t. \quad \dot{V}_E^* = V_T \cdot freq$$

where $\alpha = 0.1$, $\beta = 37$ Torr and $\dot{V}_{Emax} = 160L/min$ (Poon, 1987a).

A mechanical limitation factor $\left(1 - \dot{V}_E / \dot{V}_{Emax}\right)^4$ is included in Eq. 4.10 to

produce a more realistic prediction. (\dot{V}_{Emax} defines the maximal ventilation that can be sustained by the respiratory muscle.)

The optimal total ventilation \dot{V}_E^* is determined by minimizing the sum of chemical and mechanical cost similar to (Poon, 1987b) (Eq. 4.10). The second optimization equation (Eq. 4.11) gives the optimal combination of tidal volume and breathing frequency corresponding to \dot{V}_E^* by minimizing the mechanical cost index, \dot{W} . In the present study, only tidal volume and frequency are of concern. The underlying assumption for separating the breathing pattern optimization from the ventilation optimization is that the chemoafferent signal has little effect in altering the breathing pattern. We argue that the swing of chemical signal is comparatively slower than breath-to-breath variation. Therefore, it is beyond the bandwidth of the pattern controller. As such, breathing pattern is primarily determined by mechanical factors.

It is assumed that the mechanical cost index, \dot{W} of breathing is the weighted sum of the power output required for inspiration and the mean squared acceleration which accounts for the smoothness of muscle movement. Similar cost index has been considered in various studies (Yamashiro & Grodins, 1971; Hämäläinen & Viljanen, 1978a; Hämäläinen & Viljanen, 1978b; Hämäläinen & Sipilä, 1984; Poon *et al.*, 1992b). Furthermore, a linear dynamic model of the lung mechanics is assumed. Hence, the mechanical cost index can be formulated as follow:

$$\dot{W} = freq \int \left[\frac{P\dot{V}}{\left(1 - \frac{V_T}{V_C}\right)^n} + \lambda\ddot{V}^2 \right] dt, \text{ s.t. } P(t) = R\dot{V}(t) + EV(t) \quad (4.12)$$

where $P(t)$ is the driving pressure, $V(t)$, $\dot{V}(t)$ and $\ddot{V}(t)$ are the airflow volume, velocity and acceleration respectively; V_T is the tidal volume; $freq$ is the breathing frequency; R ($= 3\text{cmH}_2\text{O L}^{-1} \text{s}^{-1}$) and E ($= 10 \text{cmH}_2\text{O L}^{-1}$) are the overall system resistance and stiffness respectively; V_C ($= 5 \text{L}$) is the lung vital capacity.

Without assuming a specific airflow pattern, the mechanical cost of breathing is estimated as follows:

$$\begin{aligned} V &\sim V_T \\ \dot{V} &\sim V_T \cdot freq \\ \ddot{V} &\sim V_T \cdot freq^2 \end{aligned}$$

Such that,

$$\begin{aligned} \dot{W} &= freq \int \left[\frac{P\dot{V}}{\left(1 - \frac{V_T}{V_C}\right)^n} + \lambda\ddot{V}^2 \right] dt, \quad \text{s.t. } P = R\dot{V} + EV \\ &= freq \int \left[\frac{(R\dot{V} + EV)\dot{V}}{\left(1 - \frac{V_T}{V_C}\right)^n} + \lambda\ddot{V}^2 \right] dt \\ &\sim \frac{\eta_1 R V_T^2 \cdot freq^2 + \eta_2 E V_T^2 \cdot freq}{\left(1 - \frac{V_T}{V_C}\right)^n} + \lambda' (V_T \cdot freq^2)^2 \end{aligned} \quad (4.13)$$

The four parameters η_1 , η_2 , n and λ' are dependent on the actual airflow profile and the relative weight between the two terms in \dot{W} (Yamashiro & Grodins, 1971;

Hämäläinen & Sipilä, 1984). To produce a realistic breathing pattern, they are determined here by fitting the simulated pattern to the clinical data of a normal subject from (Wasserman *et al.*, 1997), and it is assumed that these parameters remain relatively constant over the range of conditions tested.

To determine the parameters, the mean values of the data point in Fig. 3 in Wasserman *et al.* (1997) were extracted graphically, denoted as $V_{T,Data}$, $freq_{Data}$ and $\dot{V}_{E,Data}$. The optimal set of the parameters to predict the clinical data was determined by minimizing the following error function:

$$e^2 = \sum_{i=1}^9 [(V_{T,Data_i} - V_{T,Predicted_i})^2 + (freq_{Data_i} - freq_{Predicted_i})^2] \quad (4.14)$$

where $V_{T,Predicted}$ and $freq_{Predicted}$ are the tidal volume and breathing frequency predicted by Eq. 4.13 based on $\dot{V}_{E,Data}$.

The fitting result with the clinical data is shown in Figure 4.3. The values of parameters obtained are as follow:

$$\eta_1 = 1; \eta_2 = 1; n = 1; \text{ and } \lambda' = 0.005$$

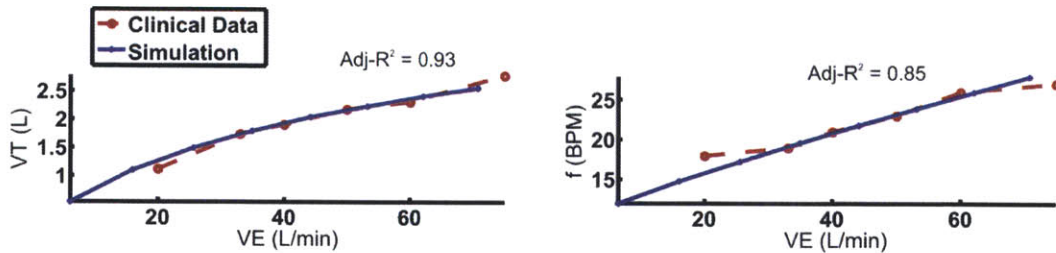


Figure 4.3 Simulated breathing pattern fitted to clinical data to determine parameter values for mechanical work index.

4.5 GAS EXCHANGE EQUATION UNDER DIFFERENT PULMONARY GAS EXCHANGE DEFECTS

4.5.1 Congestive heart failure

Congestive heart failure (CHF) patients suffer from reduced cardiac output. This leads to reduced or no pulmonary perfusion to well ventilated lung unit (Wasserman *et al.*, 1997). The condition can be simplified with a parallel dead space (Figure 4.4), where a portion of the tidal volume is wasted in a lung unit of volume V_D which does not receive perfusion, hence no gas exchange occurs. As a result, gas in the perfused lung unit ($V_T - V_D$) will be in equilibrium with P_{aCO_2} while gas in the non-perfused unit (V_D) will remain at the partial pressure as the inspired gas ($P_{CO_2} = 0$). During expiration, the gas from the two units will mix together. The result is that the mixed expired P_{CO_2} will be lower than P_{aCO_2} as shown in the expired CO_2 trace in Figure 4.4.

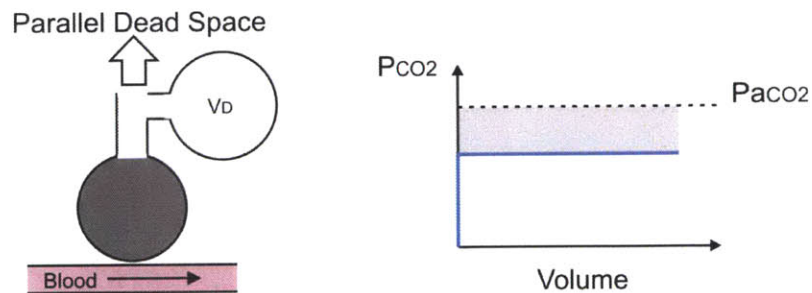


Figure 4.4 Illustration of parallel dead space, V_D , and the corresponding expired CO_2 trace.

Assuming complete mixing, the gas exchange equation can be shown:

$$\begin{aligned}
 freq \cdot (V_T - V_D) \cdot P_{aCO_2} + freq \cdot V_D \cdot 0 &= freq \cdot V_T \cdot P_{\bar{E}CO_2} \\
 P_{aCO_2} &= P_{\bar{E}CO_2} + \frac{V_D}{V_T} P_{aCO_2} \\
 P_{aCO_2} &= \frac{K\dot{V}_{CO_2}}{\dot{V}_E} + \frac{V_D}{V_T} P_{aCO_2} \\
 &= \frac{K\dot{V}_{CO_2}}{\dot{V}_E (1 - V_D/V_T)}
 \end{aligned} \tag{4.15}$$

where the severity of the disease can be reflected by the ratio V_D/V_T . V_D/V_T remains relatively constant from rest to exercise in these patients (Wasserman *et al.*, 2005).

Furthermore, these patients are also found to develop lung restriction and reduced vital capacity (Wasserman *et al.*, 1997).

4.5.2 Right-to-left shunts

Patients with significant right-to-left shunt have a portion of blood flow by-passing the ventilated lung unit (shunt blood). Hence, a shunt allows venous blood of higher P_{CO_2} to reach the end capillary side without undergoing gas exchange. When the clean blood (blood that passes through the ventilated lung unit and is in equilibrium with the alveolar gas at P_{ACO_2}) reaches the end capillary side, it will mix with the shunt blood and the resultant blood P_{aCO_2} will be increased by the shunt blood, and hence higher than P_{CO_2} in the expired gas as shown in the expired CO_2 trace in Figure 4.5. The expired CO_2 trace is similar to CHF (Figure 4.4) and hence right-to-left shunt is often confused with a true alveolar dead space (Hedenstierna & Sandhagen, 2006).

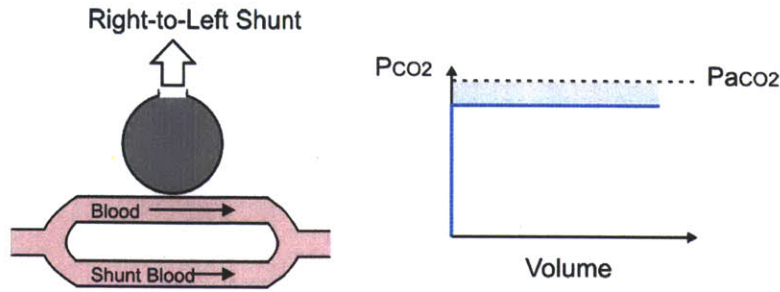


Figure 4.5 Illustration of right-to-left shunt and the corresponding expired CO₂ trace.

The effect of shunt can be modeled based on conservation of mass (Kuwabara & Dencalf, 1969; Mecikalski *et al.*, 1984). The gas exchange equation will become:

$$P_{aCO_2} = \frac{K\dot{V}_{CO_2}}{\dot{V}_E} + \frac{(\dot{Q}_S / \dot{Q}_T)\dot{V}_{CO_2}}{S\dot{Q}_T(1 - \dot{Q}_S / \dot{Q}_T)} \quad (4.16)$$

where \dot{Q}_T and \dot{Q}_S are the total cardiac blood flow and shunt blood flow; S is the CO₂ solubility in blood. \dot{Q}_T is taken as a linear function of \dot{V}_{CO_2} (Åstrand *et al.*, 1964).

$$\dot{Q}_T = 8.51 \cdot \dot{V}_{CO_2} + 3.66 \quad (4.17)$$

Equation 4.16 suggests that the shunt is like a pseudo “inhaled CO₂”, which is dependent on the shunt ratio, \dot{Q}_S / \dot{Q}_T ratio, CO₂ solubility and the ratio of $\dot{V}_{CO_2} / \dot{Q}_T$.

4.5.3 External Dead Space

External dead space has been commonly used for challenging the respiratory system. However, the underlying mechanism is very unclear. External dead space (e.g. equipment dead space in a ventilatory circuit) is usually taken as an additional component to the physiological dead space indicated by its physical volume (Wasserman *et al.*, 2005). However, we show that it is of quite a different nature compared to an alveolar (parallel) dead space like in CHF.

To gain some qualitative insight regarding the problem, we examined the evolution of CO₂ along the airway pathway during a breath cycle by considering the one-dimensional convection-diffusion equation (derived in Scherer *et al.*, 1972; Scherer *et al.*, 1988):

$$\left(1 + \frac{V_A}{V_c}\right) \frac{\partial P_{CO_2}}{\partial t} + \left(\frac{\dot{Q}}{V_c}\right) \frac{\partial P_{CO_2}}{\partial z} = \frac{1}{V_c} \frac{\partial}{\partial z} \left[\frac{D_{mol} A}{L} \frac{\partial P_{CO_2}}{\partial z} \right] + \frac{S}{V_c} \quad (a)$$

$$S(z, t) = \frac{N_A(z)}{N_T} \dot{Q}_B \lambda (\sqrt{P_{BCO_2}} - \sqrt{P_{CO_2}(z, t)}) \quad (b)$$
(4.18)

where

z	Weibel's generational (geometric) coordinates
t	time
$V_A(z, t)$	Alveolar volume at generation z at time t to account for tidal volume
$V_c(z)$	Airway volume of generation z
$\dot{Q}(z, t)$	Volumetric air flow rate in generation z at time t
D_{mol}	Molecular diffusivity of CO ₂
$A(z)$	Total airway cross sectional area of generation z
$L(z)$	Airway length in generation z
$N_A(z)$	Number of alveoli in generation z
N_T	Total number of alveoli in Weibel's lung
\dot{Q}_B	Total cardiac output
P_{BCO_2}	Pulmonary arterial blood P _{CO₂}
λ	CO ₂ solubility in blood

The term $S(z, t)$ in Eq. 4.18 represents the evolution of CO₂ from the blood into lung air space. It is a function of local concentration gradient of CO₂ between the blood and alveolar; as well as local blood flow. A sinusoidal air flow pattern is assumed.

A modified Weibel's Lung Model was used to describe the geometry of the lung system, which provides realistic human dimensions of airway (Weibel, 1963; Schwardt *et al.*, 1991). Briefly, the Weibel's lung model divides the trachio-bronchial tree into 24 generations of airway branching (0th generation being the opening of trachea). This model provides detailed anatomic dimensions of each generation from measurement of a human

lung ($V(z)$, $L(z)$, $A(z)$, $N_A(z)$). In this simulation, generations 0-16 are conductive pathways while generations 17-23 are alveolated airways which can expand ($V_A(z,t)$) to account for the tidal volume. (Refer to (Scherer *et al.*, 1988; Schwardt *et al.*, 1991) for more details)

To account for the change of blood CO₂ tension due to change in total ventilation (and breathing pattern), we incorporated the following dynamics of CO₂ in a tissue compartment. It is assumed that blood leaves the lung at tension in equilibrium with the alveolar gas. The blood passes through a tissue compartment which generates CO₂ at a rate of \dot{V}_{CO_2} and is carried away by the blood. The blood will leave the tissue compartment at a concentration of P_{BCO_2} and circulate to the lung. Diffusion is assumed to reach equilibrium very quickly.

$$\begin{aligned} \frac{dP_{BCO_2}}{dt} &= \frac{\dot{Q}_B}{V_{TCO_2}} (\bar{P}_{ACO_2} - P_{BCO_2}) + \frac{\dot{V}_{CO_2}}{bV_{TCO_2}} & (a) \\ \bar{P}_{ACO_2}(t) &= \frac{\sum_z V_A(z,t) \cdot P_{CO_2}(z,t)}{\sum_z V_A(z,t)} & (b) \end{aligned} \quad (4.19)$$

where \bar{P}_{ACO_2} is the mean P_{CO_2} over the alveolar space, \dot{V}_{CO_2} is the metabolic CO₂ production; V_{TCO_2} is the tissue CO₂ storage, and b is the tissue CO₂ dissociation. See Appendix A for details of numerical simulation method.

To simulate the effect of external dead space (Tube), additional conductive airway was added beyond the 0th generation of the Weibel's lung model. To account for the concentration gradient inside the tube, the tube was divided into M_{DS} generations of equal length and cross-sectional area. Hence, the dead space volume can be changed by changing M_{DS} . A sample simulation programmed in Matlab using $M_{DS} = 10$ (resulting in a tube of volume $V_{Dex} = 1L$) is shown in Figure 4.6.

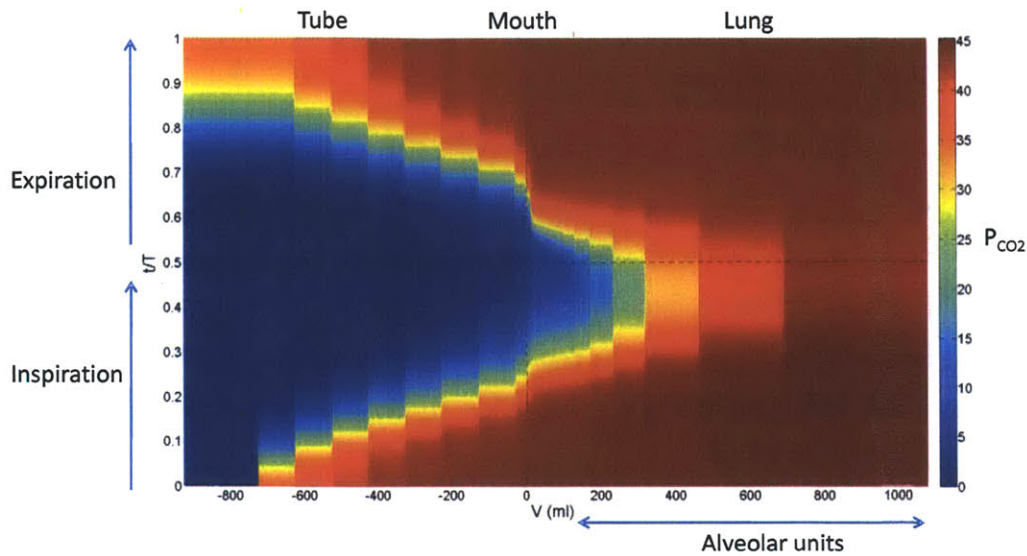


Figure 4.6 Distribution of P_{CO_2} along the airway over a breath cycle in the presence of an external dead space. Tube volume $V_{Dex} = 1L$.

This simulation shows a significant amount of residue CO_2 left in the tube at the end of expiration. The residual CO_2 significantly clogs the airway during the subsequent inspiration to the extent that it takes 60% of the inspiratory duration before fresh air reaches the alveolar units. Figure 4.7 shows the expired CO_2 trace as measured at both the mouth and the end of the tube. Here, the ΔP_{CO_2} in external dead space has two components. The area between the two curves indicates the amount of CO_2 that would be re-inhaled in the next breath cycle, while the area between P_{aCO_2} and the mouth curve indicates other intrinsic gas exchange defects of the body and additional gas exchange defects due to the dead space volume and gas mixing.

Figure 4.8 shows ΔP_{CO_2} increases with the size of the dead space. As a result, the amount of CO_2 rebreathing significantly increases with larger the dead space. In practice, a finite amount of CO_2 is always reinhaled as a result of the presence of external dead space. It is also shown that ΔP_{CO_2} is dependent on the breathing pattern (Figure 4.9). For

the same external dead space, ΔP_{CO_2} is reduced as breathing becomes deeper and slower with the same total ventilation.

Figure 4.10A summarizes the results from a series of simulations with a range of combinations of V_T and breathing frequency. This figure shows that ΔP_{CO_2} decreases with increasing total ventilation (or tidal volume) at fixed breathing frequency, and ΔP_{CO_2} increases with high breathing frequency and small tidal volume combinations at fixed total ventilation. This breathing pattern dependence is a result of changes of gas diffusion efficiency, where larger V_T and slower breathing allows more thorough gas mixing and deeper penetration of fresh air.

Figure 4.10B shows ΔP_{CO_2} as a function of \dot{V}_E over a range \dot{V}_{CO_2} when V_T and breathing frequency are obtained from minimization of Eq. 4.12. ΔP_{CO_2} decreases monotonically with \dot{V}_E and increases with \dot{V}_{CO_2} .

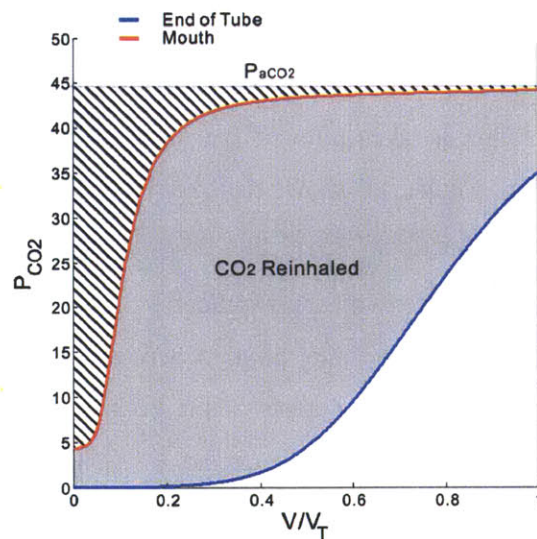


Figure 4.7 Expired CO_2 trace at mouth (red) and at end of tube (blue). Two components of ΔP_{CO_2} are illustrated.

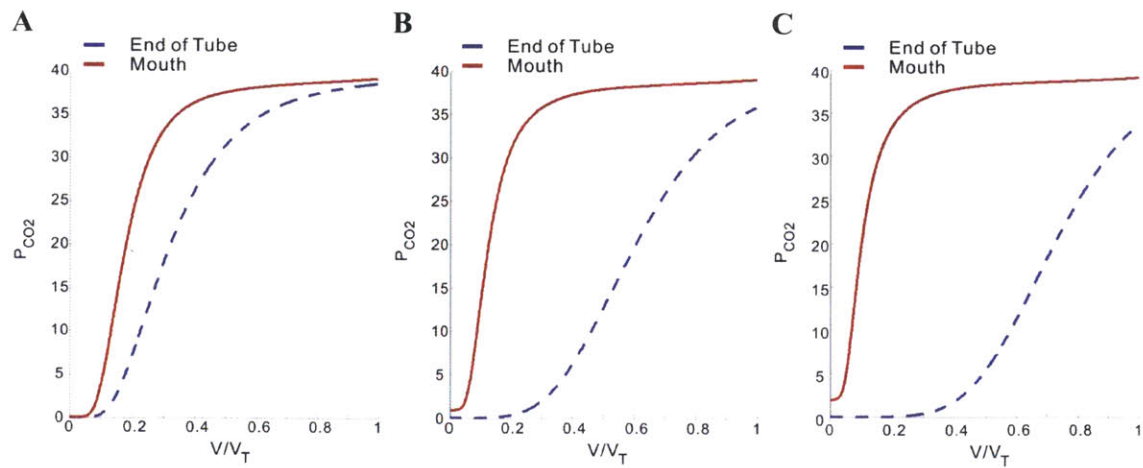


Figure 4.8 Change of ΔP_{CO_2} as a function of external dead space volume. (A) 200ml; (B) 600ml; (C) 1000ml.

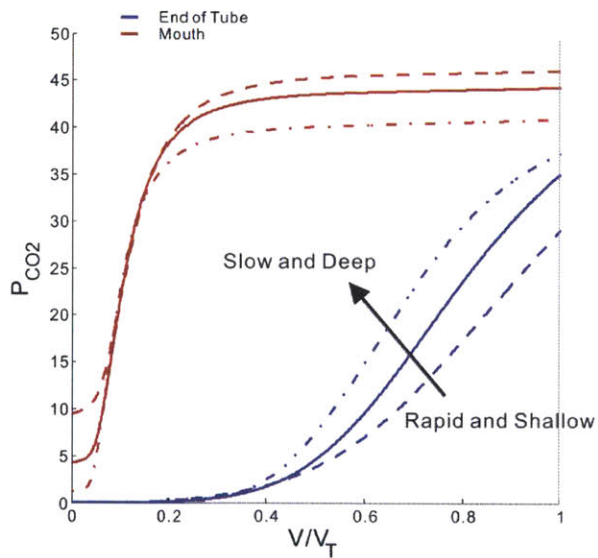


Figure 4.9 Dependence of ΔP_{CO_2} on breathing pattern (1) rapid shallow (dashed lines); (2) normal (solid line) and (3) slow deep (dash-dot lines) with constant total ventilation. (Red lines represent expired CO₂ trace at mouth and blue lines represent expired CO₂ trace at end of tube.)

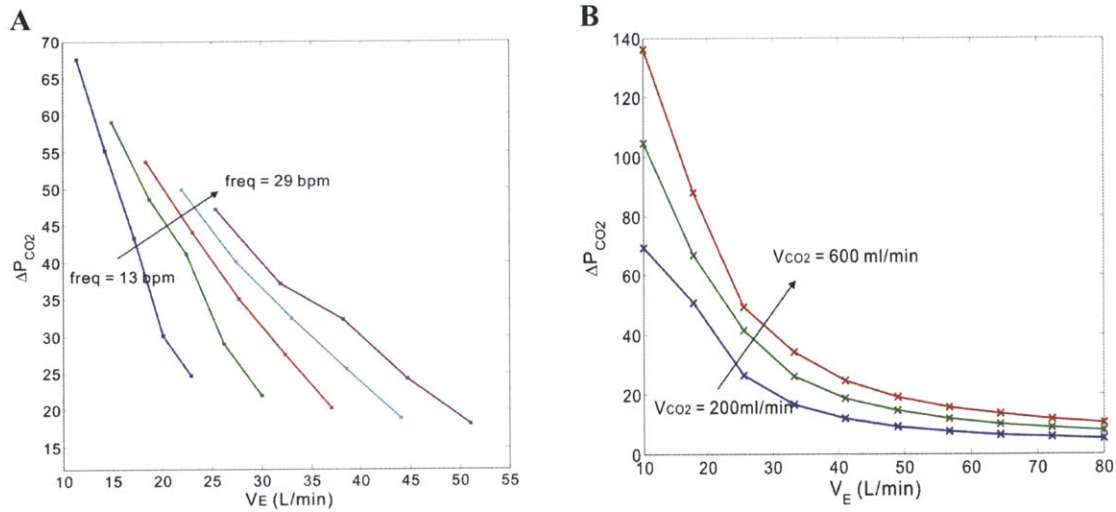


Figure 4.10 (A) ΔP_{CO_2} as a function of total ventilation and breathing frequency; (B) ΔP_{CO_2} as a function of \dot{V}_E at three levels of \dot{V}_{CO_2} (V_T and breathing frequency are obtained from minimization of Eq.4.12). ($V_{Dex} = 1L$).

These simulation results showed that

$$\Delta P_{CO_2} = \Delta P_{CO_2}(\dot{V}_E, f, V_{Dex}, \dot{V}_{CO_2}) \quad (4.20)$$

In fact, ΔP_{CO_2} now represents CO_2 breathing from the tube and its concentration is breathing pattern dependent. ΔP_{CO_2} reaches significant size especially with a large dead space, which is high enough to result in hypercapnia (Poon, 1992).

4.6 THE EFFECT OF EXTERNAL DEAD SPACE, PARALLEL DEAD SPACE AND SHUNT ON OPTIMIZATION OF RESPIRATORY CONTROL

4.6.1 Congestive heart failure

Using Eq. 4.15, the optimal respiratory response of CHF can be shown as follow by referring to Eq. 4.9:

$$\dot{V}_E^* = \alpha^2 (P_{aCO_2} - \beta) \frac{K \dot{V}_{CO_2}}{1 - V_D/V_T} \quad (4.21)$$

Eq. 4.21 predicts an augmented exercise ventilatory response as the metabolic CO₂ was effectively “scaled up” by a factor of $1/(1 - V_D/V_T)$. To illustrate the idea, the condition of CHF was simulated as follows.

The increase in dead space to tidal volume ratio was modeled on the basis of (Jones *et al.*, 1966), where the dead space was shown to be a linear function of tidal volume:

$$V_D = C_1 \cdot V_T + C_2 \quad (4.22)$$

In normal subjects, $C_1 = 0.077$ and $C_2 = 0.138$ (L) as suggested by (Jones *et al.*, 1966). For CHF, the values were chosen as $C_1 = 0.45$ and $C_2 = 0.005$ (L). The choice of these values so that the V_D/V_T ratio was higher than normal and it remained relatively constant as exercise became more vigorous as suggested in (Sullivan *et al.*, 1988; Wasserman *et al.*, 2005). Clark *et al.* (1995) has shown that increased breathing frequency in CHF patient does not contribute to increased $\dot{V}_E - \dot{V}_{CO_2}$ slope. In addition, V_C (= 3.5L) and E (= 20 cmH₂O L⁻¹) were decreased and increased, respectively, in CHF patients.

Figure 4.11 shows the results of our simulation of exercise responses in healthy subjects and CHF patients. The simulation shows several key clinical observations in

CHF patients compared to healthy subjects (Wasserman *et al.*, 1997). First, the augmented exercise response in CHF shows an increased slope in $\dot{V}_E - \dot{V}CO_2$ curve. Second, Pa_{CO_2} remains in the normal range in CHF patient over the range of exercise level concerned. Furthermore, the rapid shallow breathing pattern in CHF is reproduced as a result of increased lung stiffness and reduced vital capacity. The simulated pattern was compared with the clinical data in (Wasserman *et al.*, 1997).

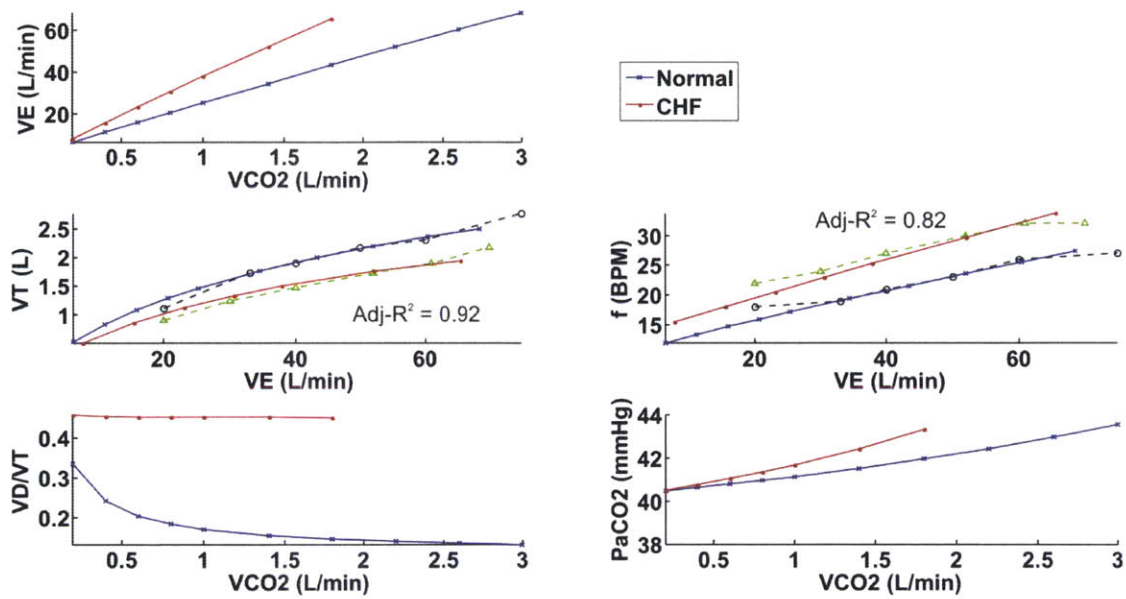


Figure 4.11 Simulated exercise respiratory response of CHF patient compared with normal subject. CHF patients demonstrated augmented ventilation, with a rapid shallow pattern. The dashed lines are clinical data adopted from (Wasserman, K., Y.-Y. Zhang, et al., *Circulation*, 1997.). Prediction of breathing pattern is characterized by adj-R² values.

4.6.2 Right-to-left shunts

Using Eq. 4.16, the optimal respiratory response of right-to-left shunt can be shown as:

$$\begin{aligned} \dot{V}_E^* &= \alpha^2 (P_{aCO_2} - \beta) K \dot{V}_{CO_2} \quad (a) \\ P_{iCO_2} &= \frac{(\dot{Q}_S / \dot{Q}_T) \dot{V}_{CO_2}}{S \dot{Q}_T (1 - \dot{Q}_S / \dot{Q}_T)} \quad (b) \end{aligned} \quad (4.23)$$

Here, from the perspective of control of breathing, the exercise ventilatory response is not different from breathing CO₂. The inhaled CO₂ partial pressure is indicated by Eq. 4.23b.

Figure 4.12A shows the results of our simulation. This simulation is consistent with two key clinical observations in right-to-left shunt (Sietsema *et al.*, 1988). First, the exercise response is augmented with increasing shunt, as a result of multiplicative “CO₂”-exercise interaction. Second, P_{aCO₂} remains within the normal range (<45mmHg) even when the shunt reaches 50% at relatively high exercise intensity. Figure 4.12B shows the change of the size of the equivalent "inhaled CO₂" as shunt increases at rest ($\dot{V}_{CO_2} = 0.2L/min$) and a moderate exercise level ($\dot{V}_{CO_2} = 1.4L/min$). The curve is relatively flat when $\dot{Q}_S / \dot{Q}_T < 60\%$ but increases quickly beyond that. Hence, the normocapnia in shunt is a result of generally low concentrations of “inhaled CO₂”. However, it increasingly challenges the respiratory system, and when, for instance, the cardiac output fails to catch up with increasing work rate, patients may become hypercapnic.

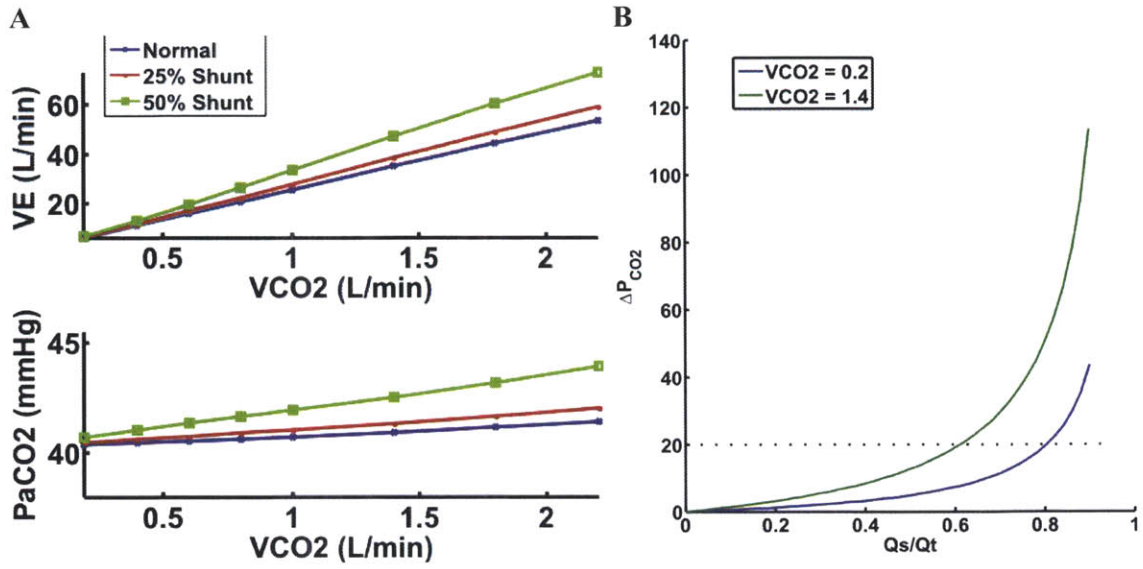


Figure 4.12 (A) Simulated exercise respiratory response of two levels of right-to-left shunt compared with normal. Increased shunt fraction is associated with augmented ventilation. (B) Change of ΔP_{CO_2} as a function of shunt fraction and metabolic CO_2 .

4.6.3 External Dead Space

Equation 4.20 shows that ΔP_{CO_2} is now an explicit function of total ventilation \dot{V}_E (and breathing pattern). Referring to the optimal solution in Eq. 4.9, which is repeated here:

$$\dot{V}_E^* = \alpha^2 (P_{aCO_2} - \beta) \left(K \dot{V}_{CO_2} - \dot{V}_E^2 \frac{\partial \Delta P_{CO_2}}{\partial \dot{V}_E} \right) \quad (a) \quad (4.24)$$

$$P_{ICO_2} = \Delta P_{CO_2} > 0 \quad (b)$$

Note, we have assumed that breathing pattern (V_T, f) is determined solely by mechanical factor (Eq. 4.13), and V_T and f can be expressed as functions in only \dot{V}_E . Therefore,

$$\Delta P_{CO_2} = \Delta P_{CO_2}(\dot{V}_E, f(\dot{V}_E), V_{Dex}, \dot{V}_{CO_2}) = \Delta P_{CO_2}(\dot{V}_E, V_{Dex}, \dot{V}_{CO_2}) \quad (4.25)$$

From Figure 4.10B, we can deduce that $\frac{\partial \Delta P_{CO_2}}{\partial \dot{V}_E} \leq 0$. Therefore, the external dead space leads to an effective metabolic CO₂ load larger than the true metabolic CO₂ load:

$$K\dot{V}_{CO_2} - \dot{V}_E^2 \frac{\partial \Delta P_{CO_2}}{\partial \dot{V}_E} \geq K\dot{V}_{CO_2} \quad (4.26)$$

Equations 4.24 and 4.26 predict stronger potentiation of $\dot{V}_E - \dot{V}_{CO_2}$ slope by external dead space compared to CO₂ breathing ($\frac{\partial \Delta P_{CO_2}}{\partial \dot{V}_E} = 0$) with matched P_{aCO_2} (hypercapnia or normocapnia). Intuitively, increasing \dot{V}_E in dead space loading can remove the additional CO₂ load in both of terms $\frac{K\dot{V}_{CO_2}}{\dot{V}_E}$ and ΔP_{CO_2} in the gas exchange equation, while ΔP_{CO_2} is constant independent of \dot{V}_E in CO₂ breathing. As such, one has more incentive to increase \dot{V}_E to restore P_{aCO_2} towards normal level. Consequently, the augmented potentiation of $\dot{V}_E - \dot{V}_{CO_2}$ in dead space loading is consistent with an optimal strategy for homeostasis. Equation 4.24 shows that external dead space has a primary effect of inhaled CO₂ ($P_{ICO_2} = \Delta P_{CO_2}$) and with secondary effect like an apparent parallel dead space effect (Eq. 4.26).

To illustrate the idea, we obtain the following empirical expression of ΔP_{CO_2} from the above simulations, with parameters adjusted to mimic the results in (Poon, 1992):

$$\begin{aligned} \Delta P_{CO_2} &= A \exp\left(\frac{-(\dot{V}_E + 20)}{20}\right) + B \\ A &= 256.5\dot{V}_{CO_2} + 90 \\ B &= 8.7\dot{V}_{CO_2} + 11 \end{aligned} \quad (4.27)$$

Figure 4.13 shows the result of the simulation of external dead space loading compared with CO₂ inhalation. The simulation shows several key observations from experimental studies on healthy human subjects breathing through an external dead space (Poon, 1992). First, exercise ventilatory response is augmented by both external dead space and inhaled CO₂, while the $\dot{V}_E - \dot{V}_{CO_2}$ slope is larger in dead space breathing than in CO₂ breathing. Second, both experimental conditions result in hypercapnia. Furthermore, under both situations, normal breathing patterns are acquired.

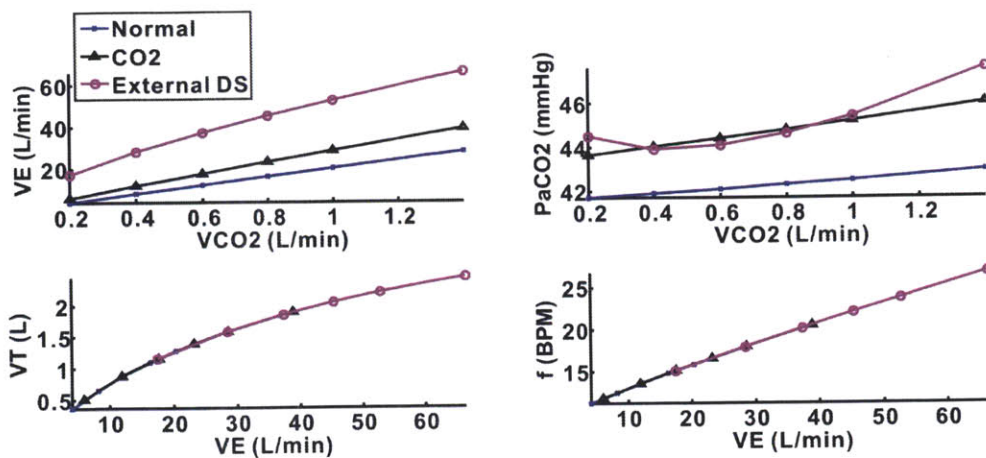


Figure 4.13 Simulated exercise respiratory response of external dead space loading compared with normal and inhaled CO_2 . External dead space resulted in a stronger augmented exercise ventilatory response than inhaled CO_2 . Both cases results in hypercapnia with normal breathing pattern.

4.7 DISCUSSION

The present study shows that an optimal respiratory control model of mechanical-chemical interaction consistently predicts some key characteristics of exercise ventilatory response in a range of pulmonary gas exchange defect problems (Figure 4.14). It provides a powerful framework to understand the mechanisms underlying control of a complex physiological system, which significantly surpasses the capability of the traditional reductionist approach.

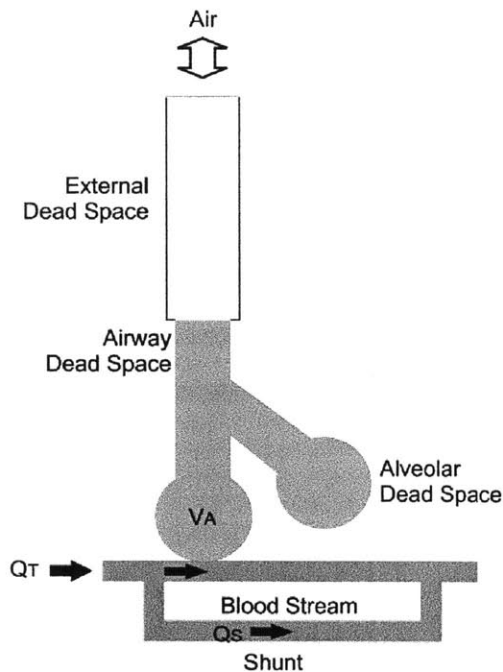


Figure 4.14 Compartment model indicating pulmonary gas exchange defect problem under present study.

4.7.1 Optimization as a framework for afferent interaction in homeostatic control

Optimization strategy in respiratory control has been well recognized as in other biological systems, owing its root to Darwinian theory. The fact that infinitely many combinations of tidal volume and frequency can achieve the same ventilation suggests that there is a specific strategy for a natural choice of breathing pattern. The optimization of breathing pattern based on a certain mechanical work index has been addressed by a number of investigators (Mead, 1960b; Yamashiro & Grodins, 1971; Hämäläinen & Viljanen, 1978a; Hämäläinen & Viljanen, 1978b; Hämäläinen & Sipilä, 1984). The implicit assumption is that ventilation is determined solely by the reflex response to various chemical stimuli (chemoreceptors and exercise stimulus). Instead, the optimal respiratory control hypothesis proposed by Poon (1983a, 1987a) suggests that the brainstem may adaptively adjust its controller gain to track the metabolic CO_2 , instead of using an independent exercise stimulus adding linearly to the chemoreflex, in order to maintain isocapnia.

The present study shows that the optimization model is capable of reproducing some key characteristics of exercise ventilatory response under different conditions of pulmonary gas exchange defects as observed clinically and experimentally. The model provides a convenient framework to understanding the overall effect of multiple risk factors impacting the system from a behavioral level. This integrative model may be extended to explain behaviors involving multi-systems. For instance, the conflict between thermoregulation and respiration is well recognized (von Euler, 1961; Squire, 2006), especially in furred animals. These animals are not able to remove excess heat by sweating. Hence, they have to rely on panting for thermoregulation during exercise, especially under high ambient temperature (Schmidt-Nielsen *et al.*, 1970; Goldberg *et al.*, 1981; Baker, 1982; Schroter *et al.*, 1987; Nijland & Baker, 1992; Entin *et al.*, 2005; Robertshaw, 2006). As such, thermoregulation and blood gas homeostasis compete for the same machinery, the act of breathing, especially when the animal is stressed by environmental heat/coldness or exercise. The conflict can be resolved by optimizing the overall need for homeostasis of body temperature and blood gas chemistry. Recent studies show that feedback afferent signal of inspiratory drive by central chemoreceptor and feedforward signal of body temperature by cutaneous thermoreceptor converge at LPBN in the dorsolateral pons (Nakamura & Morrison, 2008; Poon, 2009). These studies support the notion of brain computation involving simultaneous information about blood gas concentration and body temperature. In light of this example, the concept of optimization deserves further exploration to generalize to other homeostatic systems.

4.7.2 Different mechanisms underlying isocapnic augmented exercise hyperpnea in CHF and shunt

CHF patients and patients with significant right-to-left shunts are found to maintain normal P_{aCO_2} even during exercise. These seemingly similar behaviors were shown to result from different mechanisms from the perspective of control of breathing. The effect of CHF on gas exchange is a homogenous increase of dead space while right-to-left shunt mimics airway CO_2 loading. The optimization model predicts augmented

exercise ventilatory response as a result of increased effective “metabolic CO₂” and CO₂-exercise synergistic interaction respectively. The model also provides a quantitative predictor for the impacts of various physiological factors on the exercise response and blood gas homeostasis.

4.7.3 Mechanisms of potentiation of exercise ventilatory response by added dead space: Optimization vs. short term modulation

In a series of goat and human studies (Mitchell, 1990; Wood *et al.*, 2008, 2009), Mitchell and colleagues demonstrated that exercise ventilatory response was potentiated by added dead space, similar to the report in (Poon, 1992). The authors called the potentiation “short term modulation (STM)”. They proposed that STM is elicited by feedforward excitation of serotonin release in ventral spinal cord as a result of increased resting ventilatory drive in added dead space. Serotonin receptor activation on respiratory motor neurons would increase their excitability and hence amplify the descending respiratory drive from brainstem respiratory premotor neurons.

In the present study, we demonstrate mathematically that such potentiation by added dead space can be explained with a general optimization scheme of respiratory control (Section 4.6.3). Hence, the serotonin-dependent STM may represent the execution of such optimal decision computed in the brain stem respiratory control center.

4.7.4 Influence of chemical afferent signal on breathing pattern revealed by comparing airway CO₂ and dead space loading

Hypercapnia resulting from external dead space loading in subjects adopting a normal breathing pattern (Poon, 1992) suggests that the brainstem controller does not use the degrees of freedom of V_T and breathing frequency independently to minimize the dead space effect to restore normocapnia (hence, reducing chemical cost). In this case,

Equations 4.10 and 4.11 are integrated into one single optimization problem. For instance, one can increase ventilation by increasing V_T alone such that a smaller ΔP_{CO_2} can be obtained compared to the other way.

This provides the basis for considering chemical factor in ventilation optimization but not breathing pattern optimization. This distinction may result from the different bandwidth between dynamics of chemical afferent signals (slower) and phasic mechanical feedback (faster, breath-by-breath). On the other hand, McParland et al. (1991) reported bradypnea at high work rate during dead space loading. More investigation will be required to further elucidate the role of chemical signal on determining breathing pattern.

4.8 CONCLUSIONS

This study show that an integrative optimization respiratory control model provides consistent prediction of exercise respiratory response under a variety of chemical challenges. The model demonstrates, from the behavior level, an adaptive mechanism of the respiratory control by integrating mechanical, chemical and metabolic factors.

Appendix A: Numerical simulation for external dead space

See also (Scherer *et al.*, 1988)

Assuming a sinusoidal airflow pattern,

$$\dot{V} = \frac{1}{2} V_T \omega \sin \omega t \quad (\text{A.1})$$

where $\omega = 2\pi f/60$ and f is the breathing frequency.

The numerical simulation is formulated as following. We used Δt as the time step and the time index $n = 1, 2, \dots, N$; Δz as the lung airway generational step and the generational index $i = 1, 2, \dots, M$. For the simulation here, $\Delta z = 1$ and $\Delta t = 1 \times 10^{-5} \sim 5 \times 10^{-3}$ sec with specific time step chosen to produce a stable simulation.

$$\begin{aligned} \text{if } i < z_A, \quad \dot{Q}(i, n) &= \dot{V}(n) \\ \text{if } i \geq z_A, \quad \dot{Q}(i, n) &= \dot{V}(n) \left(1 - \sum_{k=z_A}^i \frac{N_A(k, n)}{N_T} \right) \end{aligned} \quad (\text{A.2})$$

where z_A is the first alveolar generation.

$$V_A(i, n) = \frac{N_A(i)}{N_T} (V(n) + V_{AT}^0) \quad (\text{A.3})$$

where V_{AT}^0 is the total alveolar volume at the beginning of inspiration.

For inspiration:

$$\begin{aligned}
& \left[1 + \frac{V_A(i, n)}{V_c(i)} \right] \left[\frac{P_{CO_2}(i, n+1) - P_{CO_2}(i, n)}{\Delta t} \right] + \frac{\dot{Q}(i, n)}{V_c(i)} \left[\frac{P_{CO_2}(i, n) - P_{CO_2}(i-1, n)}{\Delta z} \right] \\
& = \frac{D_{mol}}{V_c(i)} \left\{ \left[\frac{P_{CO_2}(i, n) - P_{CO_2}(i-1, n)}{\Delta z} \right] \left[\frac{A(i)/L(i) - A(i-1)/L(i-1)}{\Delta z} \right] \right. \\
& \quad \left. + \frac{A(i)}{L(i)} \left[\frac{P_{CO_2}(i+1, n) - 2P_{CO_2}(i, n) + P_{CO_2}(i-1, n)}{\Delta z^2} \right] \right\} \\
& \quad + \frac{1}{V_c(i)} \frac{N_A(i)}{N_T} \dot{Q}_B \lambda (\sqrt{P_{BCO_2}(n)} - \sqrt{P_{CO_2}(i, n)})
\end{aligned} \tag{A.4}$$

The boundary conditions are:

$$P_{CO_2}(0, n) = 0$$

$$\begin{aligned}
& \left[1 + \frac{V_A(M, n)}{V_c(M)} \right] \left[\frac{P_{CO_2}(M, n+1) - P_{CO_2}(M, n)}{\Delta t} \right] \\
& = - \frac{D_{mol}}{V_c(M)} \frac{A(M-1)}{L(M-1)} \left[\frac{P_{CO_2}(M, n) - P_{CO_2}(M-1, n)}{\Delta z^2} \right] \\
& \quad + \frac{1}{V_c(M)} \frac{N_A(M)}{N_T} \dot{Q}_B \lambda (\sqrt{P_{BCO_2}} - \sqrt{P_{CO_2}(M, n)})
\end{aligned} \tag{A.5}$$

For expiration:

$$\begin{aligned}
& \left[1 + \frac{V_A(i, n)}{V_c(i)} \right] \left[\frac{P_{CO_2}(i, n+1) - P_{CO_2}(i, n)}{\Delta t} \right] + \frac{\dot{Q}(i, n)}{V_c(i)} \left[\frac{P_{CO_2}(i+1, n) - P_{CO_2}(i, n)}{\Delta z} \right] \\
& = \frac{D_{mol}}{V_c(i)} \left\{ \left[\frac{P_{CO_2}(i+1, n) - P_{CO_2}(i, n)}{\Delta z} \right] \left[\frac{A(i+1)/L(i+1) - A(i)/L(i)}{\Delta z} \right] \right. \\
& \quad \left. + \frac{A(i)}{L(i)} \left[\frac{P_{CO_2}(i+1, n) - 2P_{CO_2}(i, n) + P_{CO_2}(i-1, n)}{\Delta z^2} \right] \right\} \\
& \quad + \frac{1}{V_c(i)} \frac{N_A(i)}{N_T} \dot{Q}_B \lambda (\sqrt{P_{BCO_2}} - \sqrt{P_{CO_2}(i, n)})
\end{aligned} \tag{A.6}$$

The boundary conditions are:

$$\begin{aligned}
& P_{CO_2}(0, n) = P_{CO_2}(1, n) \\
& \left[1 + \frac{V_A(M, n)}{V_c(M)} \right] \left[\frac{P_{CO_2}(M, n+1) - P_{CO_2}(M, n)}{\Delta t} \right] \\
& = - \frac{D_{mol}}{V_c(M)} \frac{A(M-1)}{L(M-1)} \left[\frac{P_{CO_2}(M, n) - P_{CO_2}(M-1, n)}{\Delta z^2} \right] \\
& \quad + \frac{1}{V_c(M)} \frac{N_A(M)}{N_T} \dot{Q}_B \lambda (\sqrt{P_{BCO_2}} - \sqrt{P_{CO_2}(M, n)})
\end{aligned} \tag{A.7}$$

For blood-tissue gas exchange,

$$\frac{P_{BCO_2}(n+1) - P_{BCO_2}(n)}{\Delta t} = \frac{\dot{Q}_B}{V_{TCO_2}} (\bar{P}_{ACO_2}(n) - P_{BCO_2}(n)) + \frac{\dot{V}_{CO_2}}{bV_{TCO_2}}$$

$$\bar{P}_{ACO_2}(n) = \frac{\sum_{i=ZA}^M P_{CO_2}(i,n) V_A(i,n)}{\sum_{i=ZA}^M V_A(i,n)}$$

(A.8)

Parameters values:

D_{mol}	0.17 cm ² /s
V_{AT}^0	1440 cm ³
λ	86.3
V_{TCO_2}	15L
b	0.0065 ml/ml mmHg

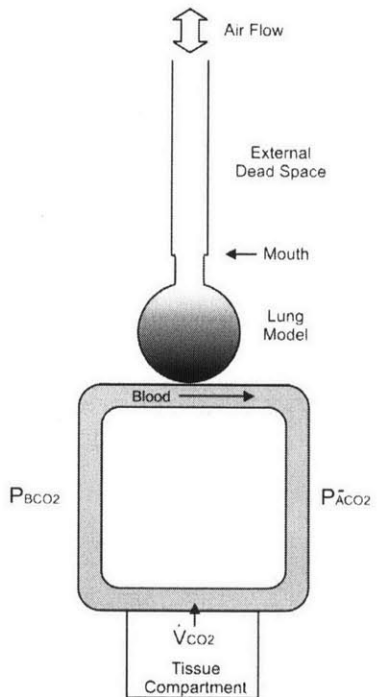


Figure 4.15 Schematic diagram of external dead space simulation

4.9 REFERENCES

- Åstrand PO, Cuddy TE, Saltin B & Stenberg J. (1964). Cardiac output during submaximal and maximal work. *Journal of applied physiology* 19, 268.
- Baker MA. (1982). Brain cooling in endotherms in heat and exercise. *Annual Review of Physiology* 44, 85-96.
- Bartels J, Severinghaus JW, Forster RE, Briscoe WA & Bates DV. (1954). The respiratory dead space measured by single breath analysis of oxygen, carbon dioxide, nitrogen or helium. *J Clin Invest* 33, 41-48.
- Bohr C. (1891). Ueber die lungenathmung. *Skand Arch Physiol* 2, 236-268.
- Clark A, Chua T & Coats A. (1995). Anatomical dead space, ventilatory pattern, and exercise capacity in chronic heart failure. *British heart journal* 74, 377.
- De Robertis E, Sigurdsson SE, Drefeldt B & Jonson B. (1999). Aspiration of airway dead space. A new method to enhance CO₂ elimination. *American journal of respiratory and critical care medicine* 159, 728-732.
- De Robertis E, Uttman L & Jonson B. (2010). Re-inspiration of CO₂ from ventilator circuit: effects of circuit flushing and aspiration of dead space up to high respiratory rate. *Critical care (London, England)* 14, R73.
- Drummond G & Fletcher R. (2006). Editorial II: Dead-space: invasive or not? *British journal of anaesthesia* 96, 4.
- Eldridge FL, Morin D, Romaniuk JR, Yamashiro S, Potts JT, Ichiyama RM, Bell H, Phillipson EA, Killian KJ, Jones NL & Nattie E. (2006). Supraspinal locomotor centers do/do not contribute significantly to the hyperpnea of dynamic exercise in humans. *J Appl Physiol* 100, 1743-1747.
- Enghoff H. (1938). Volumen inefficax. *Ups Laekarefoeren Foerh* 44, 191-218.
- Entin PL, Robertshaw D & Rawson RE. (2005). Reduction of the PaCO₂ set point during hyperthermic exercise in the sheep. *Comparative Biochemistry and Physiology - A Molecular and Integrative Physiology* 140, 309-316.
- Fletcher R, Jonson B, Cumming G & Brew J. (1981). The concept of deadspace with special reference to the single breath test for carbon dioxide. *Br J Anaesth* 53, 77-88.
- Fowler WS. (1948). Lung function studies; the respiratory dead space. *Am J Physiol* 154, 405-416.

- Goldberg MB, Langman VA & Taylor CR. (1981). Panting in dogs: Paths of air flow in response to heat and exercise. *Respiration Physiology* 43, 327-338.
- Hämäläinen RP & Sipilä A. (1984). Optimal control of inspiratory airflow in breathing. *Optimal Control Applications and Methods* 5, 177-191.
- Hämäläinen RP & Viljanen A. (1978a). A hierarchical goal-seeking model of the control of breathing. *Biological Cybernetics* 29, 151-158.
- Hämäläinen RP & Viljanen AA. (1978b). Modelling the respiratory airflow pattern by optimization criteria. *Biological Cybernetics* 29, 143-149.
- Hedenstierna G & Sandhagen B. (2006). Assessing dead space. A meaningful variable? *Minerva Anesthesiol* 72, 521-528.
- Jones N, McHardy G, Naimark A & Campbell E. (1966). Physiological dead space and alveolar-arterial gas pressure differences during exercise. *Clinical science* 31, 19.
- Kuwabara S & Dencalf D. (1969). Effect of anatomic shunt on physiologic deadspace-to-tidal volume ratio-a new equation. *Anesthesiology* 31, 575.
- Langley F, Even P, Duroux P, Nicolas R & Cumming G. (1976). Ventilatory consequences of unilateral pulmonary artery occlusion. *Distribution des échanges gazeux pulmonaires INSERM*, 209–212.
- Lucangelo U & Blanch L. (2004). Dead space. *Intensive Care Med* 30, 576-579.
- Mapleson WW. (1954). The elimination of rebreathing in various semi-closed anaesthetic systems. *British Journal of Anaesthesia* 26, 323.
- Mateika JH & Duffin J. (1995). A review of the control of breathing during exercise. *Eur J Appl Physiol Occup Physiol* 71, 1-27.
- McParland C, Mink J & Gallagher CG. (1991). Respiratory adaptations to dead space loading during maximal incremental exercise. *Journal of applied physiology* (Bethesda, Md : 1985) 70, 55-62.
- Mead J. (1960). Control of respiratory frequency. *J Appl Physiol* 15, 325-336.
- Mecikalski MB, Cutillo AG & Renzetti AD, Jr. (1984). Effect of right-to-left shunting on alveolar dead space. *Bull Eur Physiopathol Respir* 20, 513-519.
- Mitchell GS. (1990). Ventilatory control during exercise with increased respiratory dead space in goats. *J Appl Physiol* 69, 718-727.

- Nakamura K & Morrison SF. (2008). A thermosensory pathway that controls body temperature. *Nature Neuroscience* 11, 62-71.
- Nijland MJ & Baker MA. (1992). Effects of hydration state on exercise thermoregulation in goats. *American Journal of Physiology - Regulatory, Integrative and Comparative Physiology* 263, R201-R205.
- Nuckton TJ, Alonso JA, Kallet RH, Daniel BM, Pittet JF, Eisner MD & Matthay MA. (2002). Pulmonary dead-space fraction as a risk factor for death in the acute respiratory distress syndrome. *New England Journal of Medicine* 346, 1281-1286.
- Poon C-S. (1983). Optimal control of ventilation in hypoxia, hypercapnia and exercise. In *Modeling and Control of Breathing*, ed. Whipp & Wiberg. Elsevier, New York.
- Poon C-S. (1987a). Ventilatory control in hypercapnia and exercise: optimization hypothesis. *J Appl Physiol* 62, 2447-2459.
- Poon C-S. (2009). Optimal interaction of respiratory and thermal regulation at rest and during exercise: Role of a serotonin-gated spinoparabrachial thermoafferent pathway. *Respiratory physiology & neurobiology* 169, 234-242.
- Poon C. (1992). Potentiation of exercise ventilatory response by airway CO₂ and dead space loading. *Journal of Applied Physiology* 73, 591.
- Poon CS. (1987b). Ventilatory control in hypercapnia and exercise: optimization hypothesis. *J Appl Physiol* 62, 2447-2459.
- Poon CS, Lin SL & Knudson OB. (1992). Optimization character of inspiratory neural drive. *J Appl Physiol* 72, 2005-2017.
- Riley RL & Cournand A. (1949). "Ideal" Alveolar Air and the Analysis of Ventilation-Perfusion Relationships in the Lungs. *Journal of Applied Physiology* 1, 825-847.
- Riley RL & Cournand A. (1951). Analysis of Factors Affecting Partial Pressures of Oxygen and Carbon Dioxide in Gas and Blood of Lungs: Theory. *Journal of Applied Physiology* 4, 77-101.
- Robertshaw D. (2006). Mechanisms for the control of respiratory evaporative heat loss in panting animals. *Journal of Applied Physiology* 101, 664-668.
- Scherer P, Shendalman L & Greene N. (1972). Simultaneous diffusion and convection in single breath lung washout. *Bulletin of Mathematical Biology* 34, 393-412.
- Scherer PW, Gobran S, Aukburg SJ, Bartkowski R, Neufeld GR & Baumgardner JE. (1988). Numerical and experimental CO₂ and inert study of steady-state. *J Appl Physiol* 64 1022-1029.

- Schmidt-Nielsen K, Bretz WL & Taylor CR. (1970). Panting in dogs: Unidirectional air flow over evaporative surfaces. *Science* 169, 1102-1104.
- Schroter RC, Robertshaw D, Baker MA, Shoemaker VH, Holmes R & Schmidt-Nielsen K. (1987). Respiration in heat stressed camels. *Respiration Physiology* 70, 97-112.
- Schwardt JD, Gobran SR, Neufeld GR, Aukburg SJ & Scherer PW. (1991). Sensitivity of CO₂ washout to changes in acinar structure in a single-path model of lung airways. *Annals of biomedical engineering* 19, 679-697.
- Secher N, Poon C-S, Ward S, Whipp B & Duffin J. (2006). Supraspinal locomotor centers do/do not contribute significantly to the hyperpnea of dynamic exercise in humans. *J Appl Physiol* 100, 1417-1418.
- Sietsema KE, Cooper DM, Perloff JK, Child JS, Rosove MH, Wasserman K & Whipp BJ. (1988). Control of ventilation during exercise in patients with central venous-to-systemic arterial shunts. *J Appl Physiol* 64, 234-242.
- Squire LR. (2006). *The history of neuroscience in autobiography*. Academic Pr.
- Sullivan M, Higginbotham M & Cobb F. (1988). Increased exercise ventilation in patients with chronic heart failure: intact ventilatory control despite hemodynamic and pulmonary abnormalities. *Circulation* 77, 552.
- Tang Y, Turner MJ & Baker AB. (2005). Effects of alveolar dead-space, shunt and V/Q distribution on respiratory dead-space measurements. *Br J Anaesth* 95, 538-548.
- von Euler C. (1961). *PHYSIOLOGY AND PHARMACOLOGY OF TEMPERATURE REGULATION*. *Pharmacological Reviews* 13, 361-398.
- Waldrop TG, Iwamoto GA & Haouzi P. (2006). Point:Counterpoint: Supraspinal locomotor centers do/do not contribute significantly to the hyperpnea of dynamic exercise. *J Appl Physiol* 100, 1077-1083.
- Ward SA. (2000). Control of the exercise hyperpnoea in humans: a modeling perspective. *Respir Physiol* 122, 149-166.
- Wasserman K, Hansen JE, Sue DY, Stringer WW & Whipp BJ. (2005). *Principles of Exercise Testing and Interpretation*. Lippincott Williams & Wilkins, Philadelphia, PA.
- Wasserman K, Zhang YY, Gitt A, Belardinelli R, Koike A, Lubarsky L & Agostoni PG. (1997). Lung function and exercise gas exchange in chronic heart failure. *Circulation* 96, 2221-2227.

- Weibel E. (1963). Morphometry of the human lung.
- Wood HE, Mitchell GS & Babb TG. (2008). Short-term modulation of the exercise ventilatory response in young men. *J Appl Physiol* 104, 244-252.
- Wood HE, Mitchell GS & Babb TG. (2009). Breathing mechanics during exercise with added dead space reflect mechanisms of ventilatory control. *Respiratory physiology & neurobiology* 168, 210-217.
- Yamashiro SM & Grodins FS. (1971). Optimal regulation of respiratory airflow. *J Appl Physiol* 30, 597-602.
- Yu Y & Poon C-S. (2006). Critique of 'Control of arterial PCO₂ by somatic afferents'. *J Physiol* 572, 897-898.

Chapter 5 Central-peripheral Chemoreceptors Interaction Revealed a Form of Pavlovian Conditioning

5.1 INTRODUCTION

Respiratory chemoreflex response is determined by signal from the central and peripheral chemoreceptors. Extensive research in past decades has afforded rich understanding of the complex patterns, development and mechanisms of the ventilatory responses to hypoxia (Powell *et al.*, 1998; Waters & Gozal, 2003; Kumar & Prabhakar, 2007; Teppema & Dahan, 2010) and hypercapnia (Sovik & Lossius, 2004; Guyenet *et al.*, 2010; Hodges & Richerson, 2010; Nattie, 2011) in health and in disease. A generally accepted simplification in current mathematical models of human respiratory system is that the two feedback signals add linearly (pure additive) to determine the total "reflex".

However, a significant number of reports presented contradictory observations of purely additive (Van Beek *et al.*, 1983; Daristotle & Bisgard, 1989; Clement *et al.*, 1995; StCroix *et al.*, 1996), hypoadditive (Gesell *et al.*, 1940; Tenney & Brooks, 1966; Ou *et al.*, 1976; Berger *et al.*, 1978; Giese *et al.*, 1978; Eldridge *et al.*, 1981; Adams & Severns, 1982; Smith *et al.*, 1984; Day & Wilson, 2007, 2009) or hyperadditive (Adams *et al.*, 1978; Robbins, 1988; Blain *et al.*, 2010) interaction of the two chemoreceptor feedback signals. These reports suggest that central and peripheral chemoreceptor afferents are not simply relayed by pontinemedullary respiratory neurons to the respiratory controller. Rather, they are likely to be integrated in a more sophisticated manner in modulating ventilatory pattern.

Acute hypoxia is known to exert complex time-dependent influences on both inspiratory drive and inspiratory/expiratory rhythms through the induction of short-term potentiation (STP)(Gesell *et al.*, 1942; Eldridge & Millhorn, 1986b; Fregosi, 1991a; Wagner & Eldridge, 1991; Hayashi *et al.*, 1993; Poon *et al.*, 1999b; Poon & Siniaia, 2000; Young *et al.*, 2003a) and depression (STD, or post-hypoxia frequency decline) (Hayashi *et al.*, 1993; Coles & Dick, 1996; Poon *et al.*, 2000). Poon (Poon *et al.*, 1999a) proposed that carotid sinus nerve (CSN) drive likely enhances the efficacy of neurotransmission from a tonic (e.g. central chemoreceptor) drive through STP, which has a computational equivalent as a neural integrator (Poon, 1996a). Young *et al.* (Young *et al.*, 2003b) showed that a bank of such neural integrators operate in parallel in modulating the respiratory pattern by providing necessary frequency and temporal filtering. Hence, central and peripheral chemoreceptors may also interact dynamically through STP/STD.

The question of interest is where in the brain does this interaction occur. Traditionally, the pontine “pneumotaxic center” (Lumsden, 1923b; Song *et al.*, 2006) is thought to contribute importantly to the post-inspiratory (post-I) phase of the respiratory rhythm controlling the inspiratory off-switch (IOS) (Dutschmann & Herbert, 2006; Smith *et al.*, 2007) and provide a fail-safe mechanism for the IOS secondary to vagal feedback. In recent years, it has been increasingly recognized that the dorsolateral and ventrolateral pontine regions may contribute importantly to the modulation of both mechanoreceptor and chemoreceptor reflexes in regulating the respiratory rhythm (Alheid *et al.*, 2004;

Song & Poon, 2004). Lesioning of various regions in the dl-pons, including Kölliker-Fuse nucleus (KFN) and medial (MPBN) and lateral parabrachial nucleus (LPBN), has distinct effects on phrenic response to hypoxia and hypercapnia (Song & Poon, 2009a, 2009b). These sites may constitute the potential loci for the hypercapnia-hypoxia interaction to occur.

By applying the state-of-art in-vivo multielectrode recording system, we identify and characterize respiratory neurons in dl-pons that respond to hypoxia and/or hypercapnia, as well as the form of interaction that occurs when the stimuli are presented together. Our findings suggest that the hypercapnia-hypoxia hypoaddivitive interaction represents a form of associative learning for activity-dependent and pairing-specific STP and STD of chemoreflex responses.

5.2 METHODS

5.2.1 Animal preparation

Experiments were performed on 27 adult, male Sprague-Dawley rats (330–380 g, Charles River Laboratories, Wilmington, MA). All experimental protocols were reviewed and approved by the M.I.T. Committee on Animal Care in accordance with published guidelines. Animal were injected with atropine sulphate (0.025 mg, s.c.), then anesthetized with urethane (Sigma, 1.5 g/kg, i.p.). Trachea was intubated for artificial ventilation. The femoral vein and artery were cannulated for administration of infusing solution (Lactated Ringer's solution, 0.05–0.1 ml/min) or monitoring arterial blood pressure, respectively.

Rats were paralyzed with pancuronium bromide (Sigma, initial dose 0.5 mg, i.v., supplemented every hour at 0.1 mg, i.v.) and ventilated with hyperoxic medical air (40% O₂ balance N₂) using a CWE AVS-1 ventilator. A respiratory gas analyzer (CWE Gemini) was used to monitor end-tidal O₂ and CO₂ levels (P_{ET}O₂ and P_{ET}CO₂). The latter was maintained at 5.0±0.2% (38±1.5 mmHg) or 5.5±0.2% (41.8±1.5 mmHg), which was the CO₂-recruitment threshold (Boden *et al.*, 1998) plus 1.0% or 1.5%. Body temperature

was maintained at 36.5 ± 0.2 °C with a temperature controller (CWE, TC-831). During the experiment, the depth of anesthetization was checked regularly. Whenever a noxious stimulus (clamping the hind paw) caused changes in pupil size, respiration and heart rate or elicited a withdrawal reflex, a supplemental dose of urethane (1/10 original dosage) was given intravenously to maintain adequate depth of anesthesia.

The right phrenic nerve and both vagus nerves were isolated and severed at the cervical level using a ventral approach. The head of the rat was then fixed in a stereotaxic frame (KOPF 1430, David Kopf Instruments, Tujunga, CA) in a tilted position (with Bregma 1.5 mm higher than Lambda) with the dorsolateral pons being readily accessible from a vertical dorsal approach. A craniotomy was performed at interaural level. Dura and pia were carefully removed. The exposed brain surface was covered with petroleum jelly.

5.2.2 Microelectrode arrays

Two different layouts of microelectrode arrays (2×8 or 4×4) were used to record neuronal signals from the dorsolateral pons (Microprobes, Inc., Gaithersburg, MD). Each electrode in the array was spaced by 250 μm in rows and columns. The impedance of each individual electrode ranged from 0.5 - 2 $\text{M}\Omega$ as measured at 1 kHz, 5 nA. The electrode array was inserted into the dorsolateral pons (stereotaxic coordinates: -0.20 (caudal) $\rightarrow +0.2$ mm (rostral) to the level of lambda, 2.3 – 2.4 mm lateral to midline, and 7.0– 8.5 mm below lambda surface) with a direct drive micropositioner (David Kopf Instruments, CA) at a speed of 1 $\mu\text{m}/\text{sec}$.

5.2.3 Recording

The pontine area of interest was first searched with low impedance single tungsten microelectrode, based on stereotaxic coordinates, for loci where electrical

microstimulation produces specific respiratory response (Baxter & Olszewski, 1955; Cohen, 1971). Once located, neuronal activities were recorded and data acquired with a microelectrode array using a multichannel acquisition processor (MAP, Plexon Inc. TX), sampled at 40 kHz. Single-unit activities with $\geq 3:1$ signal-to-noise ratio were sorted on-line and later confirmed with an off-line sorting algorithm based on PCA decomposition (OfflineSorter, Plexon Inc.). Only single units with clear separation from the noise cluster (Figure 5.1) and with minimal spike collisions (spikes with >1 msec Interspike interval) were used for further analyses. Recording loci were confirmed with electrical lesioning of the recording location.

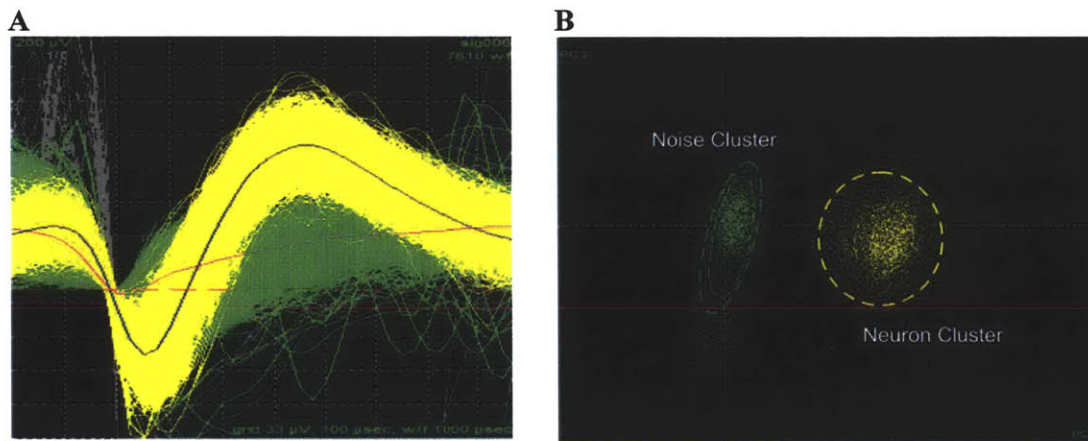


Figure 5.1 A. Local field potential recording in one channel of multielectrode array. B. PCA decomposition of signals in (A) indicating that the neuron cluster is readily distinguishable from the noise cluster.

To monitor respiratory motor output, the separated right phrenic nerve was exposed from dorsal approach and mounted on a bipolar platinum wire electrode (FHC, Bowdoin, ME). The raw phrenic discharge signal (Phr) was amplified (CyberAmp 380, Axon Instruments, Molecular Devices, Sunnyvale, CA) and integrated with a Paynter filter (time constant 15 ms). Raw and integrated phrenic nerve discharge, tracheal pressure, end-tidal CO_2 and stimulation marks were filtered, digitized (5 kHz) and fed into the MAP system through A/D subsystem (National Instruments, TX) and recorded along with neuronal spike trains.

5.2.4 Protocols

The animal was normally ventilated with hyperoxic gas (40% O₂). The CO₂ recruitment threshold (CO₂-RT) was determined by hyperventilation to apnea followed by gradual return to normal ventilation. The end-tidal CO₂ at the reappearance of first phrenic inspiratory burst was the CO₂-RT (~4.3% or 32.7mmHg). The end-tidal CO₂ was then further increased to ~5.3% (CO₂-RT plus 1%) and maintained at this value for baseline ventilation. Three types of tests were performed with brief hypoxia being applied under (1) hypercapnic (*H*), (2) eucapnic (*N*), or (3) hypocapnic (*L*) background. For hypoxia test under eucapnic background, the animal was maintained at baseline ventilation whereas for hypoxia test under hypocapnic background, the animal was first hyperventilated with hyperoxic gas until the end-tidal CO₂ was decreased to the CO₂-RT (rhythmic phrenic discharge remains). In both cases, after stabilizing for 3-5 min at the eucapnic or hypocapnic levels the ventilation gas was switched to 8% O₂ (balance N₂) for 30-45 sec before switching back to normal. For hypoxia test under hypercapnic background, the ventilation gas was first switched to carbogen (5% CO₂ balance O₂) for 5 min until the phrenic discharge stabilized, and then to 8% O₂ - 5% CO₂ (balance N₂) gas mixture for 30-45 sec before switching back to carbogen. In all cases the flow rate of test gases was carefully adjusted to be identical to that of baseline ventilation. At least 15 min was allowed between any two tests until the phrenic discharge completely returned to pre-test levels.

5.2.5 Data analysis

Inspiratory duration (T_I), expiratory duration (T_E) and breathing frequency were computed for each respiratory cycle from Phrenic signal. Amplitude of inspiratory motor output (\dot{V}_{Phr}) was measured as the peak of the integrated Phr signal.

Only neurons that showed clear respiration modulation were of interest in this study. Respiration-modulated neurons were first classified as I- or E-neurons depending

on whether they fire during the I- or E-phase of phrenic activity. Further categorization was based on the temporal firing pattern referencing to the breathing cycle using a perievent raster analysis, following standard procedures as in (Song, et al. 2006). Average firing frequencies of the neurons were calculated for inspiratory (I-activity) and expiratory (E-activity) phases respectively. They were calculated for each breath cycle as the number of spikes/ T_I or number of spikes/ T_E .

Phrenic and neuronal hypoxic responses were fitted with multi-exponential (order 1 ~ 4) functions using least squares regression analysis (see Discussions).

$$\text{ON: } y = y_0 + \sum_i A_i (1 - e^{-t/T_i}) \quad \text{and} \quad \text{OFF: } y = y_0 + \sum_i A_i e^{-t/T_i}$$

where **ON** referred to hypoxic response and **OFF** referred to post-hypoxia recovery. $y(t)$ is the phrenic motor output (amplitude, frequency, T_I and T_E) or neuronal firing frequency at time t , y_0 is the pre-hypoxia baseline level, A_i and T_i are the gains and time constants of the exponential functions.

Time constants were first obtained separately for each CO_2 background by the best exponential fit using Origin (OriginLab Inc., MA). The average time constant values over the three CO_2 background were then used as the common time constant for all three levels of CO_2 for further fitting.

Least squares regression of the phrenic discharge and neuronal firing frequency determined A_i for different CO_2 level as follow:

$$\begin{pmatrix} 1 - e^{-t_1/T_1} & 1 - e^{-t_1/T_2} & \dots & 1 - e^{-t_1/T_m} \\ \vdots & \vdots & \vdots & \vdots \\ 1 - e^{-t_N/T_1} & 1 - e^{-t_N/T_2} & \dots & 1 - e^{-t_N/T_m} \end{pmatrix} \begin{pmatrix} A_1 \\ A_2 \\ \vdots \\ A_m \end{pmatrix} = \begin{pmatrix} y_1 - y_0 \\ y_2 - y_0 \\ \vdots \\ y_N - y_0 \end{pmatrix}$$

where m is the order of the multi-exponential function and N is the number of data points. Typically, $1 \leq m \leq 4$ and $N > 20$.

or

$$\begin{aligned}\mathbf{MA} &= \mathbf{Y} \\ \Rightarrow \mathbf{A}^* &= (\mathbf{M}^T\mathbf{M})^{-1}\mathbf{M}^T\mathbf{Y}\end{aligned}$$

Similar computation was used for **OFF** data as well.

The relative gains, A_i , of the exponentials under the three conditions for each data set was normalized with the overall average gain under normocapnic condition. The normalized gains were then averaged across neurons/animals for testing statistical significance. Statistical significance was tested using Student's t-test with confidence level of 95%.

5.2.6 Histology

At the end of the experiment, electrolytic lesions were made at the recording sites with a tungsten microelectrode (tip diameter 1–2 μm , impedance 0.5–1 $\text{M}\Omega$; Micro Probes, Gaithersburg, MD). The lesion current was 100 μA , anodal D.C., lasting 30 sec. Then the animal was euthanized with an overdose of urethane (2 g/kg , i.v.) and immediately perfused transcardially with 300 ml of heparinized saline followed by another 300 ml of chilled paraformaldehyde solution (4% in 0.05 M PBS). The brain was removed, post-fixed and cut into 100- μm coronal sections on a vibratome (Leica VTS 1000, Leica Microsystems, Richmond, IL). Sections were then stained with cresyl violet and checked microscopically for the loci of recording.

5.3 RESULTS

5.3.1 Interaction of hypercapnia and hypoxia in phrenic motor output

Hypoxia under normocapnia elicited the typical phrenic response as shown in earlier studies in our group and others (Song & Poon, 2009a) (Figure 5.2). Specifically, hypoxia induced a gradual increase in $\int\text{Phr}$ amplitude and a gradual decrease of T_I , followed by a slow recovery of both components towards baseline values upon withdrawal of hypoxia. In other words, hypoxia elicited short term potentiation (STP) in both $\int\text{Phr}$ amplitude and T_I . Alternatively, T_E was initially shortened rapidly which was followed by a gradual prolongation, showing short term depression (STD). Upon removal of hypoxia, T_E rebounded above the baseline value and then decreased gradually back to baseline. The response of breathing frequency essentially mirrored that of T_E .

Our data demonstrate hypoadditive hypercapnia-hypoxia interaction in phrenic motor response similar to the recent reports by Day and Wilson (Day & Wilson, 2007, 2009). In Figure 5.2, it is clear that the strength of the hypoxia response was modulated by the level of CO_2 background the animals were exposed to. In particular, the response of $\int\text{Phr}$ amplitude and breathing frequency (as well as T_E) was stronger under lower CO_2 background. The interaction was also revealed in the post-hypoxic frequency decline (PHFD) but in a more complex manner. In addition, despite the initial apneusis, T_I response under hypocapnic background was able to catch up with those under higher CO_2 level, showing hypoadditive interaction as well, this response was not demonstrated in Day's study (Day & Wilson, 2009). Hence, it was shown that phrenic hypoxic response was conditioned on the central input.

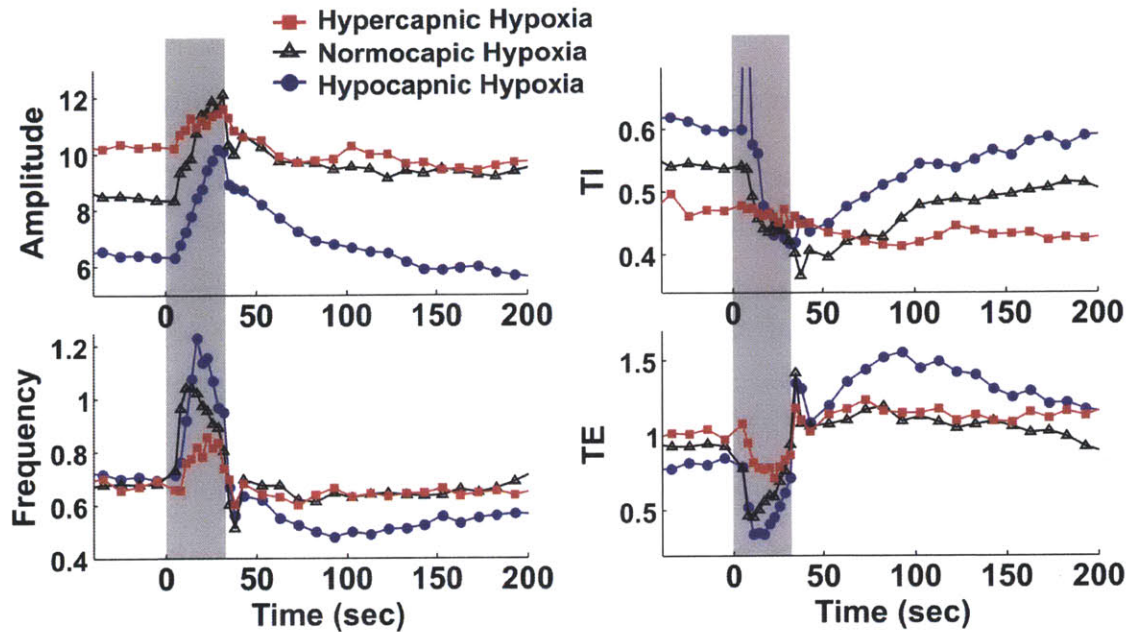


Figure 5.2 Response of phrenic discharge amplitude and timing components to hypoxia under varying CO₂ backgrounds in one rat.

5.3.2 Neuronal recording loci

Next, we determined whether the dl-pons respiratory neurons demonstrated similar chemoreflex conditioning.

Respiratory neurons were recorded in the dl-pons region including both LPBN and KFN to investigate their relevance to the hypoxia-hypercapnia interaction. Figure 5.3A shows an image of the brain slice with a lesion next to scp (superior cerebellar peduncle) to show the recording location. The neurons that were tested for hypoxia-hypercapnia interaction were marked in Figure 5.3B to show the spread of recording loci.

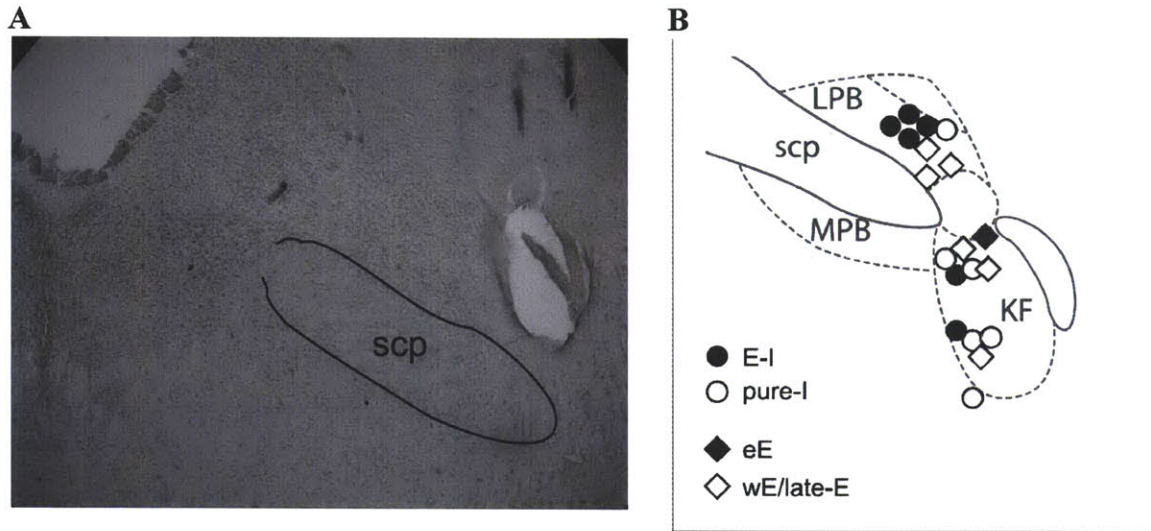


Figure 5.3 Recording loci. (A) Electrolytic lesion was made at the end of the experiment to mark the recording site. (B) Loci of 4 types of respiratory-related neurons in KFN and LPBN exhibiting hypoaddivitive CO_2 - O_2 interaction.

5.3.3 Neuronal response to hypoxia and hypercapnia

A total of 166 respiratory neurons were tested against hypoxia (I-neurons: 140 vs. E-neurons: 26) and 159 neurons were tested against hypercapnia (I-neurons: 127 vs. E-neurons: 32) (Table 5.1). Neurons are considered responsive if the peak stimulated firing frequency is beyond 1SD from the mean baseline firing frequency.

The neurons recorded were heterogeneous both in the baseline firing and their response to hypoxia and hypercapnia. Their baseline firing frequency spanned two orders of magnitude and the percentage change induced by the stimuli spanned as much as three orders of magnitude.

	Hypoxia				Hypercapnia			
	Total	Excited	Inhibited	No response	Total	Excited	Inhibited	No response
E-I	118	93	1	24	100	49	12	39
Pure-I	17	12	0	5	9	5	0	4
Recruited I	5	5	0	0	18	18	0	0
eE	17	2	14	1	22	3	15	4
wE/late-E	9	9	0	0	10	10	0	0

Table 5.1 Summary of types and corresponding response to hypoxia and hypercapnia for all respiratory neurons recorded.

Overall Hypoxic Response of Respiratory Neurons

We surveyed the overall responsiveness of I- and E-neurons to hypoxia and hypercapnia respectively, to further support the role of dl-pons in chemoafferent signaling.

The recorded neurons showed about 83% of the I-neurons were excited by hypoxia challenge. Average firing frequency increase was comparable between I-phase and E-phase (79% vs. 77%). 5 neurons, which were originally silent, were recruited by hypoxia.

On the other hand, all except one E-neuron were responsive to hypoxia. 11 of these neurons were excited by hypoxia. The excitation was primarily evoked in the E activities of the neurons, while 3 of them had also significantly extended the firing into the I-phase.

Overall Hypercapnic Response of Respiratory Neurons

About 66% of the I-neurons were responsive to hypercapnia. 54 neurons increased their firing during hypercapnia and 12 of them were suppressed (mostly in the E-activity). In addition, 18 neurons were primarily silent and were recruited by hypercapnia.

All except 4 E-neurons were responsive to hypercapnia. 8 of them had only their firing in E-phase increased by hypercapnia with no significant change in I-activity. 15 of them were initially suppressed.

5.3.4 Neuron subtypes and their hypoxic responses

Four subtypes of respiratory neurons are of specific interest for CO₂-O₂ interaction in the current study. 12 inspiratory neurons and 7 expiratory neurons were tested for the interaction.

Pure-I neuron (Figure 5.4)

Pure-I neurons (I neuron in (Song *et al.*, 2006)) fired exclusively during I-phase both in baseline and during hypoxia/hypercapnia stimulation. Both hypoxia and hypercapnia increased their firing frequency. Most of these neurons only increased their firing in I-phase and remained silent during E-phase all through. However, a subset of them had pre-I activity recruited by hypoxia but not hypercapnia. Upon removal of hypoxia, their firing frequency gradually returned to the pre-hypoxia level. These neurons showed hypoxic STP similar to $\int\text{Phr}$ amplitude and T_I.

The effect of hypoxia on I-activity of these neurons was significantly reduced as the level of CO₂ background increased, demonstrating similar hypoadditive interaction as in phrenic discharge. These neurons tended to reach a similar peak I-firing frequency during hypoxia under all three CO₂ backgrounds. But for some neurons, the peak firing frequency was relatively smaller under hypocapnia background possibly due to delayed hypoxic response under low central excitatory input.

E-I neuron (Figure 5.5)

The E-I neurons were the majority of respiratory neurons recorded. They started their firing from the E-phase with an augmenting firing frequency and acquired maximum firing frequency in early or mid I-phase. The firing continued until the end of inspiration phase or trailing into the post-inspiratory phase. They responded to hypoxia and hypercapnia by increasing both I- and E-activity. Hypoxia induced STP in these neurons, followed by a gradual after-discharge, in similar way as in pure-I neurons. The effects of hypoxia on both I- and E-activity of these neurons were significantly reduced as the level of CO₂ background increased, demonstrating similar hypoadditive interaction as in phrenic discharge.

eE neuron (Figure 5.6)

The eE neurons fired almost exclusively in the E-phase and acquired peak firing frequency in early E-phase, followed by a decremental firing pattern. They showed similar hypoxic response as the inspiratory neurons, except that only E-activity was excited. Some eE neurons were suppressed by hypercapnia and hypoxia, but they were not included for further investigation in this study.

The sample neuron in Figure 5.7 also demonstrated hypoadditive CO₂-O₂ interaction. But now, the peak firing frequency during hypoxia under hypocapnic background exceeded that under hypercapnia.

(eE neurons were not including in the averaging of E-neurons)

wE (whole phase E)/late-E neuron (Figure 5.7)

wE/late-E neurons recorded fired almost exclusively during E-phase. They had flat (wE) or augmenting (late-E) firing pattern over the E-phase of respiration. Their E-activity increased rapidly when subject to hypoxia, and soon flattened out or even started to decrease. Furthermore, some neurons extended their firing into the I-phase during

hypoxia but not hypercapnia alone. Upon removal of hypoxia, their average E-firing frequency dropped quickly in the first few breaths due to both increased inter-spike intervals and shortened firing duration, where they tended to fire only in the later phase of expiration. Neuronal firing may further decrease gradually beyond the baseline level. Eventually, neuronal firing slowly returned to the pre-hypoxic baseline.

The wE/late-E neurons showed STD response similar to phrenic T_E and breathing frequency. Peak firing of these E-neurons was even higher under low CO_2 despite the delayed response in some of them.

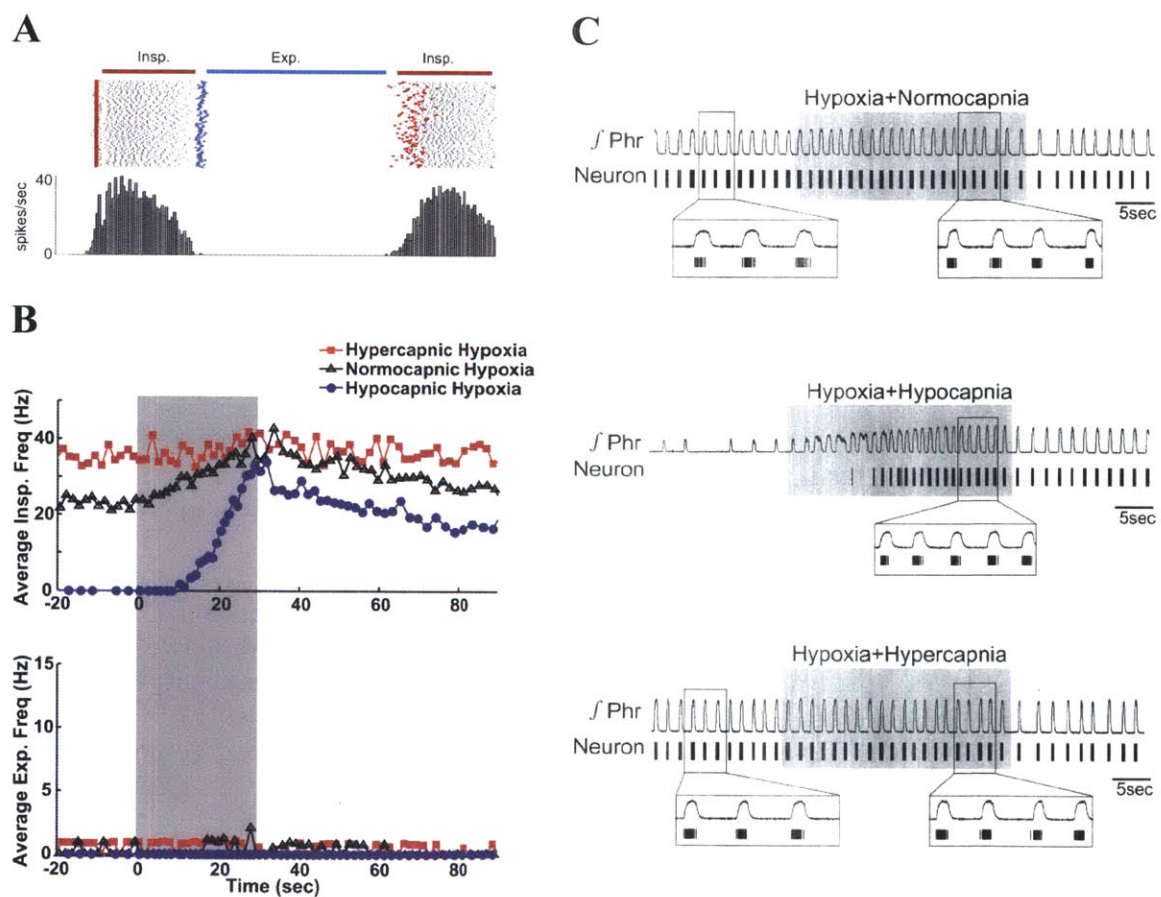


Figure 5.4 A sample pure-I neuron (A) Firing pattern of neuron presented as perievent raster referenced to respiratory cycle; (B) Hypoxic response (separated into inspiratory and expiratory components) under different CO_2 background showing hypoaddivitive interaction; (C) Time-stamped spike trains representaiton of hypoxic response under different CO_2 background.

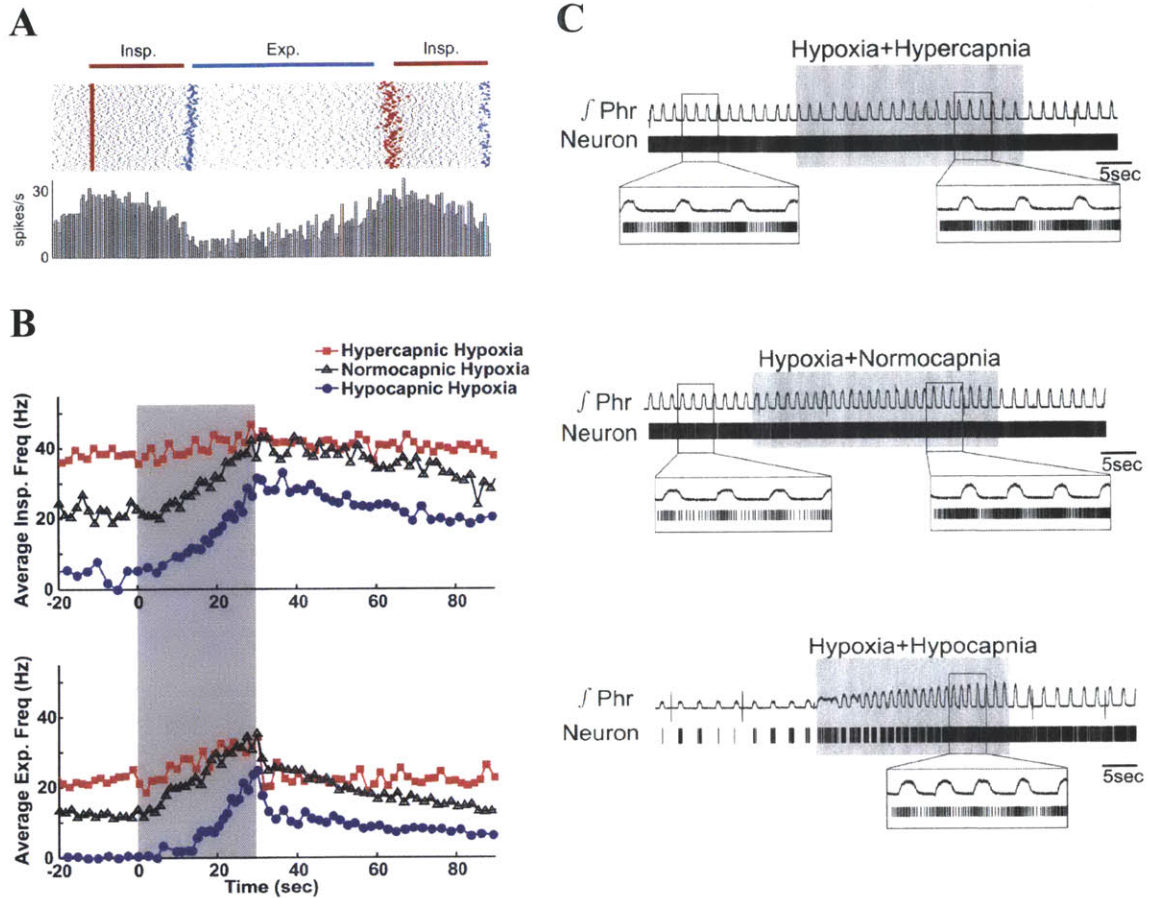


Figure 5.5 A sample E-I neuron (A) Firing pattern of neuron presented as perievent raster referenced to respiratory cycle; (B) Hypoxic response (separated into inspiratory and expiratory components) under different CO₂ background showing hypoadditive interaction; (C) Time-stamped spike trains representation of hypoxic response under different CO₂ background.

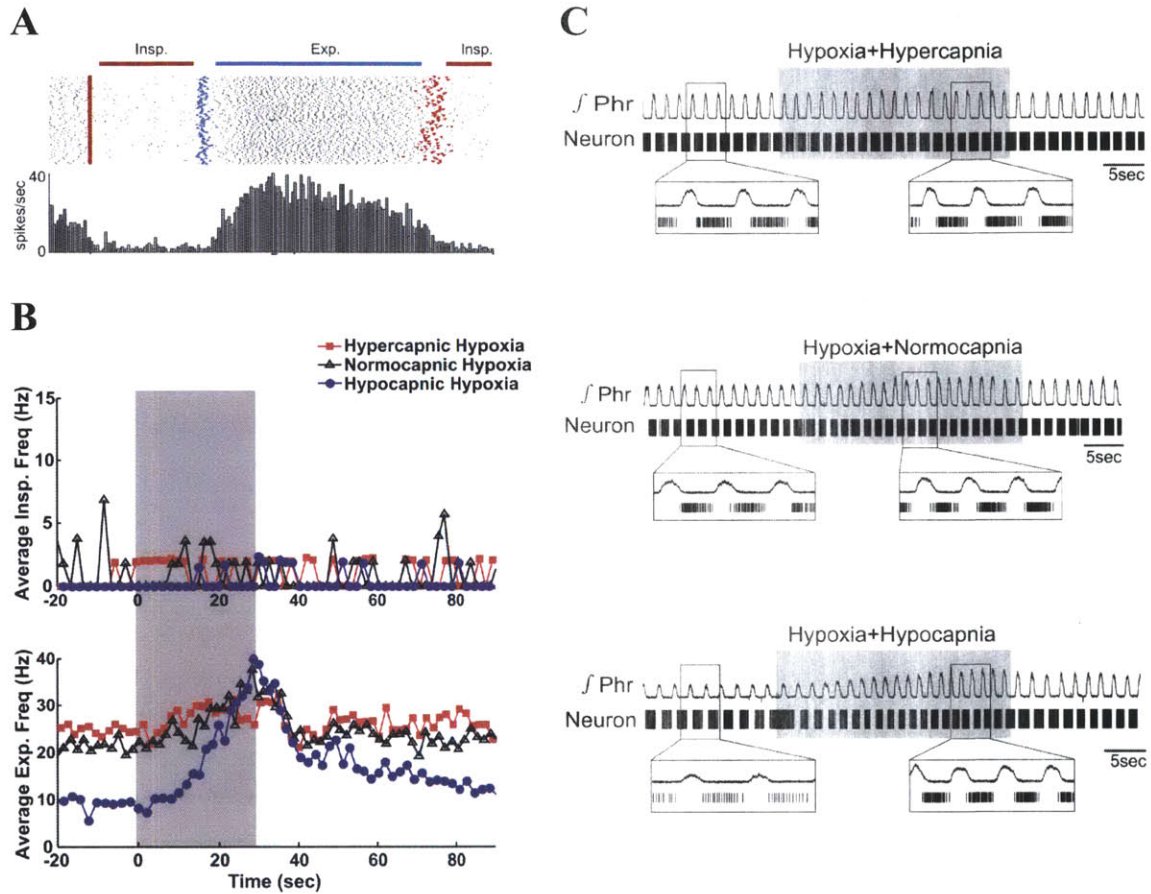


Figure 5.6 A sample eE neuron (A) Firing pattern of neuron presented as perievent raster referenced to respiratory cycle; (B) Hypoxic response (separated into inspiratory and expiratory components) under different CO₂ background showing hypoadditive interaction; (C) Time-stamped spike trains representaiton of hypoxic response under different CO₂ background.

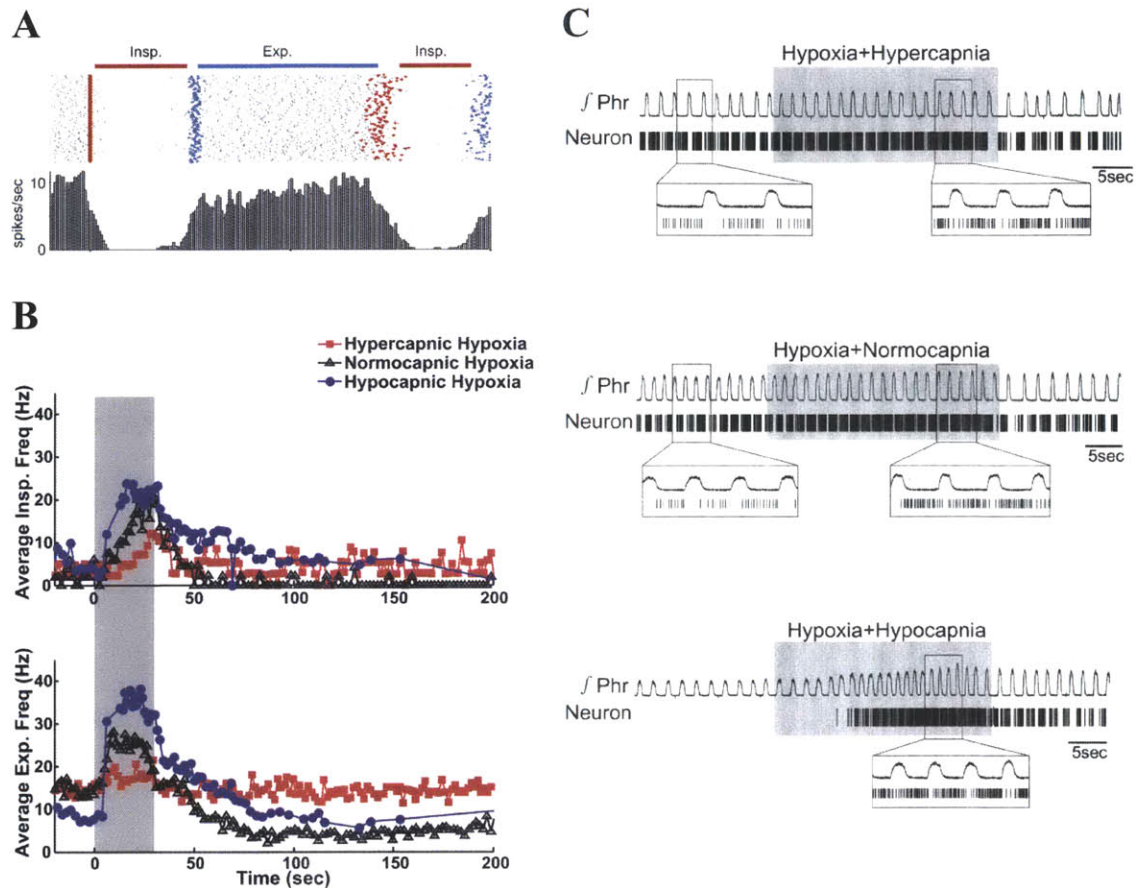


Figure 5.7 A sample wE/lateE neuron (A) Firing pattern of neuron presented as perievent raster referenced to respiratory cycle; (B) Hypoxic response (separated into inspiratory and expiratory components) under different CO₂ background showing hypoadditive interaction; (C) Time-stamped spike trains representation of hypoxic response under different CO₂ background.

5.3.5 Model Fitting

Overlaying the normalized phrenic/neuronal hypoxic response under different CO₂ backgrounds suggested that CO₂ input has no significant influence on the time constants of the dynamic responses. To investigate this hypothesis, we fitted the data in Figure 5.2 with multi-exponential curves using least-squares regression analysis (See section 5.2.5).

Figure 5.8 shows that the STP and STD effects of all phrenic components for all three CO₂ backgrounds can be well fitted by multi-exponential models with the same time constants for all three conditions but with varying amplitudes (Table 5.2). This remarkable consistency of the STP and STD time constants under all three conditions suggests that the hypoadditive effect of hypoxia and hypercapnia is due to a negative influence of hypercapnia on the gains (but not time constants) of the STP and STD integrators and differentiators. The goodness of fits was revealed by the adjusted-R² values. Adjusted-R² values averaged to 82% for **ON** phase over hypocapnic and normocapnic background. The low Adjusted-R² values in hypercapnic background was primarily due to the small hypoxic response compared to the intrinsic variance. Furthermore, better fits were obtained in the **ON** phase compared to **OFF** phase.

In a similar fashion as in Figure 5.8, we performed the same multi-exponential curve fitting on an E-I neuron and a late-E neuron (Figure 5.9). Again, we show that the neuronal response can be well fitted by multi-exponential models with the same time constants for all three conditions but with varying amplitudes. The quality of fitting was similar as in phrenic data, while the fitting in **OFF** phase seemed to be better (Table 5.3).

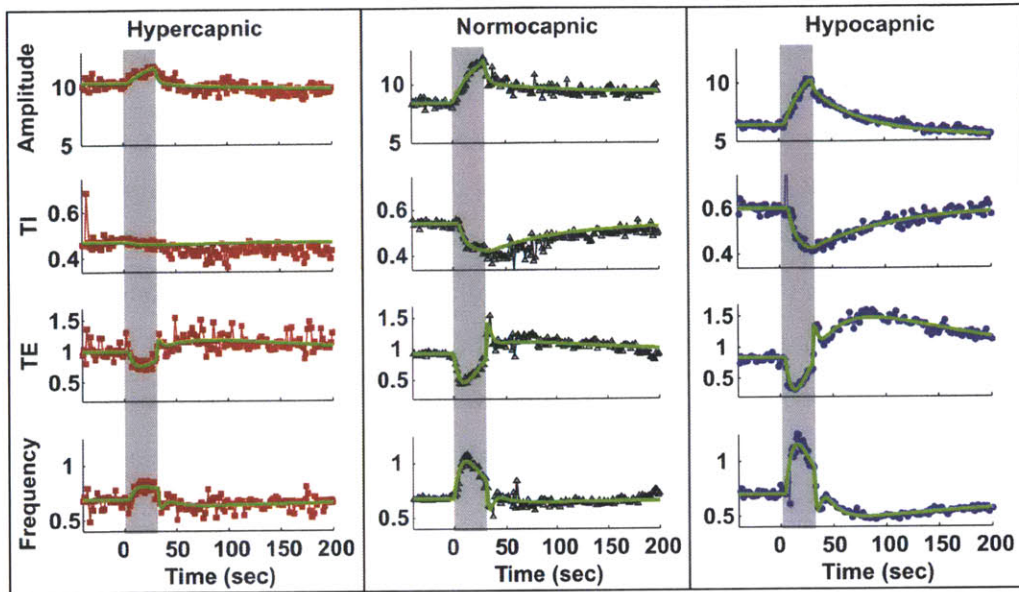


Figure 5.8 Multiexponential curve fitting to breath-by-breath phrenic data, using the same time constants over three different CO₂ background. Results suggested that hypercapnic input altered only the gains of the learning dynamics but had little influence on its time course.

Amp	ON T1 = 22.67s			OFF T1 = 126.99s, T2 = 2.99s		
	<i>Hypercapnic</i>	<i>Normocapnic</i>	<i>Hypocapnic</i>	<i>Hypercapnic</i>	<i>Normocapnic</i>	<i>Hypocapnic</i>
A1	1.93	4.78	5.76	0.49	0.78	0.91
A2				1.23	2.01	4.01
Adj-R ²	0.17	0.90	0.96	0.36	0.56	0.90
T1	ON T1 = 7.43s			OFF T1 = 71.45s		
	<i>Hypercapnic</i>	<i>Normocapnic</i>	<i>Hypocapnic</i>	<i>Hypercapnic</i>	<i>Normocapnic</i>	<i>Hypocapnic</i>
A1	0.011	0.12	0.19	0.011	0.12	0.18
Adj-R ²	0.13	0.86	0.88	<0	0.41	0.88
TE	ON T1 = 11.82s, T2 = 11.54s			OFF T1 = 119.23s, T2 = 31.45s; T3 = 2.34s, T4 = 1.44s		
	<i>Hypercapnic</i>	<i>Normocapnic</i>	<i>Hypocapnic</i>	<i>Hypercapnic</i>	<i>Normocapnic</i>	<i>Hypocapnic</i>
A1	-28.96	-68.61	-91.09	-0.39	-0.32	-1.41
A2	28.93	68.83	91.56	0.37	0.20	1.41
A3				-1.07	-2.21	-2.68
A4				1.24	2.45	2.79
Adj-R ²	0.34	0.86	0.63	0	0.43	0.79
Frequency	ON T1 = 11.82s, T2 = 11.18s			OFF T1 = 233.27s, T2 = 11.52s; T3 = 2.64s, T4 = 2.59s		
	<i>Hypercapnic</i>	<i>Normocapnic</i>	<i>Hypocapnic</i>	<i>Hypercapnic</i>	<i>Normocapnic</i>	<i>Hypocapnic</i>
A1	-7.65	-16.72	-36.21	-0.072	-0.044	-0.27
A2	7.62	16.72	35.91	0.18	0.20	0.74
A3				-19.11	-28.14	-51.62
A4				19.11	28.16	51.40
Adj-R ²	0.46	0.79	0.66	0.04	0.19	0.83

Table 5.2 Coefficients of curve fitting for phrenic data in one animal (Figure 5.8). Adjusted-R² values were shown. **ON** referred to hypoxic response and **OFF** referred to post-hypoxia recovery.

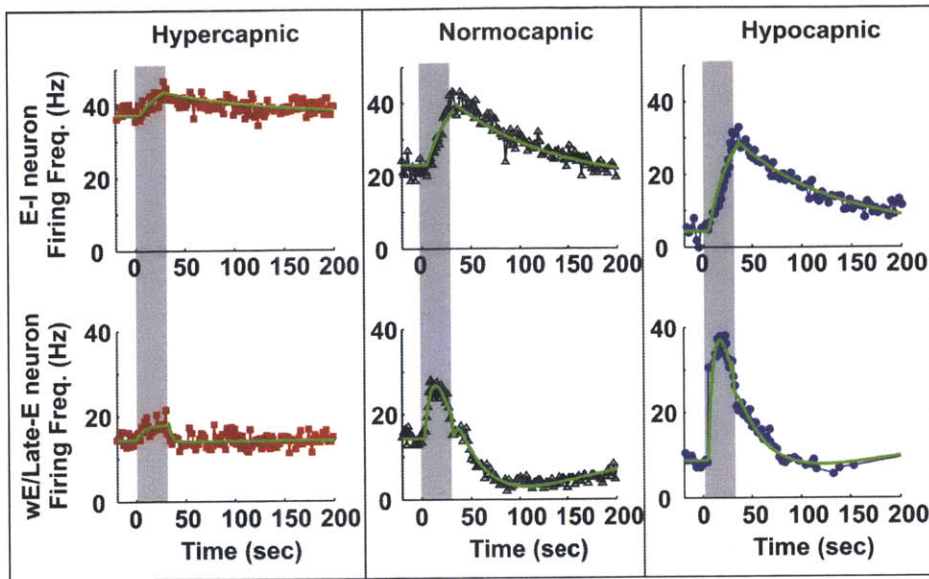


Figure 5.9 Multiexponential curve fitting to breath-to-breath neuronal firing (top: E-I inspiratory firing; bottom: wE/late-E expiratory firing) data, using the same time constants over three different CO₂ background. Results suggested that hypercapnic input altered only the gains of the learning dynamics but had little influence on its time course.

	<i>ON</i>			<i>OFF</i>		
	<i>Hypercapnic</i>	<i>Normocapnic</i>	<i>Hypocapnic</i>	<i>Hypercapnic</i>	<i>Normocapnic</i>	<i>Hypocapnic</i>
E-I neuron	T1 = 23.63s			T1 = 98.52s		
A1	8.79	25.09	32.80	6.25	22.01	24.06
Adj-R ²	0.32	0.85	0.84	0.23	0.88	0.94
wE/lateE neuron	T1 = 10.27s, T2 = 17.01s			T1 = 133.07s, T2 = 35.67s; T3 = 1.95s, T4 = 1.87s		
A1	4.60	88.14	154.37	-0.91	-27.45	-19.20
A2	-0.81	-95.37	-154.40	1.24	36.66	33.18
A3				-18.06	-393.53	-205.42
A4				-21.45	390.31	208.40
Adj-R ²	0.14	0.67	0.71	0.64	0.89	0.95

Table 5.3 Coefficients of curve fitting for neuronal data in two sample neurons (Figure 5.9). Adjusted-R² values were shown. **ON** referred to hypoxic response and **OFF** referred to post-hypoxia recovery.

Figure 5.10A1 and Figure 5.10B1 show the overall curve fitting results of all I- and E-neurons as compared to phrenic T_I and T_E respectively. Hypoadditive $\text{CO}_2\text{-O}_2$ interaction in both neuronal activity and phrenic T_I/T_E was revealed by the decrease in gains of the exponential terms as the CO_2 background increased (difference between bars under different CO_2 backgrounds are all statistically significant, $p < 0.05$). STP in I-neuron and phrenic T_I comprised one exponential term while STD in E-neurons and phrenic T_E comprised two exponential terms (positive and negative). Relative gains of I-neuron and phrenic T_I STP decreased as CO_2 level was raised, similarly in E-neuron and phrenic T_E STD. Moreover, the two gains of the STD changed in parallel, suggesting that CO_2 input has homogenous effects on the two exponential components.

Figure 5.10A2 and Figure 5.10B2 show that neuronal and phrenic activities were highly correlated in both inspiratory and expiratory components ($R^2 = 0.80$ and 0.92 respectively). This suggests that they may share a common mechanistic basis.

Figure 5.11 show similar plots as in Figure 5.10 for post-hypoxia recovery. Phrenic T_I and I-neuron activity still showed hypoadditive interaction, following the stimulated response (difference between bars were statistically significant, except for phrenic T_I between *Low* and *Normal* CO_2 background) (Figure 5.11A1). A weak positive correlation was shown ($R^2 = 0.32$) (Figure 5.11A2). On the other hand, hypoadditive interaction in the recovery of phrenic T_E and E-neuron activity was unclear (Figure 5.11B1) and no apparent correlation was observed (Figure 5.11B2).

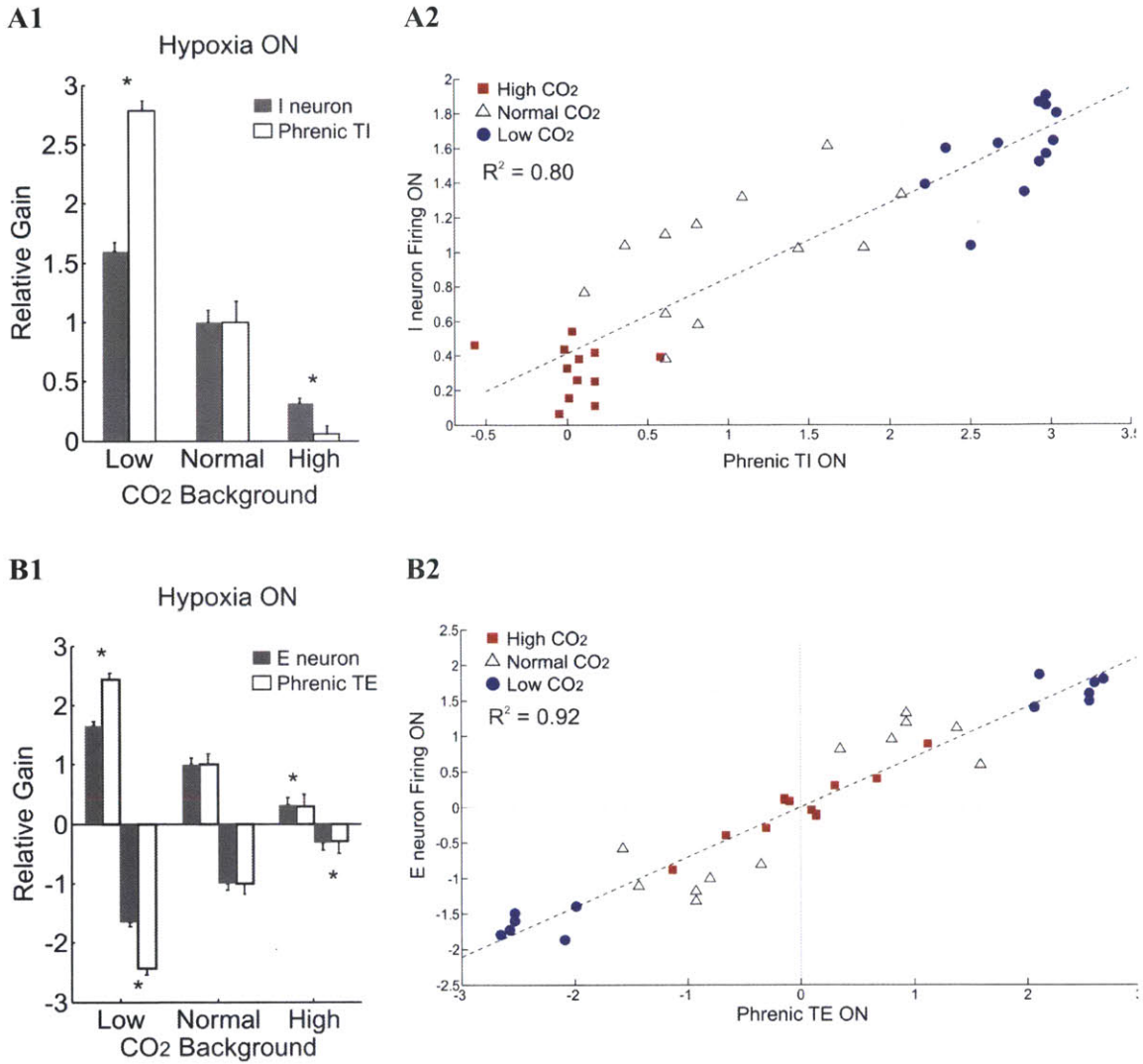


Figure 5.10 Left panels: Averaged gains of multiexponential curve fitting (normalized to normocapnic condition) for phrenic and neuronal activity over three different CO₂ background during hypoxia stimulation. Right panels: Correlation between gains of phrenic T_I/T_E and I/E-neurons multiexponential curve fitting. (A) Phrenic T_I vs. I-neurons (n=12); (B) Phrenic T_E vs. E-neurons (n=7). * indicates statistically significant difference from normal CO₂ condition (p<0.05).

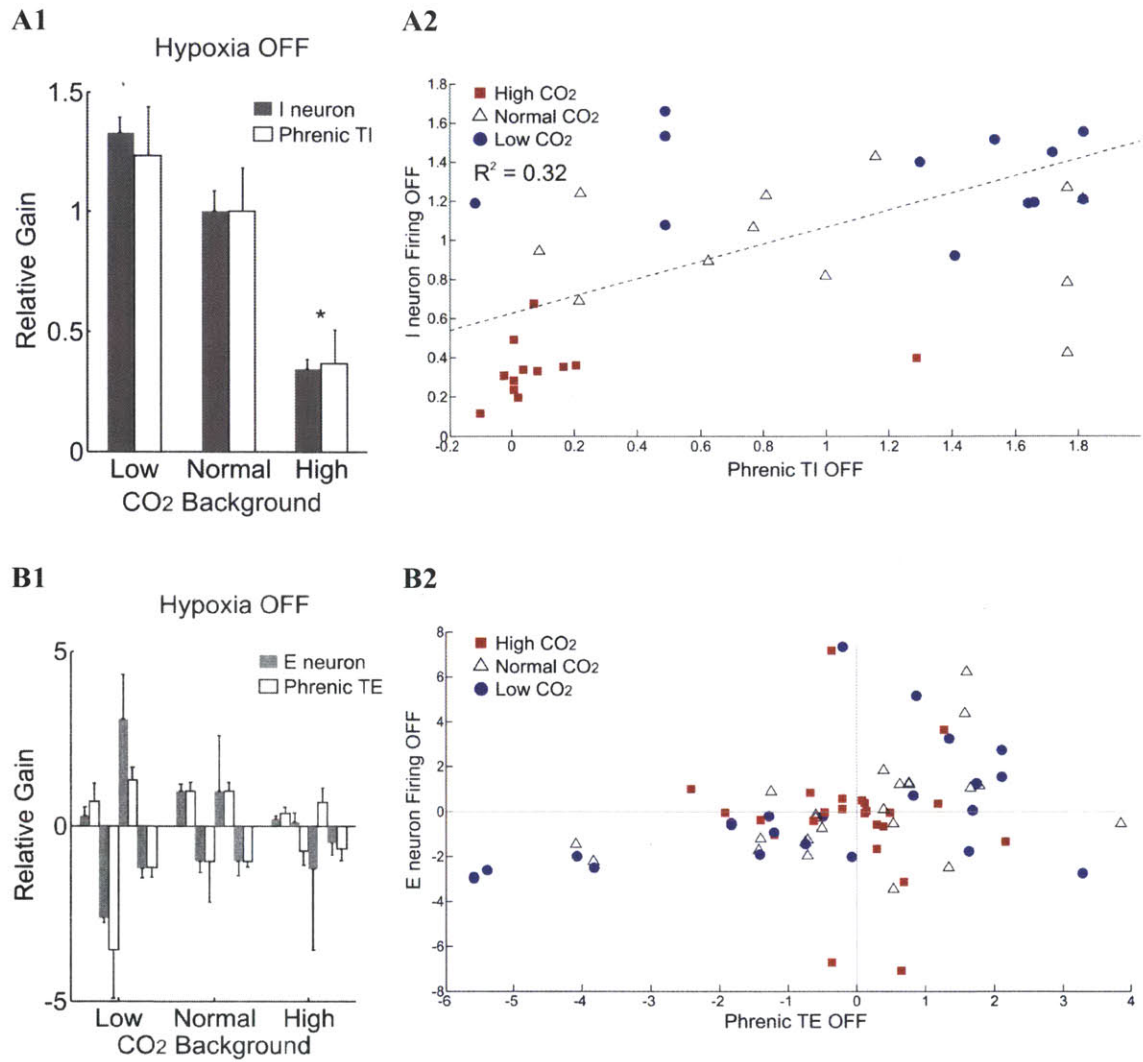


Figure 5.11 Left panels: Averaged gains of multiexponential curve fitting (normalized to normocapnic condition) for phrenic and neuronal activity over three different CO₂ background during post-hypoxia recovery. Right panels: Correlation between gains of phrenic T_I/T_E and I/E-neurons multiexponential curve fitting. (A) Phrenic T_I vs. I-neurons (n=12); (B) Phrenic T_E vs. E-neurons (n=7). * indicates statistically significant difference from normal CO₂ condition (p<0.05).

5.4 DISCUSSION

In summary, our results show that: 1) hypoadditive CO₂-O₂ interaction in phrenic motor output, consistent with the recent report in (Day & Wilson, 2009); 2) a significant number of respiratory neurons in dl-pons were chemosensitive; 3) demonstrate hypoadditive CO₂-O₂ interaction in multiple types of respiratory neurons in the dl-pons; and 4) hypoadditive CO₂-O₂ interaction was primarily due to a negative influence of hypercapnia on the gains (but not time constants) of the STP and STD. Such activity-dependent and pairing-specific modulation of hypoxic response indicates a certain form of associative learning or Pavlovian conditioning underlying CO₂-O₂ interactions. The strong correlations between phrenic and neuronal activity in CO₂-O₂ interactions suggest that dl-pons are likely neuronal correlates for such interactions.

5.4.1 Controversy about chemoreceptors interaction in phrenic motor output

Day and Wilson (Day & Wilson, 2009) used a dual perfused rodent preparation to show hypoadditive interaction between central and peripheral chemoreceptors. They showed that the most apparent interaction happened in respiratory frequency (mainly through the effects of TE), which also translated into neural total ventilation (*total ventilation = freq × tidal volume*).

In the present study, we have shown similar CO₂-O₂ interaction in all the phrenic variables, including \int Phr amplitude, TI, TE and breathing frequency, suggesting that the interaction is a general phenomenon for various components of phrenic motor output. These additional findings may be a result of using different animal preparations or stimulation protocols. The homogenous effect of chemoafferent interactions over all respiratory variables also suggests that chemoreceptors information may play a small role in determining breathing pattern.

Conversely, (Blain *et al.*, 2010) showed hyperadditive central-peripheral chemoreceptors interaction in awake animals. They argued that state of consciousness could affect the interaction (Smith *et al.*, 2010b). On the other hand, their study differed from the study of Day and Wilson and our study in that they administrated central chemoreceptor stimulation under different background of peripheral chemoreceptor activity. We suggest that the way of conditioning, central-to-peripheral or peripheral-to-central, may result in different interactions. Further studies addressing these hypotheses will help to clarify the contradicting reports.

5.4.2 Recording loci of respiratory neurons

Using microelectrode arrays in neuronal recording has the advantage of increasing the chance of hitting the neurons of interest. However, the drawback is the difficulty in identifying the exact loci of recording of individual electrode. At the end of each experiment, the electrode array was replaced by a single tungsten electrode for electrical lesioning to mark the approximate location of recording, with an inevitable small error in the reinsertion location. A previous study showed that phasic respiratory neurons mainly populated around PBN and KFN in dl-pons (Song *et al.*, 2006). By referencing to the stereotaxic coordinates of these brain regions, it helped to confine our search for phasic respiratory neuron in these specific regions.

5.4.3 Role of dl-pons in chemoafferent signaling

In the present study, we have shown that respiratory neurons in LPBN and KF, two subdivisions of the dorsolateral pons "pneumotaxic center" in the rat (Song *et al.*, 2006), are chemosensitive. Such capability of processing chemoreceptor inputs is consistent with previous studies that showed that lesions of LPBN change the hypoxic and hypercapnic response of phrenic motor output (Song & Poon, 2009a, 2009b). The hypoxic/hypercapnic response of individual respiratory neurons in these regions has not

been previously addressed in detail. A recent report (Nuding *et al.*, 2009) investigated the general excitatory/depression nature of PRG neurons. They showed that roughly 1/3 of the neurons (including both respiratory modulated and tonic neurons) in PRG were responsive to at least one of the chemoreceptor stimulation. Our current results show that a majority of neurons recorded (all respiration modulated) over a wide area of dl-pons were responsive to either central or peripheral stimulation.

Most current models of respiratory central pattern generator assume that the pons provides only a tonic drive to the medullary rhythmogenic network where the three-phase inspiratory, expiratory (I, E) and post-I rhythm is thought to arise (Smith *et al.*, 2007; Abdala *et al.*, 2009; Rubin *et al.*, 2009; Molkov *et al.*, 2010; Rubin *et al.*, 2010). This basic assumption is being challenged by our present demonstration that many pontine inspiratory and expiratory-modulated neurons contribute to hypoxic-hypercapnic afferents integration in a phase-specific (instead of tonic) manner. These new findings suggest necessary revision of these models which will improve their predicting capability.

5.4.4 Associative learning (Pavlovian conditioning) in respiratory chemoreflex control

An important implication of the hypoadditive CO₂-O₂ interaction is that the hypoxic ventilatory response is not simply reflexogenic as generally thought. Rather, the activity-dependent and pairing-specific induction of STP and STD by hypoxic-hypercapnic stimuli suggests a unique form of classical (Pavlovian) conditioning, in which the response to a “conditioned stimulus” (hypoxia) is modulated (in this case, depressed) by temporal pairing with an “unconditioned stimulus” (hypercapnia) (Pavlov, 1960; Poon & Siniatia, 2000), similar to classical studies in *Aplysia* (Glanzman, 1995) and cerebellum (Thompson, 1988) except that the memory is short-term instead of long-term. Such associative learning challenges traditional models of respiratory control based on a Sherringtonian long-loop reflex paradigm (Sherrington, 1906; Tin *et al.*, 2010) and

support an optimization model we proposed (Poon, 1993, 1996b; Poon, 1996c; Young & Poon, 2001a; Poon *et al.*, 2007). The current study further provides the first systematic investigation of the neural correlates of these learning processes that will potentially unify our findings at cellular level.

The mechanism of this CO₂-O₂ associative learning is still unknown but it seems to play an important role in gain modulation of STP/STD of hypoxic response. Young's (Young *et al.*, 2003b) studies suggested that peripheral chemoreceptor inputs are relayed centrally by a bank of parallel neural integrator and differentiator pathways that provide STP and STD modulations of inspiratory amplitude, T_I and T_E with varying time constants and gains. STP/STD have been proposed to be a computational equivalence of a neural integrator/differentiator in processing peripheral chemoafferents to the respiratory central pattern generator (Poon, 1996e; Poon *et al.*, 1999a). The neural integrator can be described by the following first-order linear dynamic system:

$$\frac{Y(s)}{X(s)} = \frac{A_i}{(s/T_i + 1)} \quad i = 1, 2, \dots, n$$

Equivalently the overall response of these neural integrators, assuming mutual independence, can be described by the following multi-exponential functions:

$$\text{ON: } y = y_0 + \sum_i A_i (1 - e^{-t/T_i}) \quad \text{and} \quad \text{OFF: } y = y_0 + \sum_i A_i e^{-t/T_i}$$

Each (A_i, T_i) pair described the gain and the time constant of an individual neural integrator. Note that the time constants may be different between the stimulated response and the recovery (Poon *et al.*, 1999b; Young *et al.*, 2003b). Here, real-valued exponents are used since Young's (Young *et al.*, 2003b) studies using 4 min electrical stimulation of carotid sinus nerve did not demonstrate any oscillatory response.

Using this model fitting, we show that STP and STD in both phrenic and neuronal activities can be well fitted by the neural integrator models with the same time constants over all three CO₂ background but with varying gains. This remarkable consistency of

the STP and STD time constants under all three conditions suggests that the hypoadditive effect of hypoxia and hypercapnia is due to a negative influence of hypercapnia on the gains (but not time constants) of the STP and STD integrators and differentiators. Thus, Pavlovian conditioning or associative learning of the hypoxic response occurs when paired with a CO₂ stimulus and this learning effect affects only the amplitude of learning but not its time course.

The post-hypoxic recovery demonstrates a more complex behavior, particularly in the expiratory components and no apparent trend of interaction (hypoadditive, additive or hyperadditive) was shown (Figure 5.11B). This suggests that a different form of CO₂-O₂ interaction may underlie post-hypoxic recovery. In fact, ventrolateral pons (vl-pons) contains many wE (Dick & Coles, 2000) and eE (Guyenet *et al.*, 1993) neurons and they have been shown to mediate post-hypoxic frequency decline of respiration (Dick & Coles, 2000). Consequently, vl-pons may constitute another potential site for chemoreceptor interaction, and potentially exert additional influence specifically at the recovery phase of expiratory activities.

5.4.5 Implications for respiratory rhythmogenesis, respiratory instability/apnea and acclimatization

These new findings impact the traditional view of pure summation of chemoreceptor inputs in mathematical modeling. As such, the concept of relative contribution of peripheral and central chemoreceptors (Berkenbosch *et al.*, 1979; Heeringa *et al.*, 1979) has to be taken with caution.

The present work will also have profound implications in transforming current models of respiratory instability in obstructive sleep apnea or central apnea. Sleep apnea has been suggested to arise from respiratory instability which leads to periodic breathing in sleep. Sleep apnea incidence is correlated with higher respiratory loop gain and/or increased feedback delays (Khoo *et al.*, 1982). All of these models assume additive chemoreceptor feedbacks to the exclusion of pontine-mediated STP/STD or Pavlovian

conditioning effects during apnea-induced hypoxia episodes (Cherniack & Longobardo, 2006; Topor *et al.*, 2007; Sands *et al.*, 2009; Cheng *et al.*, 2010; Duffin, 2010). The hypoadditive effect presently demonstrated between hypoxic and hypercapnic stimuli in inducing inspiratory STP and expiratory STD implies that the overall chemoreceptor gain (and hence, loop gain) is decreased during apnea episodes with concurrent hypoxia and hypercapnia. Such apnea-induced decrease in loop gain provides an “automatic gain control” (AGC) mechanism (Green, 1983) that adaptively mitigates respiratory instability, in agreement with a self-tuning optimization model of respiratory control we proposed (Poon, 1993, 1996b; Poon, 1996c; Young & Poon, 2001a; Poon *et al.*, 2007).

Finally, the hypoadditive CO₂-O₂ interaction in inducing STP and STD via Pavlovian conditioning may also contribute to the increased hypoxic-hypercapnic ventilatory chemosensitivity during early acclimatization to high altitude (Rahn *et al.*, 1953; Forster *et al.*, 1971; Sato *et al.*, 1992; Fatemian & Robbins, 1998) (reviewed in (Smith *et al.*, 2010a)), an important survival strategy allowing increased responsiveness to abrupt hypoxia in the face of ensuing hypocapnia and respiratory alkalosis. Such an increase in loop gain during poikilocapnic hypoxia explains the increased incidence of sleep apnea at high altitude (Khoo *et al.*, 1982; Waggener *et al.*, 1984). Elucidation of the pontine neuromodulation processes integrating hypoxic and hypercapnic inputs at the cellular level will provide a mechanistic basis for understanding and managing such respiratory control abnormalities.

5.5 CONCLUSIONS

The present studies show a form of associative learning of central-peripheral chemoreceptor interaction, which is modulated by respiratory neurons in the dl-pons. Such adaptive control paradigm provides a powerful gain modulation mechanism in respiratory control, which is hitherto evidenced only in the higher brain (Salinas & Thier, 2000; Chance *et al.*, 2002).

5.6 REFERENCES

- Abdala AP, Rybak IA, Smith JC & Paton JF. (2009). Abdominal expiratory activity in the rat brainstem-spinal cord in situ: patterns, origins and implications for respiratory rhythm generation. *J Physiol* **587**, 3539-3559.
- Adams JM, Attinger FM & Attinger EO. (1978). Medullary and carotid chemoreceptor interaction for mild stimuli. *Pflügers Archiv European Journal of Physiology* **374**, 39-45.
- Adams JM & Severns ML. (1982). Interaction of chemoreceptor effects and its dependence on the intensity of stimuli. *Journal of Applied Physiology* **52**, 602-606.
- Alheid GF, Milsom WK & McCrimmon DR. (2004). Pontine influences on breathing: an overview. *Respir Physiol Neurobiol* **143**, 105-114.
- Baxter DW & Olszewski J. (1955). Respiratory responses evoked by electrical stimulation of pons and mesencephalon. *Journal of Neurophysiology* **18**, 276.
- Berger W, Berger K, Berndt J & Giese K. (1978). Interaction of peripheral and central respiratory drives in cats I. Effects of sodium cyanide as a peripheral chemoreceptor stimulus at different levels of CSF pH. *Pflügers Archiv European Journal of Physiology* **374**, 205-210.
- Berkenbosch A, Van Dissel J, Olievier C, De Goede J & Heeringa J. (1979). The contribution of the peripheral chemoreceptors to the ventilatory response to CO₂ in anaesthetized cats during hyperoxia* 1. *Respiration Physiology* **37**, 381-390.
- Blain GM, Smith CA, Henderson KS & Dempsey JA. (2010). Peripheral chemoreceptors determine the respiratory sensitivity of central chemoreceptors to CO₂. *The Journal of Physiology* **588**, 2455-2471.
- Boden AG, Harris MC & Parkes MJ. (1998). Apneic threshold for CO₂ in the anesthetized rat: fundamental properties under steady-state conditions. *Journal of Applied Physiology* **85**, 898-907.
- Chance FS, Abbott LF & Reyes AD. (2002). Gain modulation from background synaptic input. *Neuron* **35**, 773-782.
- Cheng LM, Ivanova O, Fan HH & Khoo MCK. (2010). An integrative model of respiratory and cardiovascular control in sleep-disordered breathing. *Resp Physiol Neurobi* **174**, 4-28.

- Cherniack NS & Longobardo GS. (2006). Mathematical models of periodic breathing and their usefulness in understanding cardiovascular and respiratory disorders. *Experimental Physiology* **91**, 295-305.
- Clement ID, Pandit JJ, Bascom DA, Dorrington KL, O'Connor DF & Robbins PA. (1995). An assessment of central-peripheral ventilatory chemoreflex interaction using acid and bicarbonate infusions in humans. *The Journal of Physiology* **485**, 561-570.
- Cohen MI. (1971). Switching of the respiratory phases and evoked phrenic responses produced by rostral pontine electrical stimulation. *The Journal of Physiology* **217**, 133-158.
- Coles SK & Dick TE. (1996). Neurones in the ventrolateral pons are required for post-hypoxic frequency decline in rats. *J Physiol* **497 (Pt 1)**, 79-94.
- Daristotle L & Bisgard GE. (1989). Central-peripheral chemoreceptor ventilatory interaction in awake goats. *Respiration Physiology* **76**, 383-391.
- Day TA & Wilson RJA. (2007). Brainstem PCO₂ modulates phrenic responses to specific carotid body hypoxia in an in situ dual perfused rat preparation. *The Journal of Physiology* **578**, 843-857.
- Day TA & Wilson RJA. (2009). A negative interaction between brainstem and peripheral respiratory chemoreceptors modulates peripheral chemoreflex magnitude. *The Journal of Physiology* **587**, 883-896.
- Dick TE & Coles SK. (2000). Ventrolateral pons mediates short-term depression of respiratory frequency after brief hypoxia. *Respir Physiol* **121**, 87-100.
- Duffin J. (2010). The role of the central chemoreceptors: A modeling perspective. *Resp Physiol Neurobi* **173**, 230-243.
- Dutschmann M & Herbert H. (2006). The Kolliker-Fuse nucleus gates the postinspiratory phase of the respiratory cycle to control inspiratory off-switch and upper airway resistance in rat. *Eur J Neurosci* **24**, 1071-1084.
- Eldridge FL, Gill-Kumar P & Millhorn DE. (1981). Input-output relationships of central neural circuits involved in respiration in cats. *The Journal of Physiology* **311**, 81-95.
- Eldridge FL & Millhorn DE. (1986). Oscillation, gating, and memory in the respiratory control system. In *Handbook of Physiology, Section 3: The Respiratory System, Vol II: Control of Breathing, part 1*, ed. Fishman AP, Cherniack NS & Widdicombe JG, pp. 93-114. American Physiological Society, Bethesda, MD.

- Fatemian M & Robbins PA. (1998). Human ventilatory response to CO₂ after 8 h of isocapnic or poikilocapnic hypoxia. *J Appl Physiol* **85**, 1922-1928.
- Forster HV, Dempsey JA, Birnbaum ML, Reddan WG, Thoden J, Grover RF & Rankin J. (1971). Effect of chronic exposure to hypoxia on ventilatory response to CO₂ and hypoxia. *J Appl Physiol* **31**, 586-592.
- Fregosi RF. (1991). Short-term potentiation of breathing in humans. *J Appl Physiol* **71**, 892-899.
- Gesell R, Brassfield CR & Hamilton MA. (1942). An acid-neurohumoral mechanism of nerve cell activation. *American Journal of Physiology* **136**, 604-608.
- Gesell R, Lapedes J & Levin M. (1940). THE INTERACTION OF CENTRAL AND PERIPHERAL CHEMICAL CONTROL OF BREATHING. *American Journal of Physiology -- Legacy Content* **130**, 155-170.
- Giese K, Berndt J & Berger W. (1978). Interaction of central and peripheral respiratory drives in cats II. Peripheral and central interaction of hypoxia and hypercapnia. *Pflügers Archiv European Journal of Physiology* **374**, 211-217.
- Glanzman DL. (1995). The cellular basis of classical conditioning in *Aplysia californica*-it's less simple than you think. *Trends Neurosci* **18**, 30-36.
- Green DN. (1983). Global stability analysis of automatic gain-control circuits. *IEEE Transactions on Circuits and Systems* **30**, 78-83.
- Guyenet PG, Koshiya N, Huangfu D, Verberne AJ & Riley TA. (1993). Central respiratory control of A5 and A6 pontine noradrenergic neurons. *American Journal of Physiology - Regulatory, Integrative and Comparative Physiology* **264**, R1035-R1044.
- Guyenet PG, Stornetta RL & Bayliss DA. (2010). Central respiratory chemoreception. *J Comp Neurol* **518**, 3883-3906.
- Hayashi F, Coles SK, Bach KB, Mitchell GS & McCrimmon DR. (1993). Time-dependent phrenic nerve responses to carotid afferent activation: intact vs. decerebellate rats. *Am J Physiol* **265**, R811-819.
- Heeringa J, Berkenbosch A, De Goede J & Olievier C. (1979). Relative contribution of central and peripheral chemoreceptors to the ventilatory response to CO₂ during hyperoxia* 1. *Respiration Physiology* **37**, 365-379.
- Hodges MR & Richerson GB. (2010). The role of medullary serotonin (5-HT) neurons in respiratory control: contributions to eupneic ventilation, CO₂ chemoreception, and thermoregulation. *J Appl Physiol* **108**, 1425-1432.

- Khoo MC, Kronauer RE, Strohl KP & Slutsky AS. (1982). Factors inducing periodic breathing in humans: a general model. *J Appl Physiol* **53**, 644-659.
- Kumar P & Prabhakar N. (2007). Sensing hypoxia: carotid body mechanisms and reflexes in health and disease. *Respir Physiol Neurobiol* **157**, 1-3.
- Lumsden T. (1923). Observations on the respiratory centres in the cat. *J Physiol London* **57**, 153-160.
- Molkov YI, Abdala AP, Bacak BJ, Smith JC, Paton JF & Rybak IA. (2010). Late-expiratory activity: emergence and interactions with the respiratory CpG. *J Neurophysiol* **104**, 2713-2729.
- Nattie E. (2011). Julius H. Comroe, Jr., Distinguished Lecture: Central chemoreception: then ... and now. *J Appl Physiol* **110**, 1-8.
- Nuding S, Segers L, Shannon R, O'Connor R, Morris K & Lindsey B. (2009). Central and peripheral chemoreceptors evoke distinct responses in simultaneously recorded neurons of the raphé-pontomedullary respiratory network. *Philosophical Transactions of the Royal Society B: Biological Sciences* **364**, 2501.
- Ou LC, Miller MJ & Tenney SM. (1976). Hypoxia and carbon dioxide as separate and interactive depressants of ventilation. *Respiration Physiology* **28**, 347-358.
- Pavlov IP. (1960). *Conditioned reflexes; an investigation of the physiological activity of the cerebral cortex*. Dover Publications, New York,.
- Poon C-S. (1993). Adaptive neural network that subserves optimal homeostatic control of breathing. *Ann Biomed Eng* **21**, 501-508.
- Poon C-S. (1996a). Synaptic plasticity and respiratory control. In *Bioengineering Approaches to Pulmonary Physiology and Medicine*, ed. Khoo MCK, pp. 93-113. Plenum, Los Angeles.
- Poon C-S. (1996b). Synaptic Plasticity and Respiratory Control. In *Bioengineering Approaches to Pulmonary Physiology and Medicine*, ed. Khoo MCK, pp. 93-113. Plenum, Los Angeles.
- Poon C-S, Siniaia MS, Young DL & Eldridge FL. (1999a). Short-term potentiation of carotid chemoreflex: an NMDAR-dependent neural integrator. *NeuroReport* **10**, 2261-2265.
- Poon CS. (1996c). Self-tuning Optimal Regulation of Respiratory Motor Output by Hebbian Covariance Learning. *Neural Netw* **9**, 1367-1383.

- Poon CS. (1996d). Synaptic Plasticity and Respiratory Control. In *Bioengineering Approaches to Pulmonary Physiology and Medicine*, ed. Khoo MCK, pp. 93-113. Plenum, Los Angeles.
- Poon CS & Siniatia MS. (2000). Plasticity of cardiorespiratory neural processing: classification and computational functions. *Respir Physiol* **122**, 83-109.
- Poon CS, Siniatia MS, Young DL & Eldridge FL. (1999b). Short-term potentiation of carotid chemoreflex: an NMDAR-dependent neural integrator. *Neuroreport* **10**, 2261-2265.
- Poon CS, Tin C & Yu Y. (2007). Homeostasis of exercise hyperpnea and optimal sensorimotor integration: the internal model paradigm. *Respir Physiol Neurobiol* **159**, 1-13; discussion 14-20.
- Poon CS, Young DL & Siniatia MS. (2000). High-pass filtering of carotid-vagal influences on expiration in rat: role of N-methyl-D-aspartate receptors. *Neurosci Lett* **284**, 5-8.
- Powell FL, Milsom WK & Mitchell GS. (1998). Time domains of the hypoxic ventilatory response. *Respir Physiol* **112**, 123-134.
- Rahn H, Stroud RC, Tenney SM & Mithoefer JC. (1953). Adaptation to high altitude: respiratory response to CO₂ and O₂. *J Appl Physiol* **6**, 158-162.
- Robbins PA. (1988). Evidence for interaction between the contributions to ventilation from the central and peripheral chemoreceptors in man. *The Journal of Physiology* **401**, 503-518.
- Rubin JE, Bacak BJ, Molkov YI, Shevtsova NA, Smith JC & Rybak IA. (2010). Interacting oscillations in neural control of breathing: modeling and qualitative analysis. *J Comput Neurosci*.
- Rubin JE, Shevtsova NA, Ermentrout GB, Smith JC & Rybak IA. (2009). Multiple rhythmic states in a model of the respiratory central pattern generator. *J Neurophysiol* **101**, 2146-2165.
- Salinas E & Thier P. (2000). Gain modulation: a major computational principle of the central nervous system. *Neuron* **27**, 15-21.
- Sands SA, Edwards BA, Kelly VJ, Davidson MR, Wilkinson MH & Berger PJ. (2009). A model analysis of arterial oxygen desaturation during apnea in preterm infants. *PLoS Comput Biol* **5**, e1000588.

- Sato M, Severinghaus JW, Powell FL, Xu FD & Spellman MJ. (1992). Augmented hypoxic ventilatory response in men at altitude. *Journal of Applied Physiology* **73**, 101-107. .
- Sherrington C. (1906). *The Integrative Action of the Nervous System*. Yale University Press, New Haven.
- Smith CA, Forster HV, Blain GM & Dempsey JA. (2010a). An interdependent model of central/peripheral chemoreception: Evidence and implications for ventilatory control. *Respiratory physiology & neurobiology* **173**, 288-297.
- Smith CA, Forster HV, Blain GM & Dempsey JA. (2010b). An interdependent model of central/peripheral chemoreception: evidence and implications for ventilatory control. *Respir Physiol Neurobiol* **173**, 288-297.
- Smith CA, Jameson LC, Mitchell GS, Musch TI & Dempsey JA. (1984). Central-peripheral chemoreceptor interaction in awake cerebrospinal fluid-perfused goats. *Journal of Applied Physiology* **56**, 1541-1549.
- Smith JC, Abdala AP, Koizumi H, Rybak IA & Paton JF. (2007). Spatial and functional architecture of the mammalian brain stem respiratory network: a hierarchy of three oscillatory mechanisms. *J Neurophysiol* **98**, 3370-3387.
- Song G & Poon C-S. (2009a). Lateral parabrachial nucleus mediates shortening of expiration during hypoxia. *Respiratory physiology & neurobiology* **165**, 1-8.
- Song G & Poon C-S. (2009b). Lateral parabrachial nucleus mediates shortening of expiration and increase of inspiratory drive during hypercapnia. *Respiratory physiology & neurobiology* **165**, 9-12.
- Song G & Poon C. (2004). Functional and structural models of pontine modulation of mechanoreceptor and chemoreceptor reflexes. *Respir Physiol Neurobiol* **143**, 281-292.
- Song G, Yu Y & Poon CS. (2006). Cytoarchitecture of pneumotaxic integration of respiratory and nonrespiratory information in the rat. *J Neurosci* **26**, 300-310.
- Sovik S & Lossius K. (2004). Development of ventilatory response to transient hypercapnia and hypercapnic hypoxia in term infants. *Pediatr Res* **55**, 302-309.
- StCroix CM, Cunningham DA & Paterson DH. (1996). Nature of the interaction between central and peripheral chemoreceptor drives in human subjects. *Can J Physiol Pharmacol* **74**, 640-646.
- Tenney SM & Brooks JG. (1966). Carotid bodies, stimulus interaction, and ventilatory control in unanesthetized goats. *Respiration Physiology* **1**, 211-224.

- Teppema LJ & Dahan A. (2010). The ventilatory response to hypoxia in mammals: mechanisms, measurement, and analysis. *Physiol Rev* **90**, 675-754.
- Thompson RF. (1988). The neural basis of basic associative learning of discrete behavioral responses. *Trends Neurosci* **11**, 152-155.
- Tin C, Wasserman K, Cherniack NS & Poon CS. (2010). Paradoxical potentiation of exercise hyperpnea in congestive heart failure contradicts Sherrington chemoreflex model and supports a respiratory optimization model. *Adv Exp Med Biol* **669**, 69-72.
- Topor ZL, Vasilakos K, Younes M & Remmers JE. (2007). Model based analysis of sleep disordered breathing in congestive heart failure. *Resp Physiol Neurobi* **155**, 82-92.
- Van Beek JHGM, Berkenbosch A, De Goede J & Olievier CN. (1983). Influence of peripheral O₂ tension on the ventilatory response to CO₂ in cats. *Respiration Physiology* **51**, 379-390.
- Waggener TB, Brusil PJ, Kronauer RE, Gabel RA & Inbar GF. (1984). Strength and cycle time of high-altitude ventilatory patterns in unacclimatized humans. *Journal of Applied Physiology* **56**, 576.
- Wagner PG & Eldridge FL. (1991). Development of short-term potentiation of respiration. *Respir Physiol* **83**, 129-139.
- Waters KA & Gozal D. (2003). Responses to hypoxia during early development. *Respir Physiol Neurobiol* **136**, 115-129.
- Young DL, Eldridge FL & Poon CS. (2003a). Integration-differentiation and gating of carotid afferent traffic that shapes the respiratory pattern. *J Appl Physiol* **94**, 1213-1229.
- Young DL, Eldridge FL & Poon CS. (2003b). Integration-differentiation and gating of carotid afferent traffic that shapes the respiratory pattern. *J Appl Physiol* **94**, 1213-1229.
- Young DL & Poon C-S. (2001). A Hebbian feedback covariance learning paradigm for self-tuning optimal control. *IEEE Trans Systems, Man, and Cybernetics* **31 (Part B)**, 173-186.

Chapter 6 Conclusions and Future Work

This thesis challenges the traditional Sherringtonian reflexogenic view of respiratory control, which assumed that response is linearly additive due to multiple factors. In a series of computational and experimental studies, we have shown that:

1. At the behavior level, the respiratory response in humans during muscular exercise under a variety of pulmonary gas exchange defects seems to follow an optimization strategy of mechanical and chemical afferents interaction. Model predictions are consistent with some key clinical and experimental observations in a range of pulmonary gas exchange defect problems. The optimization model provides a powerful tool to help understanding the underlying control mechanism in the face of various pulmonary gas exchange defects, including CHF, right-to-left shunt and external dead space. We also discuss the risk factors that would impacts the capability to maintain blood gas homeostasis. The model also suggests that mechanical-chemical afferent interaction has a stronger influence on total ventilation than breathing pattern.

2. At the neuronal level, certain respiratory neurons in the dorsolateral pons in the rat brain stem integrate central and peripheral chemoreceptor afferent signals in a hypoadditive manner, evidencing classical (Pavlovian) conditioning of chemoreceptor inputs that modulate the respiratory rhythm and respiratory motor output. This shows the first neuronal correlates of CO₂-O₂ interaction. Such a unique form of associative learning provides a powerful gain modulation mechanism that has profound implications in respiratory stability during sleep apnea. Elucidation of the pontine neuromodulation processes integrating central and peripheral chemical inputs at the cellular level will provide a mechanistic basis for understanding and managing such respiratory control abnormalities.

The top-down and bottom-up approaches both point to a novel adaptive control paradigm underlying the autonomic regulation of respiration, which is beyond the scope of the traditional Sherringtonian reflex framework.

M. Tenney once exhorted: “The physiologist keeps the whole always in mind. He accepts the tactical necessity of reductionism to understand the parts, but, once done, it is for him only the beginning, never the end. Synthesis is his overriding strategy.” (quoted from Remmers (2005)).

Consideration of such system complexity is challenging but essential for understanding how the physiological systems function in disease states, which is not likely to be explained by a single genetic or molecular deficit.

6.1 FUTURE WORKS

6.1.1 Modeling

The optimization model provides a convenient framework for integrating multiple factors by incorporating their mutual interactions. It is of great interest to further examine

the model in a wider scope of physiological and clinical conditions. For instance, the paradox of obesity hypoventilation syndrome (OHS) (a.k.a. Pickwickian syndrome) is a clinical paradox (Mokhlesi & Tulaimat, 2007; Piper & Grunstein, 2007) that is distinguishable from eucapnic obesity (Olson & Zwillich, 2005) and obstructive sleep apnea (Rapoport *et al.*, 1986; Kessler *et al.*, 2001; Banerjee *et al.*, 2007). The alveolar hypoventilation is characterized by a marked reduction in V_T and increase in V_D/V_T (Auchincloss *et al.*, 1955). The pathogenesis of OHS is not fully understood, but it has commonly been ascribed to either “can’t breathe” (chest wall and respiratory muscle disorder) and “won’t breathe” (ventilatory drive disorder) mechanisms (Teichtahl, 2001; Jubber, 2004). However, neither of them alone has proved to totally account for hypercapnia in OHS (Gilbert *et al.*, 1961; Zwillich *et al.*, 1975; Leech *et al.*, 1991; Cherniack, 2008b, a).

Another longstanding clinical paradox is that some patients with chronic obstructive pulmonary disease (COPD) appear to be more prone to CO_2 retention and hypoxemia (“blue bloaters”) than others (“pink puffers”). COPD patients are faced with combined mechanical (increased resistance in small airways, hyperinflation) and chemical (mismatch of pulmonary ventilation and perfusion) challenges. Early studies ascribed such discrepancy to the manifestation of two distinct phenotypes of COPD (bronchitis and emphysema) with differing impairments of pulmonary mechanics and pulmonary gas exchange (Filley *et al.*, 1968). In a group of patients with mixed presentations of COPD, blue bloaters reportedly had a fivefold greater incidence of chronic bronchitis and a seven-fold greater incidence of cor pulmonale (failure of the right side of the heart brought on by long-term high blood pressure in the pulmonary arteries and right ventricle of the heart) than pink puffers (Javaheri *et al.*, 1981). However, the etiologies of COPD may be highly heterogeneous and the phenotypes are often mixed (Makita *et al.*, 2007), so the situation is more complicated than originally thought.

These clinical paradoxes represent complex physiological problems which cannot be resolved by traditional reductionist approach. Hence, the optimization model is a useful tool to examine the relative contributions of varying chemical, mechanical and metabolic factors with direct clinical implications.

6.1.2 Experimental

This thesis has focused on the role of respiratory neurons in dl-pons on CO₂-O₂ interaction. Similar experimental approach can be applied to other brain stem regions, which may also contribute to this or other form on respiratory afferent interactions, for instance, vl-pons and intertrigeminal nucleus.

On the other hand, the limitation of the multi-electrode recording technique used here is that it does not allow further characterization of the neurochemical basis of the afferents integration. Instead, a multibarrel extracellular recording/microiontophoresis-pressure microinjection technique can be employed, which will allow us to functionally characterize the recorded neurons both electrophysiologically and neurochemically simultaneously. These techniques will provide further knowledge about the pharmacological mediator for the afferent interactions of interest.

6.2 REFERENCES

- Auchincloss JH, Jr., Cook E & Renzetti AD. (1955). Clinical and physiological aspects of a case of obesity, polycythemia and alveolar hypoventilation. *J Clin Invest* **34**, 1537-1545.
- Banerjee D, Yee BJ, Piper AJ, Zwillich CW & Grunstein RR. (2007). Obesity hypoventilation syndrome: hypoxemia during continuous positive airway pressure. *Chest* **131**, 1678-1684.
- Cherniack NS. (2008a). The obesity hyperventilation syndrome. *Current Respiratory Medicine Reviews* **4**, 100-104.
- Cherniack NS. (2008b). What causes hypercapnia? Won't breathe, can't breathe or something in between? *Respiration* **75**, 251-252.
- Filley GF, Dart GA & Mitchell RS. (1968). Emphysema and chronic bronchitis: clinical manifestations and their physiological significance. *Aspen Emphysema Conf* **9**, 339-349.
- Gilbert R, Sipple JH & Auchincloss JH, Jr. (1961). Respiratory control and work of breathing in obese subjects. *J Appl Physiol* **16**, 21-26.
- Javaheri S, Blum J & Kazemi H. (1981). Pattern of breathing and carbon dioxide retention in chronic obstructive lung disease. *Am J Med* **71**, 228-234.
- Jubber AS. (2004). Respiratory complications of obesity. *Int J Clin Pract* **58**, 573-580.
- Kessler R, Chaouat A, Schinkewitch P, Faller M, Casel S, Krieger J & Weitzenblum E. (2001). The obesity-hypoventilation syndrome revisited: a prospective study of 34 consecutive cases. *Chest* **120**, 369-376.
- Leech J, Onal E, Aronson R & Lopata M. (1991). Voluntary hyperventilation in obesity hypoventilation. *Chest* **100**, 1334-1338.
- Makita H, Nasuhara Y, Nagai K, Ito Y, Hasegawa M, Betsuyaku T, Onodera Y, Hizawa N & Nishimura M. (2007). Characterisation of phenotypes based on severity of emphysema in chronic obstructive pulmonary disease. *Thorax* **62**, 932-937.
- Mokhlesi B & Tulaimat A. (2007). Recent advances in obesity hypoventilation syndrome. *Chest* **132**, 1322-1336.
- Olson AL & Zwillich C. (2005). The obesity hypoventilation syndrome. *Am J Med* **118**, 948-956.

- Piper AJ & Grunstein RR. (2007). Current perspectives on the obesity hypoventilation syndrome. *Curr Opin Pulm Med* **13**, 490-496.
- Rapoport DM, Garay SM, Epstein H & Goldring RM. (1986). Hypercapnia in the obstructive sleep apnea syndrome. A reevaluation of the "Pickwickian syndrome". *Chest* **89**, 627-635.
- Remmers JE. (2005). A century of control of breathing. *Am J Respir Crit Care Med* **172**, 6-11.
- Teichtahl H. (2001). The obesity-hypoventilation syndrome revisited. *Chest* **120**, 336-339.
- Zwillich CW, Sutton FD, Pierson DJ, Greagh EM & Weil JV. (1975). Decreased hypoxic ventilatory drive in the obesity-hypoventilation syndrome. *Am J Med* **59**, 343-348.